NOAA Atlas NESDIS 91

WORLD OCEAN ATLAS 2023
Volume 3: Dissolved Oxygen, Apparent Oxygen Utilization, Dissolved Oxygen Saturation, and 30-year Climate Normal

Silver Spring, MD
February 2024

U.S. DEPARTMENT OF COMMERCE
National Oceanic and Atmospheric Administration
National Environmental Satellite, Data, and Information Service
National Centers for Environmental Information

NOAA National Centers for Environmental Information (NCEI)

Additional copies of this publication, as well as information about NCEI data holdings and services, are available upon request directly from NCEI.

NOAA/NESDIS
National Centers for Environmental Information
SSMC3, 4th floor
1315 East-West Highway
Silver Spring, MD 20910-3282
U.S.A.

Telephone: +1 (828) 271-4800
E-mail: ncei.info@noaa.gov
WEB: https://www.ncei.noaa.gov /

For updates on the data, documentation, and additional information about the WOA23 please refer to:
https://www.ncei.noaa.gov/products/ocean-climate-laboratory

This World Ocean Atlas (WOA23) Volume 3 should be cited as:

Garcia H. E., Z. Wang, C. Bouchard, S.L. Cross, C.R. Paver, J.R. Reagan, T.P. Boyer, R.A. Locarnini, A.V. Mishonov, O.K. Baranova, D. Seidov, and D. Dukhovskoy (2024). World Ocean Atlas 2023, Volume 3: Dissolved Oxygen, Apparent Oxygen Utilization, Dissolved Oxygen Saturation, and 30-year Climate Normal. A. Mishonov Technical Editor. *NOAA Atlas NESDIS 91*, 98 pp. https://doi.org/10.25923/rb67-ns53

This document is available online at https://www.ncei.noaa.gov/products/world-ocean-atlas

NOAA Atlas NESDIS **91**

WORLD OCEAN ATLAS 2023
Volume 3: Dissolved Oxygen, Apparent Oxygen Utilization, Dissolved Oxygen Saturation, and 30-year Climate Normal

Hernan E. Garcia, Zhankun Wang, Courtney Bouchard, Scott L. Cross,
Chris R. Paver, James R. Reagan, Timothy P. Boyer,
Ricardo A. Locarnini, Alexey V. Mishonov, Olga K. Baranova,
Dan Seidov, and Dmitry Dukhovskoy

Technical Editor: Alexey Mishonov

National Centers for Environmental Information

Silver Spring, Maryland
February 2024

U.S. DEPARTMENT OF COMMERCE
Gina M. Raimondo, Secretary

National Oceanic and Atmospheric Administration
Richard W. Spinrad, Under Secretary of Commerce for Oceans and Atmosphere and NOAA Administrator

National Environmental Satellite, Data, and Information Service
Stephen Volz, Assistant Administrator

To Sydney (Syd) Levitus

Syd exemplifies the craft of careful, systematic inquiry of the large-scale distributions and low-frequency variability from seasonal-to-decadal time scales of ocean properties. He was one of the first to recognize the importance and benefits of creating objectively analyzed climatological fields of measured ocean variables including temperature, salinity, oxygen, nutrients, and derived fields such as mixed layer depth. Upon publishing the Climatological *Atlas of the World Ocean* in 1982, he distributed this work without restriction, an act not common at the time. This seminal atlas moved the oceanographic diagnostic research from using hand-drawn maps to using objectively analyzed fields of ocean variables.

With his NODC Ocean Climate Laboratory (OCL) colleagues, and unprecedented cooperation from the U.S. and international ocean scientific and data management communities, he created the *World Ocean Database (WOD)*; the world's largest collection of ocean profile data that are available internationally without restriction. The *World Ocean Atlas (WOA)* series represents the gridded objective analyses of the WOD and these fields have also been made available without restriction.

The WOD and WOA series are used so frequently that they have become known generically as the "Levitus Climatology". These databases and products enable systematic studies of ocean variability in its climatological context that were not previously possible. His foresight in creating WOD and WOA has been demonstrated by their widespread use over the years. Syd has made major contributions to the scientific and ocean data management communities. He has also increased public understanding of the role of the oceans in climate. He retired in 2013 after 39 years of distinguished civil service. He distilled the notion of the synergy between rigorous data management and science; there are no shortcuts.

All of us at the Ocean Climate Laboratory would like to dedicate this atlas to Syd, his legacy, vision, and mentorship.

The OCL Team

Table of Contents

List of Acronyms Used

Acronym	Expanded Term
APB	Autonomous Pinniped Bathythermograph
AWI	Alfred Wegener Institute for Polar and Marine Research
BAMS	Bulletin of the American Meteorological Society
Argo	Core Argo program floats
BGC-Argo	BioGeoChemical Argo float, an extension of the Argo core program
CCHDO	CLIVAR and Carbon Hydrographic Data Office
CLIVAR	Climate and Ocean: Variability, Predictability and Change
CMIP	Coupled Model Inter-comparison Project
CRM	Certified Reference Material
CSV	Comma-Separated Value
CTD	Conductivity Temperature Depth dataset in the WOD
DBT	Drifting Bathythermograph
DIVA	Data-Interpolating Variational Analysis
DOC	Department of Commerce
DOE	Department of Energy
DRB	Drifting Buoy dataset in the WOD
EMODnet	European Marine Observation and Data Network
EEI	Earth Energy Imbalance
ENSO	El Niño-Southern Oscillation,
ERL	Earth Research Laboratory
EOV	Essential Ocean Variable
ETOPO2	Earth Topography 2 arc minute
FAIR	Findable, Accessible, Interoperable, and Reusable
GEOSECS	Geochemical Ocean Sections Study
GIS	Geographic Information System
GLD	Glider dataset in the WOD
GMT	Greenwich Mean Time, or Generic Mapping Tools
GO2NE	Global Ocean Oxygen Network
GLODAP	Global Ocean Data Analysis Project
GOBAI	Gridded Ocean Biogeochemistry from Artificial Intelligence for O_2
GODAR	Global Ocean Data Archaeology and Rescue
GOMO	Global Ocean Monitoring and Observing Program
GO-SHIP	Global Ocean Ship-based Hydrographic Investigations Program
GPP	Gross Primary Production
GTSPP	Global Temperature-Salinity Profile Program
IAPSO	International Association for the Physical Sciences of the Oceans
IOC	Intergovernmental Oceanographic Commission of UNESCO
IOCARIBE	Cooperative marine science activities of IOC in the Caribbean and adjacent regions
IODE	International Oceanographic Data Exchange of IOC
IPCC	Intergovernmental Panel on Climate Change
IQuOD	International Quality-controlled Ocean Database
IRI	International Research Institute for Climate and Society

Acronym	Expanded Term
IUPAC	International Union of Pure and Applied Chemistry
JPOTS	Joint Panel on Oceanographic Tables and Standards
LDEO	Lamont-Doherty Earth Observatory
MBT	Mechanical Bathythermograph
MRB	Moored Buoy
NATO	North Atlantic Treaty Organization
NCEI	National Centers for Environmental Information
NESDIS	National Environmental Satellite, Data, and Information Service
NetCDF	Network Common Data Form
NOAA	National Oceanic and Atmospheric Administration
NODC	National Ocean Data Center
OA	Objective Analysis
OSD	Ocean Station Data dataset in the WOD
O2S	Dissolved oxygen saturation (%)
O2I	Dissolved oxygen inventory
OCL	Ocean Climate Laboratory Team
ODINAFRICA	Ocean Data and Information Network for Africa
ODIS	IOC Ocean Data and Information System
ODV	Ocean Data View (Schlitzer, R., 2023)
OMZ	Oxygen Minimum Zone
PDF	Portable Document Format
PDO	Pacific Decadal Oscillation
PFL	Profiling Float dataset in in the WOD
QA	Quality Assurance
QC	Quality Control
QCF	Quality Control Flags
SST	Sea Surface Temperature
SME	Subject Matter Expert
SOCCOM	Southern Ocean Carbon and Climate Observations and Modeling project
SUR	Surface dataset in the WOD
UN	United Nations
UNESCO	United Nations Educational, Scientific and Cultural Organization
UOR	Undulating Oceanographic Recorder in the WOD
USA	United States of America
WDS	World Data System
WDS Oceanography	World Data Service for Oceanography of the WDS hosted at NCEI
WOA	World Ocean Atlas
WOA18	World Ocean Atlas 2018
WOA23	World Ocean Atlas 2023
WOA23F	World Ocean Atlas 2023 (1965-2022)
WOA23N	World Ocean Atlas 2023 “Climate Normal” (1971-2000)
WOCE	World Ocean Circulation Experiment
WOD	World Ocean Database
WOD18	World Ocean Database 2018
WOD23	World Ocean Database 2023

Acronym	Expanded Term
XBT	Expendable Bathythermograph dataset in the WOD
XCTD	Expendable Conductivity Temperature Depth dataset in the WOD

Preface

The World Ocean Atlas 2023 (WOA23) is the latest in a line of research quality oceanographic analyses of subsurface (profile) measured Essential Ocean Variables (EOV) at standard depths extending back to the groundbreaking *Climatological Atlas of the World Ocean* (Levitus, 1982). The WOA line of products has been published semi-regularly since 1994, with versions in 1998, 2001, 2005, 2009, 2013, 2018, and now 2023. Previous iterations of the WOA have proven to be of great utility to the oceanographic, climate research, geophysical, and operational environmental forecasting communities. The oceanographic variable analyses are used as boundary and/or initial conditions in numerical ocean circulation models and atmosphere-ocean models, for verification of numerical simulations of the ocean, as a form of "sea truth" for satellite measurements such as altimetric observations of sea surface height, for computation of nutrient fluxes by Ekman transport, and for planning oceanographic expeditions among others.

The WOA23 includes objective analyses on a one-degree grid for all quality-controlled variables at annual, seasonal, and monthly (temperature, salinity, dissolved inorganic nutrients, and oxygen). WOA23 also includes data analyses on a quarter-degree grid for temperature and salinity only. Since the WOA18, the ocean variable analyses are produced on 102 standard depth levels from the surface to 5,500 m (previously 33 levels within the same depth limits). The WOA23 provides one-degree 30-year climate normal for temperature, salinity, and dissolved oxygen. Ocean data and analyses of data at higher temporal and spatial resolution than previously available are needed to document ocean variability, isopycnal analysis, uncertainty, including improving diagnostics, understanding, and modeling of the physics of the ocean.

In the acknowledgment section of this publication, we have expressed our view that creation of global ocean profile and plankton databases and data analyses are only possible through the sharing of data and cooperation of data centers, scientists, data managers, and scientific administrators throughout the U.S. and international scientific community including the International Oceanographic Data and Information Exchange (IODE) of the Intergovernmental Oceanographic Commission (IOC) of UNESCO.

Ocean Climate Laboratory Team
NOAA NESDIS National Centers for Environmental Information
Silver Spring, MD USA
February 2024

Acknowledgments

This work was made possible by a grant from the National Oceanic and Atmospheric Administration (NOAA) Climate and Global Change Program, which enabled the establishment of a research group at the National Centers for Environmental Information (NCEI). The purpose of this group is to prepare research quality oceanographic databases, as well as to compute objective analyses of, and diagnostic studies based on, these databases. This work is funded in partnership with the NOAA's Global Ocean Monitoring and Observing Program (GOMO).

The measured data on which the World Ocean Atlas 2023 (WOA23, Reagan *et al.* 2023, Reagan *et al.* 2024a) is based are in the *World Ocean Database 2023* (WOD23; Mishonov *et al.* 2024) and are distributed on-line by NCEI. Many data were acquired as a result of the IOC/IODE *Global Oceanographic Data Archeology and Rescue* (GODAR) project, the IOC/IODE *World Ocean Database project* (WOD), and the World Data Service for Oceanography (WDS-Oceanography) of the World Data System hosted at NCEI. The WOD23 is the latest major update release to NOAA's World Ocean Database (WOD); the world's largest collection of uniformly formatted, quality controlled, publicly available ocean profile of Essential Ocean Variables (EOV) collected since 1772 to present.

We acknowledge the scientists, technicians, and programmers who have collected and processed data, those individuals who have submitted and shared data to national, regional, and global data centers as well as the data managers and staff at the various data centers. We are working on a more substantive and formalized way to acknowledge all those who have collected and contributed to oceanographic measurements used in the WOD including Persistent Unique Identifiers (*e.g.* Digital Object Identifiers, DOI). All of the originator's data in the WOD are archived at NCEI and includes all metadata provided by the data provider including provenance and attribution. When requested, NCEI can add a DOI to new data being archived if one does not already exist. Until we have a more comprehensive system in place within the WOD metadata to include DOIs, we direct the reader's attention to lists of primary investigators, institutions, and projects, which contributed data (See WOD Code Table Library). We thank our colleagues at the NCEI. Their efforts have made this and similar works possible. We are grateful to Dr. Annie Wong, Dr. Takamitsu Ito, and to the anonymous reviewers for their constructive comments and suggestions which significantly improved the content of this document.

We dedicate this work to Carla Coleman who always contributed with a smile and was taken from us too soon.

WORLD OCEAN ATLAS 2023
Volume 3: Dissolved Oxygen, Apparent Oxygen Utilization, Dissolved Oxygen Saturation, and 30-year Climate Normal

ABSTRACT

The World Ocean Atlas (WOA23) of dissolved oxygen (O_2), Apparent Oxygen Utilization (AOU), and O_2 saturation (O2S) is the most comprehensive observation-based global mean climatology of the past ~6 decades (1965-2022). We describe data sources, quality control (QC), statistics, and objective analysis (OA) used to estimate mean annual, seasonal, monthly fields at 102 standard depths levels (0-5500m depth) on a one-degree latitude-longitude grid resolution. The analysis uses quality-controlled O_2 measurements from chemical (Winkler titrations) and sensor-based (CTD and delayed-mode Argo as well as BGC-Argo including deep Argo) totaling ~27.4 million measurements (~1.0 million profiles) from the World Ocean Database 2023 (WOD23). The global mean difference between Winkler and CTD O_2 profile geographically and temporally matched pairs deeper than 1000m depth is about ±0.27 µmol·kg^{-1}. The delayed-mode Argo and BGC-Argo O_2 observations were globally adjusted up by ~1.34 µmol·kg^{-1} to account for the global mean difference between Winkler-CTD and Argo/BGC-Argo geographically and temporally matched pairs deeper than 1000m depth. A O_2 solubility adjustment was applied to all O_2 measurements as a function of year and depth to account for the effect of ocean warming on O_2 solubility between sampling years. The global mean difference between the statistical and analyzed values is about 0.2 ± 0.3 µmol·kg^{-1} for O_2, -0.5 ± 0.9 µmol·kg^{-1} for AOU, and 0.1 ± 0.2 % for O_2 saturation. The global annual mean ocean O_2 inventory is ~238.2 Pmol. When compared to mapped data products, the WOA23 global O_2 mean content (µmol·kg^{-1}) is slightly lower than in the WOA18 (-1.0 ± 1.0) and GLODAP (-0.4 ± 0.5) for the 0-5500 m depth layer. WOA23 is on average about 3.1 ± 0.9 µmol·kg^{-1} higher than the GOBAI-O2 for the 0-2000 m depth layer. A separate 30-year (1971-2000) "Climate Normal" of O_2, AOU, and O_2 saturation is presented using Winkler and CTD sensor-based O_2 measurements. The 1971-2000 Climate Normal annual mean O_2 inventory is ~239.1 Pmol.

1. INTRODUCTION

The content and distribution of dissolved oxygen (O_2), Apparent Oxygen Utilization (AOU), and dissolved oxygen saturation (O2S) in the global ocean water column are affected by both biogeochemical and physical processes acting on several spatial and temporal scales including climate change. Dissolved O_2 is a non-conservative Essential Ocean Variable (EOV). Biogeochemical processes include sources and sinks of O_2 due to marine biological production, respiration, redox chemistry, and respiration of labile organic matter. The photosynthetic O_2 generated (Gross Primary Production, GPP) is nearly counter balanced by respiration of the labile organic matter produced (*i.e.* biological pump); and schematically represented as $CO_2 + H_2O \leftrightarrow \text{carbon organic matter} + O_2$. While this relation is a simplification, it shows the importance of biologically-mediated O_2 production and respiration (*i.e.* remineralization). In some oceanic regions,

O_2 supersaturation may occur due to increased photosynthetic production and physical forcing (Craig and Hayward, 1987; Schudlich and Emerson, 1996). Physical processes include sources and sinks of O_2 affected by circulation, ventilation, air-sea flux exchange, gas solubility, and water mixing. counterbalanced by the supply of oxygenated waters at or near the surface, the oceanic O_2 content distribution and inventory is sensitive to natural and man-made climate change and impacts (*e.g.* Garcia *et al.* 1998; Keeling and Garcia, 2002; Matear and Hirst, 2003; Stramma *et al.* 2008; Stramma *et al.* 2012; Shaffer *et al.* 2009; Riebesell *et al.* 2009; Hofmann and Schellnhuber, 2009; Wang *et al.* 2022).

Ocean climate changes due to global warming (Ocean Heat Content, OHC) have a potentially large impact through feedbacks on ocean O_2 sources and sinks including marine ecosystems and near surface ocean O_2-rich water ventilation of the generally O_2-poor deep ocean. Even small changes in the global dissolved oxygen inventory may have large impacts on marine ecosystems (Wishner *et al.* 2018; Morée *et al.* 2023), ocean remineralization of labile organic matter (Redfield *et al.* 1963), the blue economy (Pavlov *et al.* 2024). Some of the these societal challenges are being addressed as part of the UN Decade of Ocean Science for Sustainable Development (2001-2030).

Observational studies have indicated regional to global-scale O_2 content decreases over time, a process termed "ocean deoxygenation" (deoxygenation for short). Deoxygenation refers to the decrease in O_2 content overtime due to man-induced impacts on ocean biogeochemical and physical forcing factors. Thus, the global O_2 content of the ocean in the past few decades is affected by both natural variability and anthropogenic climate impacts. While ocean warming decreases O_2 solubility content, deoxygenation appears to be impacted by other factors including reduced exchange of relatively O_2-richer near surface waters and O_2-poorer deep waters due to thermal stratification, air-sea exchange, and biochemical-mediated processes. Additional work is needed to assess deoxygenation attribution and uncertainties.

Global ocean deoxygenation trend estimates from observations and models vary greatly. Observational studies differ by more than 50%. For example, observation-based studies such as Helm *et al.* (2011) estimated a rate of -0.55 ± 0.13 Pmol·decade^{-1} (100–1000 m) between about 1970 and 1992. Schmidtko *et al.* (2017) reported trends of -0.26 (0-1200 m), -0.70 (1200-bottom) and -0.96 Pmol·decade^{-1} (0-bottom between 1960 and 2016. Ito *et al.* (2017) indicated a rate of -0.24 Pmol·decade^{-1} (0-1000 m, 1958 to 2015). Ito (2022) estimated -0.054 Pmol·decade^{-1} (0-700 m) and 0.27 Pmol·decade^{-1} for the global ocean (1965 to 2015). More recently, Ito *et al.* (2023) estimated a trend of -0.18 ± 0.02 Pmol·decade^{-1} (0-1000 m; 1965-2017). Using observations and machine learning (ML), Sharp *et al.* (2023) estimated a global mean trend of -1.19 ± 0.05 μmol·kg^{-1} (0.79 ± 0.04 %·decade^{-1}) for the 0-2000 m (2004-2022). Assuming a global ocean volume of 0.638×10^{18} m^3 (0-2000 m depth), the trend is approximately -0.88 Pmol·decade^{-1}. The variance among observational and model estimates depends on many factors including data 4-D (time, depth, latitude, and longitude) coverage, methods, and data quality (*i.e.* precision, reproducibility, uncertainty). For comparison, Coupled Model Inter-comparison Project phase 5 and 6 historical simulations (0-1000 m, 1965-2014) indicate a smaller in magnitude trend of about -0.11 ± 0.07 Pmol·decade^{-1} (Kwiatkowski *et al.* 2020; Takano *et al.* 2023).

It is critical that the ocean science community

has access to a reliable global ocean profile database of known science quality and covering the instrumental time period. For example, the International Quality-controlled Ocean Database (IQuOD) uses NOAA's World Ocean Database (WOD) data to develop a climate-quality ocean temperature database using consistent quality control standards.

The World Ocean Atlas 2023 (WOA23; Reagan *et al.* 2023, Reagan *et al.* 2024a) is part of the World Ocean Atlas (WOA) data product series. The WOA23 is a set objectively analyzed (one degree grid and quarter degree grid) climatological fields of *in situ* temperature, salinity, O_2, AOU, O2S, phosphate, silicate, and nitrate at 102 standard depth levels (0-5500 m depth) for annual, seasonal, and monthly compositing periods for the World Ocean. The WOA23 O_2 fields (as well as AOU and O2S) are available using all quality controlled bottle (Winkler titrations), CTD, and profiling float sensor-based O_2 data from 1965-2022 as well as a thirty year "climate normal" using bottle and CTD data for the 1971-2000 time period. The analyses are derived from NOAA's World Ocean Database 2023 (WOD23, Mishonov *et al.* 2024). As shown in Table 12, the WOA23 data products include analysis for dissolved oxygen (this atlas), temperature (Locarnini *et al.* 2024), salinity (Reagan *et al.* 2024a), dissolved inorganic nutrients (Garcia *et al.* 2024a), conductivity (Reagan *et al.* in preparation); density (Locarnini *et al.* in preparation), mixed layer depth (Wang *et al.* in preparation).

This WOA23 presents composite annual, seasonal, and monthly objectively analyzed (OA) and statistical fields for O_2, AOU, and O2S for data collected between January 1, 1965 and December 31, 2022. We also present a 30-year "climate normal" for data collected between January 1, 1971 and December 31, 2000) for the same variables. A "Climate Normal" is a 30-year average of a particular variable of the climate. The World Meteorological Organization (WMO) defines a climate normal as "Period averages computed for a uniform and relatively long period comprising at least three consecutive ten-year periods". This is the first time a WOA climate normal has been done for O_2, AOU, and O2S. We plan to develop additional 30-year WOA O_2 "Climate Normals" in the future subject to data availability.

In this atlas, we use several terms or definitions important to understand how the atlas is developed and made available. We use the terms "WOA23F" to denote the full 1965-2022 climatology and "WOA23N" for the 1971-2000 "Climate Normal" climatology. We use the term WOA23 where referring to both the WOA23F and WOA23N.

Climatologies in this atlas are defined as observation-based mean oceanographic 1-degree fields (360×180) at 102 standard depth levels (0-5500 m depth) based on the objective analysis of quality-controlled oceanographic profiles available in the WOD23.

The WOD23 is the latest major update release to the World Ocean Database (WOD). The WOD is world's largest collection of uniformly formatted, quality controlled, publicly available ocean profile of EOV data collected since 1772 to present. The WOD23 contains all measurements added to the WOD up to December 31, 2022. Thus, the WOD23 is a subset of the data in the WOD. Garcia *et al.* (2024b) provides a WOD23 user manual which includes descriptions of the data and metadata.

The WOD incorporates new measurements and updates to data/metadata on an ongoing basis and make them available online quarterly at the National Oceanic and Atmospheric Administration (NOAA) National Centers for Environmental

Information (NCEI) WOD webpage. All of the data in NOAA's World Ocean Atlas (WOA) and World Ocean Database (WOD) are FAIR-compliant (Findable, Accessible, Interoperable, and Reusable; Wilkinson *et al.* 2016) and available online free of charge and without restrictions on access and reuse. This is consistent with the IOC Oceanographic Data Exchange Policy and Terms of Use (2023). All of the original or primary data in the WOD are archived and freely available at the NCEI archives in the exact original format and content shared by the data provider. This enables anyone the means to recreate the WOD23 and WOA23 in their entirety from the archived data as well having all of the information available of the original data as the primary reference. The availability of the WOD23 data used in the WOA23 is discussed in Section 2.

A water column profile is here defined as a set of discrete or continuous measurements as a function of depth by a sampler or sensor such as a rosette mounted on a Conductivity-Temperature-Depth (CTD) package, gliders, profiling floats, moorings, underway systems, instrumented marine instrumented animals (*i.e.* elephant seals, turtles, *etc*.), or other platforms.

The data in the WOD23 are grouped into datasets depending on several factors such as sampling instruments, vertical resolution, and variables sampled (Table 1e). For example, the Ocean Station Dataset (OSD for short) includes all of the discreet chemical oceanographic measured variables and excludes all sensor-based observations which are stored in other datasets. Dissolved O_2 observational data are available in different datasets in the WOD (OSD, CTD, PFL, GLD, DRB, and UOR, as shown in Table 1a, Table 1b, Table 1e). The WOA23 uses O_2 data in the OSD, CTD, and PFL datasets. In the future, we plan to incorporate additional OSD, CTD, and PFL as well as O_2 data from the GLD, DRB, and UOR datasets (Figure 1a).

In our analysis, the WOA23F is defined as using the WOD23 quality-controlled measurements collected between January 1, 1965 and December 31, 2022 (*i.e.* baseline 1965-2022). WOA23N is defined as quality-controlled measurements collected between January 1, 1965 and December 31, 2001 (*i.e.* baseline 1965-2001). Table 1b shows the number of O_2 profiles and observations.

We present data quality and OA procedures used to estimate annual, seasonal, and monthly climatologies and related statistical fields at 102 standard depth levels between the surface and the ocean bottom to a maximum depth of 5500 m. The complete set of maps, statistical and objectively analyzed data fields, and documentation are all available on-line at NCEI.

The WOA23F climatology uses quality-controlled *in situ* O_2 observations estimated using chemical methods (Winkler method, Winkler, 1888; Carpenter, 1965a, Carpenter, 1965b) and sensor-based (CTD, delayed-mode Argo, and Biogeochemical Argo; BGC-Argo for short, and deep-Argo). BGC-Argo is extension of the Argo core program (Johnson *et al.* 2022) that includes biogeochemical observations including O_2, Nitrate, pH, and Chlorophyll. The previous atlas version World Ocean Atlas 2018 (WOA18, Garcia *et al.* 2019b) O_2 fields were calculated using *in situ* Winkler-based measurements collected between January 1, 1965 and December 31, 2018. The WOA13 used quality-controlled Winkler-based O_2 data collected on or after January 1, 1960. Prior to WOA13, climatologies were calculated using all available O_2 data regardless of year of observation that passed our quality control steps. The availability of more post-1965 O_2 data has increased the temporal and spatial coverage.

The WOA23F and WOA23N annual

climatology O_2 fields were calculated using all quality-controlled observational data in the WOD23 regardless of the month in which the observation was made between January 1, 1965 and December 31, 2022 for WOA23F and January 1, 1971 and December 31, 2001 for WOA23N. Seasonal (Winter, Spring, Summer, Fall) O_2 climatologies were calculated using only data from the defined season (regardless of year). The seasons are defined in this atlas as follows. Winter is defined as the months of January, February, and March. Spring is defined as April, May, and June. Summer is defined as July, August, and September. Fall is defined as October, November, and December. Monthly climatologies were calculated using data only from the given month regardless of the day of the month in which the observation was made. All of the methods, quality control tests and their metrics, original archived data, documentation, and statistical and objectively analyzed fields are available at NCEI.

Relatively large volumes of oceanographic data have been acquired because of the fulfillment of several data management projects and increased open data sharing including:

a) the Intergovernmental Oceanographic Commission (IOC), International Oceanographic Data and Information Exchange (IODE) Global Oceanographic Data Archaeology and Rescue (GODAR) project (Levitus *et al.* 2005b);

b) the IOC IODE *World Ocean Database project* (WOD) managed at NOAA NCEI;

c) the IOC Global Temperature Salinity Profile project (GTSPP);

d) The Argo project (including BGC Argo)

e) Ship board and repeat hydrography including the World Ocean Circulation Experiment (WOCE), Climate and Ocean: Variability, Predictability and Change (CLIVAR), and the Global Ocean Ship-based Hydrographic Investigations Program (GO-SHIP data.

f) The NOAA NCEI-hosted World Data Service for Oceanography of the World Data System (WDS); formerly World Data Center for Oceanography, Silver Spring).

The observational data used in WOA23 have been quality-controlled and objectively analyzed in an internally consistent objective manner on a one-degree by one-degree latitude-longitude grid at 102 standard depths (0-5500 m depth). The objective analysis procedures are identical to those used in the WOA18. Slightly different procedures were followed in earlier WOA analyses (*e.g.* Levitus, 1982; World Ocean Atlas 1994 series [Levitus and Boyer, 1994a; Levitus and Boyer 1994b). The present analysis uses 102 depth levels for annual (0-5500 m depth) and 57 for seasonal and monthly fields (0-1500 m depth) as shown in Table 2. Below 1500m, resolving seasonal and monthly variations are difficult to resolve, particularly along coastal regions.

Objective analyses shown in this atlas are constrained by the nature of the available O_2 data (*i.e.* spatial and temporal data coverage resolution, data quality, variability), characteristics of the objective analysis techniques, and the grid size used. Some of these limitations and characteristics are discussed below.

Since the publication of the WOA18, substantial amounts of additional historical and modern O_2 data from both discreet bottle samples and sensors have become available from many scientists, projects, organizations, academia worldwide too many to list individually here. It is thanks to all of these data sources that WOA23 is possible. The WOD23 includes a total of ~2.3 Million O_2 profiles (~55.4 Million measurements at

standard depth levels) collected between January 1, 1965 and December 31, 2022 (Table 1a) from all of the WOD23 datasets (Table 1e). About 92% of the available profiles were collected on or after 1965 and 2022. The number of O_2 profiles (1965-2022) from OSD, CTD, and PFL (delayed-mode Argo/BGC-Argo) after quality control combined is ~1.0 Million (~27.4 Million observations at standard depth levels) as shown in Table 1b. Prior to 1965, there are approximately 117 thousand O_2 profiles (*i.e.* manual Winkler titration method in the OSD dataset of the WOD23) which were not used in the WOA18 and WOA23.

Even with the available O_2 data, we are still hampered in a number of ways by heterogenous 4-D O_2 data coverage and quality of the data. Because of the heterogeneous data coverage, we are forced to examine the annual cycle by compositing all quality-controlled data for the time period 1965 and 2022 for WOA23F and 1971-2000 for WOA23N. The overall precision in the O_2 data collected have significantly improved over time since 1965, and particularly after 1972 with the Geochemical Ocean Sections Study (GEOSECS) research cruises (1972-1978). In some geographic areas, quality control is made difficult by the limited number of O_2 observations collected in these areas. The measurement precision of the observations is often not reported, however. Data may exist in an area for only one season, thus precluding a representative annual analysis. In some areas there may be a reasonable spatial distribution of data points on which to base an analysis, but there may be only a few (perhaps only one) data values in each one-degree latitude-longitude grid.

We note that the WOA23 is a global mean O_2 climatology based on the WOD23 quality-controlled measurements collected between 1965 and 2022. The objectively analyzed mean fields cannot represent both the mean and variability. Similarly, it is unlikely that the WOA23 data can match the values and vertical gradients of any selected individual profile of *in situ* O_2 measurements collected at any time or location; particularly in areas subjected to relatively high-frequency variability. For illustration purposes, projected global ocean O_2 content change from models and observational studies indicate a linear decrease (deoxygenation) ranging between about 0.6 and 2% since the 1960s (*i.e.* Bopp *et al.* 2013; Bopp *et al.* 2002; Schmidtko *et al.* 2017; Oschlies *et al.* 2018; Stramma *et al.* 2008) Observational studies support basin-scale O_2 variability (Garcia *et al.* 1998; Garcia *et al.* 2005a; Garcia *et al.* 2005b). Thus, O_2 profiles collected several years apart in the same geographic location and depths may be subjected to different ocean temporal processes which cannot all be represented in a single mean value. We note that we also provide statistical mean and standard deviation fields.

This atlas is divided into sections. We begin by describing the data sources and their distribution (Section 2). Then we describe the general data quality and objective analysis processing procedures (Section 3), the results (Section 4), summary (Section 5), and future work (Section 6). WOA23 provides statistical fields of the quality-controlled observations used as well as differences between the statistical mean and the objectively analyzed mean value. Sections 4.4 and 4.5 provide an estimate of the mean difference between the statistical mean and the objective analyzed fields. This provides an estimate of how quantitatively close the mapping represents the observational mean fields.

Global horizontal maps for O_2, AOU, and O2S at individual depth levels for each composite time period are available on-line or at NOAA's National Centers for Environmental Information (NCEI, https://www.ncei.noaa.gov/). We also

provide a selection of meridional sections in each major ocean basin.

2 DATA SOURCES AND QUALITY CONTROL

The WOA23 fields are based on the WOD23 which is set to be released in the early 2024. The WOD23 will contain all *in situ* ocean profiles assembled and processed by the Ocean Climate Laboratory (OCL) team at NCEI through December 31, 2022. This includes all Argo and BGC Argo measurements made up to December 31, 2022, with quality control as of April 1, 2023. Additionally, the WOD23 will contain updated quality control flags based on the quality improvements made during the construction of the WOA23. These are discussed in Section 2 of this document. The WOD23 and WOA23 are reproducible from the original data archived at NOAA NCEI.

Data sources and quality control procedures are briefly described below in Sections 2.1 and 2.2, respectively. The quality control procedures used in preparation of these analyses are described by Garcia *et al.* (2024b). The calculation of the AOU and O2S parameters is described in Section 2.3

2.1. Data sources

Historical and recent oceanographic O_2 data used in this atlas were obtained from the NCEI/WDS-Oceanography long-term data archives and include all data gathered as a result of the IODE *Global Oceanographic Data Archeology and Rescue* (GODAR) and WOD activities. GODAR aims to increase the volume of historical oceanographic data available to climate change and other researchers by locating ocean profile and plankton data sets not yet in digital form, digitizing these data, and ensuring their submission to national data centers and the World Data Service of Oceanography of the World Data System. Table 1a show the number of available O_2 profiles before QC and Table 1b the number of profiles after QC used in WOA23.

Garcia *et al.* (2019b) indicated the need to add additional O_2 data sources to the WOA Climatologies. Figure 1a shows our current World Ocean Atlas O_2 roadmap for systematically developing higher quality and more representative global climatologies. The WOD23 includes O_2 data from several observing systems arranged as datasets (Table 1e). Prior to the WOA23, WOA O_2 climatologies used quality-controlled data from OSD (Ocean Station Data) Winkler chemical titrations (*e.g.* Carpenter 1965a; Carpenter 1965b; Culberson and Huang, 1987; Knapp *et al.* 1990; Dickson, 1994; Langdon 2010). The WOA23 O_2, AOU, and O2S is our first blended climatology in the WOA data product series. In the WOA23F, we blend quality-controlled O_2 measurements from OSD (Ocean Station Data, Winkler chemical methods for the period 1965-2022), CTD (O_2 sensors mounted on a Conductivity-Temperature-Depth rosette for the period 1987-2022); and PFL (Profiling Floats with O_2 sensors from Argo and BGC-Argo delayed-mode data for the period 2005-2022). For simplicity, we refer to the Argo and BGC Argo O_2 data simply as PFL (Table 1e). In future WOA O_2 climatologies, we plan to blend additional observations from O_2 sensors in GLD (Gliders), DRB (Moored Buoys), and UOR (Undulating Oceanographic Recorder), and SUR (Surface Underway) as shown in Figure 1a.

Blending O_2 measurements collected from diverse ocean O_2 observing systems and investigators worldwide significantly increases the temporal and spatial representativeness of the climatologies. It also increases the difficulty of aggregating and integrating measurements of potentially different science quality (*i.e.* reproducibility, precision, uncertainty). Thus, we do not assume that all of the measurements are of

similar science quality. The WOA23F is based on quality-controlled Winkler chemical titrations (*e.g.* Langdon 2010) in the OSD dataset as well as sensor-based O_2 data in the CTD and PFL datasets available in the WOD23 collected on or after January 1, 1965 and December 31, 2022. The WOA23N uses quality-controlled OSD and CTD O_2 data in the WOD23 collected on or after January 1971 and December 31, 2000. Estimating the uncertainty of each O_2 measurement collected over time is not in the scope of this work.

The WOA23 O_2, AOU, and O2S fields were developed in several stages using data that passed all of our quality control steps. First, we calculated new statistical mean fields and an objectively analyzed climatology using Winkler data only (OSD). We consider the Winkler data to probably be the most reliable and higher data quality O_2 data. We compared all CTD O_2 profiles against those in the OSD dataset as well as to the statistical mean fields and flagged questionable data from further use in the WOA23. We assume that most of the CTD sensor-based O_2 data collected on or after 1987 including the WOCE and GO-SHIP eras were calibrated against Winkler data (Uchida *et al.* 2010). Nevertheless, we found several instances where the CTD O_2 profiles include questionable data, flagged, and not used further in the WOA23 analysis. We then blended in the quality-controlled OSD and CTD observational data and created new statistical and objectively analyzed fields. In a third stage, we then compared the PFL data (delayed-mode Argo and BGC-Argo) against the blended OSD and CTD climatology. We flagged PFL observations and/or profiles that did not pass this third quality control stage. Finally, we merged together the quality-controlled OSD, CTD, and PFL data and estimated new statistical and objectively analyzed fields. The fields were examined to identify the need for additional quality control. The data processing is described in more detail in Section.3.

The WOA23F provides the most comprehensive and representative observation-based O_2 global climatology to date (1965-2022). Figure 1b shows the spatial distribution of O_2 profiles available in in the WOD23 in 5-years bins from 1965 to 2022. The coverage is not uniform. The distribution illustrates the predominance of discreet data in the OSD prior to 1989 and the emergence of sensor-based data collected afterwards.

As the WOD ingests more oceanographic O_2 data, we plan to systematically add observations collected by a larger set of observing instruments and platforms to update future WOA O_2 products (Figure 1a). Figure 1c shows the number of OSD, CTD, and PFL O_2 profiles as a function of year of sampling and analysis. The majority of the historical OSD and CTD observations were collected in the northern hemisphere.

The OSD chemical data follow various modifications of the classical "Winkler titration method" using visual, amperometric, photometric end-detection methods (*e.g.* Carpenter 1965a; Carpenter 1965b; Langdon 2010; Culberson and Huang, 1987; Knapp *et al.* 1990; Dickson, 1994; Emerson *et al.* 1999, Helm *et al.* 2018). High quality historical and modern Winkler-based O_2 data have a nominal field measurement precision in the range of 0.5-1 $\mu mol \cdot kg^{-1}$ (Saunders, 1986; Langdon, 2010). Estimates of field data precision are often based on duplicate measurements and data inter-comparisons. By measurement precision we mean how quantitatively close are two or more measurements to each other. At present, there is no ocean community adopted use of O_2 chemical Certified Reference Material (CRM) or broad use of certified minimum analytical grade reagents such for KIO_3 standards for Winkler titrations. Thus, all of

the chemical (Winkler) O_2 data in the instrumental record may not necessarily be all of comparable analytical measuring science quality. In the absence of a "true value" or a community adopted reference O_2 value (*e.g.* CRM), it is difficult to estimate the accuracy of individual measurements. By data accuracy, we mean how quantitatively close in content are measurements to a "true value" or an accepted reference value. Emerson *et al.* (1999) indicated an accuracy of ±0.1% for Winkler-based O_2 measurement using KIO_3 standards corrected for impurities. This estimate is consistent with the Winkler titration ±0.1% accuracy estimated by Carpenter (1965b). In practice, it is difficult to identify which Winkler-based O_2 observations used reagent-grade and reagents corrected for impurities.

Because the number of O_2 measurements made by profiling floats in open ocean waters have now surpassed the number of O_2 Winkler titrations and CTD O_2 sensors (Figure 1c), we have chosen to carefully blend selected quality-controlled O_2 data obtained by chemical Winkler titration methods (OSD) and electronic sensors from CTD and Argo (mostly BGC-Argo) in the WOD23 to developed the WOA23F. The WOA23N blends O_2 data obtained by chemical Winkler titration methods (OSD) and electronic sensors from CTDs only.

The sensor-based O_2 measurements use a variety of electrochemical, polarographic, and optical instruments generally mounted on the Conductivity-Temperature-Depth (CTD) rosette frame, Argo and BGC-Argo profiling floats, gliders, buoys, and other observing systems (Figure 1a-c). Oxygen sensors are often calibrated using Winkler measurements.

The reproducibility or precision of sensor-based oxygen measurements in Argo/BGC-Argo floats are approximately in the range of 2-5 $\mu mol \cdot kg^{-1}$ (Grégoire *et al.* 2021; Maurer *et al.* 2021; GOOS EOV-Oxygen, 2017). The O_2 sensors mounted on profiler floats are calibrated using different methods. Sarmiento *et al.* (2023) indicated a mean difference of 0.64 ± 7.22 $\mu mol \cdot kg^{-1}$ between Southern Ocean Carbon and Climate Observations and Modeling project (SOCCOM) float BGC-Argo and ship-board O_2 samples collected near the time of the float deployment and an uncertainty of 3 $\mu mol \cdot kg^{-1}$. Mignot *et al.* (2019) indicated a mean depth offset of 2.9 ± 5.5 $\mu mol \cdot kg^{-1}$ and a root-mean-squared error (RMSE) of 5.1 ± 0.8 $\mu mol \cdot kg^{-1}$ for BGC-Argo O_2 data collected between 2013 and 2017 in the Mediterranean Sea. Bushinsky *et al.* (2016) estimated a drift rate of about -0.5%·$year^{-1}$. The deviations suggest the need to identify instrumentation and other potential issues. Some of the BGC-Argo profilers equipped with O_2 optodes (i.e., optical oxygen sensors) use an air calibration method (Nicholson and Feen, 2017).

While the precision of sensor based O_2 measurements have improved over the years (Bittig and Kortzinger, 2015; Johnson *et al.* 2015; Bushinsky *et al.* 2016; Bittig *et al.* 2018; Mignot *et al.* 2019), some of the oxygen sensor data on CTDs and Argo and BGC-Argo profilers underestimate the O_2 content when compared to historical Winkler measurements collected in the approximate same location below about 1000 m.

We found it necessary to conduct an in-depth data quality control on the CTD and PFL sensor-based O_2 data before the data could be blended with the quality-controlled Winkler data. This is discussed in Section 2.2. We conducted profile matchup comparisons to help quantify depth offset bias between the different sensor-based O_2 measurements and Winkler chemical O_2 observations. The goal was to develop an internally consistent climatology using quality-controlled O_2 measurements obtained by both chemical and

sensor-based methods.

Upon further data quality inspection, we selected O_2 data obtained by chemical Winkler titration (1965-2022), CTD (1987-2022), and PFL (Argo and BGC-Argo, 2005-2022) for developing the WOA23F and WOA23N (Table 1a,b). Although the WOD23 includes O_2 data obtained by CTD sensors as early as in 1971, we only used data collected on or after January 1, 1987 when we generally found the quality of the data to be of better quality. We found the PFL O_2 data of better quality on or after January 1, 2010. A similar data selection criterion was used for WOA23N for Winkler (1965-2001) and CTD (1971-2001) data. In Section 4.5, we estimate the mean difference between the statistical mean of the observations and the objectively analyzed O_2, AOU, and O2S fields

Dissolved oxygen solubility is non-linearly dependent on temperature and to a lesser extent on salinity and hydrostatic pressure (Garcia and Gordon, 1992). The AOU content ($\mu mol \cdot kg^{-1}$) and O2S (percent, %) parameters were calculated only when *in situ* O_2, temperature and salinity were also measured at the same geographic location, time, and depth. As a result, there are locations with O_2 measurements without simultaneous temperature and/or salinity measurements or because their data quality was deemed questionable during quality control. Further details about the calculation of dissolved oxygen solubility are provided in Section 2.3.

To understand the procedures for taking individual oceanographic observations and constructing climatological fields, definitions of the terms "standard depth level data" and "observed depth level data" are necessary. We refer to the actual measured value of an oceanographic variable *in situ* (Latin for "in place") as an "observation", and to the depth at which such a measurement was made as the "observed level depth". We refer to such data as "observed level data". Garcia *et al.* (2024b) provides technical details about the data and metadata in the WOD23.

Before the development of oceanographic instrumentation able to measure at relatively high frequencies in the water column, oceanographers often attempted to make measurements at selected "standard levels" in the water column. Sverdrup *et al.* (1942) presented the suggestions of the International Association of Physical Oceanography (IAPSO) as to which depths oceanographic measurements should be made or interpolated to for analysis.

Historically the World Ocean Atlas used a modified version of the IAPSO standard depths. However, with the increased global coverage of high depth resolution instrumentation, such as profiling floats, WOA has extended the standard depth levels from 33 to 102. The standard depth levels include the original depth levels presented up to WOA09, but have tripled the resolution in the upper 100 meters, more than doubled the depth resolution of the upper 1000 meters, and almost three and a half times the resolution for overall depth levels. For many purposes, including preparation of the present climatologies, observed level data are interpolated to 102 standard depth levels if observations did not occur at the desired standard depths (see Section 3.1 for details). The levels at which the O_2, AOU, and O2S climatologies were calculated are given in Table 2. Table 3 shows the depths of each standard depth level. Section 3.1 discusses the vertical interpolation procedures used in our work.

The O_2 data have been collected at great public monetary expense and effort over many years. It is difficult to put a monetary value to the global ocean O_2 instrumental data record.

2.2. Data quality control

Performing quality control (QC) on the historical O_2 data is a major task. By QC, we mean that the O_2 observations used to estimate the WOA23 statistical mean used in the objective analysis are of approximately internally consistent science quality. In this way, we also help ensure a consistent quality assurance process at all steps of the QC.

The main difficulty is related to lack of data of known science quality and lack of greater 4-D data coverage (at least in some areas) upon which to base our objective statistical checks. Winkler measurements collected in the 1960's are potentially of lower precision than more recent observations. Because the science quality of the measurements is not always known *a priory*, we are forced to use a uniform QC process irrespective of the year of data collection. Consequently, certain empirical criteria were applied (see Section 2), and as part of the last processing step, subjective judgment was used. Individual measurements, and in some cases entire profiles or all profiles for individual research cruises, have been flagged (not eliminated) and not used further in the analysis because these data produced ocean features that were judged to be non-representative or questionable. For comparison, Table 1a and Table 1b illustrates the number of profiles and observations before and after QC. Table 1b shows that after QC, about 20% of all available O_2 profiles were flagged and not used in the WOA23. The data are all available in the WOD23. Below about 2 km depth, the global ocean is largely under sampled. The Atlantic and the Arctic are the most and least sampled basins, respectively.

As part of our work, we have made available the WOD23 which contains both observed levels profile data and standard depth level profile data with various QC flags applied. The flags mark individual measurements or entire profiles which were not used in the next step of the procedure, either interpolation to standard depth levels for observed level data or calculation of statistical means in the case of standard depth level data.

Our knowledge of the variability of the world ocean now includes a greater appreciation and understanding of the ubiquity of ocean eddies, rings, and lenses in some parts of the world ocean as well as sub-seasonal, interannual, interdecadal variability associated with modal variability of the atmosphere such as the North Atlantic Oscillation, Pacific Decadal Oscillation (PDO), and El Niño Southern Ocean Oscillation (ENSO). Therefore, we have simply flagged data, not eliminating them from the WOD23. We note that the WOD23 preserves the QC flags by the data provider if available. Thus, individual investigators can make their own decision regarding the quality and representativeness of the O_2 data. Investigators studying the distribution of features such as eddies will be interested in those data flagged that we may regard as unrepresentative or questionable for the preparation of the analyses shown in this atlas.

2.2.1. Duplicate data flagging

Because O_2 data are received from many sources, sometimes the same data set is received at NCEI/WDS-Oceanography more than once but with slightly different time and/or position and/or data values, and hence are not easily identified as duplicate stations. Therefore, to eliminate the repetitive O_2 data values our databases were checked for the presence of exact and near exact replicates using eight different criteria. The first checks involve identifying stations with exact position/date/time and data values; the next checks involve offsets in position/date/time. Profiles identified as duplicates in the checks with a large offset were individually verified to ensure they were indeed duplicate profiles.

All replicate profiles were flagged and not used in our processing

2.2.2. Data range and gradient checks

Range checking (*i.e.* checking whether an O_2 value is within preset minimum and maximum values as a function of depth and ocean region) was performed on all O_2 values as a first QC check to flag from further use values that were grossly outside expected oceanic ranges. Range checks were prepared for individual regions of the world ocean (Garcia *et al.* 2024b).

A check as to whether excessive vertical gradients occur in the data as a function of depth has been performed for O_2 data in the WOD23 both in terms of positive and negative content vertical (depth) gradients. We flagged and not used values that exceeded these gradients.

2.2.3. Statistical checks

Statistical checks were performed as follows. All data for O_2 (irrespective of year of collection in the 1965-2022 time period), at each standard depth level, were averaged within five-degree latitude-longitude squares to produce a record of the number of observations, mean, and standard deviation in each square. Statistics were computed for the annual, seasonal, and monthly compositing periods. Below 50 m depth, if data were more than three standard deviations from the mean, the data were flagged and withheld from further use in objective analyses (OA for short). Above 50 m depth, a five-standard-deviation criterion was used in five-degree squares that contained any land area. In selected five-degree squares that are close to land areas, a four-standard-deviation check was used. In all other squares a three-standard-deviation criterion was used for the 0-50 m depth layer. For standard depth levels situated directly above the bottom, a four-standard-deviation criterion was used. We realize that the O_2 data in some geographic regions show departures from being approximately normal. While we considered using statistical test less independent of the data distribution, we opted to use a simpler approach which is consistent across the WOA23 products and previous WOA versions.

The reason for the weaker standard deviation criterion in coastal and near-coastal regions is the exceptionally large range of values in the coastal five-degree square statistics for O_2. Frequency distributions of O_2 values in some coastal regions are observed to be skewed or bimodal. Thus, to avoid flagging possibly good data in environments expected to have large variability, the standard deviation criteria were broadened.

The total number of measurements in each profile, as well as the total number of O_2 observations exceeding the standard deviation criterion, were recorded. If more than two observations in a profile were found to exceed the standard deviation criterion, then the entire profile was flagged. This check was imposed after tests indicated that surface data from particular casts (which upon inspection appeared to be questionable) were being flagged but deeper data were not. Other situations were found where questionable data from the deeper portion of a cast were flagged, while near-surface data from the same cast were not flagged because of larger natural variability in surface layers. One reason for this was the decrease of the number of observations with depth and the resulting change in sample statistics. The standard-deviation check was applied twice to the O_2 data set for each compositing period.

In summary, first the five-degree square statistics were computed, and the data flagging procedure described above was used to provide a preliminary data set. Next, new five-degree-square statistics were computed from this preliminary data set and used with

the same statistical check to produce a new, "clean" data set. The reason for applying the statistical check twice was to flag (and withhold from further use), in the first round, any grossly erroneous or non-representative data from the data set that would artificially increase the variances. The second check is then relatively more effective in identifying smaller, but questionable or non-representative, O_2 observations.

2.2.4. Subjective quality control flagging of data

The O_2 data were averaged by one-degree squares for input to the OA program. After initial OA were computed, the input set of one-degree means still contained questionable data contributing to unrealistic distributions, yielding intense bull's-eyes or spatial gradients. Examination of these features indicated that some of them were due to profiles from particular oceanographic cruises. In such cases, data from an entire cruise were flagged and withheld from further use by setting a flag on each profile from the cruise. In other cases, we flagged individual profiles and/or measurements causing such features. It is possible that some of the data and profiles flagged as questionable correspond to real sub meso-scale ocean features such as ocean eddies.

We recognize that our statistical flagging of standard level data assumes that the data within each 5-degree box are approximately normally distributed. This assumption fails in certain regions of the ocean. Therefore, we are currently investigating alternative methods for QC flagging. These include alternative statistical tests that do not require Gaussian distributions and leveraging machine learning to better cluster the data before applying statistical checks. Because not all O_2 data in the WOD23 includes temperature and salinity for calculating density or were already expressed in $\mu mol \cdot kg^{-1}$ units, we are unable to conduct the analysis on isopycnal surfaces without excluding a significant portion of the available historical data.

There are still certain regions of the global ocean that are severely under sampled (*e.g.* Arctic Ocean, South East Pacific, Indian Ocean, marginal seas) and thus large uncertainties continue to remain in the climatologies for these regions. The WOA23 provides standard error of the analysis fields.

2.2.5. Representativeness of the data

Another QC issue is the global O_2 data spatial and temporal coverage (representativeness). The general paucity of data forces the compositing of all historical data to produce "climatological" fields. In a given one-degree square, there may be data from a month or season of one particular year, while in the same or a nearby square there may be data from an entirely different year. If there is large interannual variability in a region where scattered sampling in time has occurred, then one can expect the analysis to reflect this. Because the observations are scattered randomly with respect to time, except for a few limited areas, the results cannot, in a strict sense, be considered a true long-term climatological average.

We present smoothed analyses of historical means, based (in certain areas) on relatively few observations. We believe, however, that useful information about the oceans can be gained through our procedures and that the large-scale features are representative of the real ocean. We believe that, if a hypothetical global synoptic set of oceanographic O_2 data existed and one were to smooth these data to the same degree as we have smoothed the historical means overall, the large-scale features would be similar to our results. Some differences would certainly occur because of interannual-to-decadal-scale variability.

The volume of O_2 observations diminish with increasing depth. In the upper ocean, the all-data O_2 annual and seasonal mean distributions are quite reasonable for defining large-scale features, but for the monthly periods, the database is inadequate in some regions. With respect to the deep ocean, in some areas the distribution of observations may be adequate for some diagnostic computations but inadequate for other fit for purpose applications. If an isolated deep basin or some region of the deep ocean has only one observation, then no horizontal gradient computations can be meaningful or representative. However, useful information is provided by the observations in the computation of other quantities (*e.g.* a volumetric mean or inventory over a major ocean basin).

2.2.6 Ocean warming O_2 solubility adjustment

Due to observed ocean warming (global ocean heat content, Levitus 2000; Levitus 2005a, Levitus *et al.* 2012, Boyer *et al.* 2016) over the last decades, the O_2 solubility in the ocean is expected to have slightly decreased overtime. Since the WOD23 contains O_2 data collected in different years (1965-2022), a O_2 solubility adjustment helps make the measurements comparable from year to year and depth with respect to ocean warming trends. In other words, newer O_2 observations in time were measured at a relatively higher *in situ* temperature than older observations at the same depth and location. While some ocean areas and depths may have different warming trends, we opted to use a global mean O_2 solubility adjustment rate $[\mu mol/(kg \times year)]$ to all locations as a function of depth and year. Because of the larger 4-D data coverage, volume of observations, and sampling frequency of observations, it is expected that the more recent Argo and BGC Argo O_2 data would slightly offset the representativeness of the WOA23F climatology towards waters which were nominally warmer (lower O_2 solubility) than older measurements collected in waters which were slightly colder (higher O_2 solubility).

At the sea surface, the temperature warming increase is ~0.11 decade^{-1} and at 1000 m depth is ~0.02 decade^{-1} (Figure 1d). In other words, the mean warming between 1965 and 2022 (57 years) is approximately 0.63

Thus, the gas solubility adjustment to the O_2 observations makes it possible to have a more representative mean climatology minimizing the impact of ocean warming on solubility in different years and depths.

Based on the temperature increase from 1965 to 2022 at each standard depth (Figure 1d), we calculated O_2 solubility adjustments as a function of year and depth (Table 13). Using these rates, we adjusted all of the oxygen measurements to a common year baseline of 1985 (the middle of 1971-2000 climate normal, WOA23N). Thus, the net O_2 solubility adjustment is slightly negative before 1985, 0 in 1985, and slightly positive after 1985.

Figure 1d shows the global mean temperature (°C) increase and calculated oxygen solubility content ($\mu mol \cdot kg^{-1}$) decrease between 1965 and 2020 at a constant salinity of 35.0. The linear O_2 solubility adjustment rate was applied to all of the *in situ* O_2 measurements used in the WOA23F and WOA23N as a function of time and depth. The adjustment is largest at or near the sea surface and decreases with depth. Table 13 shows the solubility adjustment rates in tabular form. The adjustment rate is larger at sea surface (about -0.05 $\mu mol \cdot kg^{-1} \cdot year^{-1}$) and smaller at 1500 m depth (about -0.01 $\mu mol \cdot kg^{-1} \cdot year^{-1}$). For illustration purposes, the 1965-2022 mean O_2 solubility adjustment in 57 years is ~ 2.9 $\mu mol \cdot kg^{-1}$ at the surface and ~ 0.6 $\mu mol \cdot kg^{-1}$ at 1500 m depth (salinity = 35). Similarly, the 1971-2000 solubility

adjustment in 30 years is approximately 1.5 $\mu mol \cdot kg^{-1}$ at the surface and 0.3 at 1500 m depth.

In summary, the purpose of the O_2 solubility adjustment is to develop a representative mean O_2 climatology which is unbiased with respect to the observations collected in any time period and warming trends. The solubility adjustments as a function of year and depth are applied to all of the oxygen observations used in the WOA23.

It is difficult to quantify the attribution and impact of different factors to ocean deoxygenation. The impact of ocean warming on solubility accounts for a significant fraction of the global ocean deoxygenation; particularly in the upper water column. A hypothetical example may help illustrate this point. Schuckmann *et al.* (2020) indicated a gain in the Earth Energy Imbalance (EEI) of 358 ± 37 zettajoules (ZJ = 1 x 10^{21} Joules) with about 89% (~319 zettajoules) being gained by the oceans (Ocean Heat Content, OHC) for the 1971-2018 time period. More recently, Schuckmann *et al.* (2023) indicated a higher earth-system accumulated EEI of 381 ± 61 ZJ for the 1971 to 2020 time period. The majority (about 89%) of the EEI is stored in the ocean. If the oceans absorbed 89% of this cumulative EEI, the OHC would then be approximately 339 ZJ over the same time period. This OHC is comparable to other assessments (*e.g.* NOAA NCEI global ocean heat content). We note that the increase in cumulative OHC is relatively small prior to 1970 (See Figure 8 in Schuckmann *et al.* 2023). This suggests that the majority of the upper global ocean deoxygenation due to decreases in O_2 solubility because of ocean warming are expected to larger after approximately the year 1975 and largest on or after 2020. For comparison, Intergovernmental Panel on Climate Change (IPCC) Sixth Assessment Report (AR6) model simulations indicate a larger cumulative OHC of ~435 ZJ for the 1971-2018 time period (Foster *et al.* 2021).

What would be the approximate change in the O_2 solubility content due to ocean warming since the 1970s (*i.e.* OHC gain)? For illustration purposes, suppose that the 1971-2020 OHC (~339 ZJ) is homogeneously distributed in the upper 2 km of the ocean. The mean temperature gain would approximately be ~0.14 °C; or about ~0.03 $°C \cdot decade^{-1}$ (assuming a seawater density of 1025 $kg \cdot m^{-3}$, seawater heat capacity of 3850 $J \cdot °C^{-1} \cdot kg^{-1}$, and a 0-2 km ocean volume of ~0.638 x 10^{18} m^3). Suppose that the only factor that affects the O_2 content of a parcel of water is its gas solubility. The estimated decrease in O_2 solubility between 1971 and 2020 due to an increase of ~0.14 °C in ocean warming depends on the starting and ending temperature of the water at constant salinity. For example, suppose that a parcel of water at the surface instantaneously warms by 0.14 °C at constant salinity of 35 from -1.00 to -0.86 °C, the resulting O_2 solubility decrease is about 1.30 $\mu mol \cdot kg^{-1}$ (*i.e.* solubility decrease from ~357.12 to 355.82 = 1.30 $\mu mol \cdot kg^{-1}$). Assuming that the ocean warming occurs over 47 years, the corresponding O_2 solubility content decrease trend is small, about 0.28 $\mu mol/(kg \times decade)$. For comparison, Schmidtko *et al.* (2017) indicated a deoxygenation rate of about 0.26 $Pmol \cdot decade^{-1}$ for the 0-1200 m layer. If 0.26 $Pmol \cdot decade^{-1}$ is hypothetically homogeneously distributed in the 0-1200 m depth layer (~0.389 × 10^{18} m^3) of the global ocean, then the O_2 content decrease after 47 years is approximately -3.07 $\mu mol \cdot kg^{-1}$ at a constant seawater density of 1025 $kg \cdot m^{-3}$. This suggests that the estimated O_2 solubility decrease after 47 years (-1.3 $\mu mol \cdot kg^{-1}$) could potentially account for as much as 47% of the deoxygenation change (-3.07 $\mu mol \cdot kg^{-1}$). While these are simple hypothetical examples, they serve to

illustrate that ocean deoxygenation is driven by a complex combination of physical and biogeochemical forcing mechanisms in addition to solubility decreases due to ocean warming.

We emphasize that the observational O_2 data in the WOD23 are not altered or modified in anyway. The adjustments are applied to the data for the purpose of calculating internally consistent statistical mean values. The data user can discover and access from the WOD23 the original O_2 data in a uniform format and units along with QC flags if provided by the data provider and/or those added during WOA23 data QC. The will also find access to the original data used in the NCEI long-term data archive.

2.2.7 Inclusion of PFL (Argo and BGC-Argo) O_2 data

The WOD23 contains about 240,287 PFL (Argo and BGC-Argo) O_2 profiles. Most of these were taken post-2010. The PFL data have become the largest continuous ocean O_2 observing system after the year 2010 (Figure 1b). The number of PFL observations have surpassed those analyzed with the Winkler method and CTD sensors. Most of the PFL data used in this study were collected on or after 2010.

PFL (*i.e.* Argo and BGC-Argo floats) O_2 data within the WOD23 are grouped into real-time, real-time adjusted, and delayed-mode. The delayed-mode data are the highest quality and are nominally available 12-18 months after the real-time measurements were collected (Thierry *et al.* 2021). If the delayed-mode O_2 data were adjusted (even if the adjustment was 0.0), this is documented in the WOD23. In the WOA23F, we use only delayed-mode PFL O_2 observations (Argo, BGC-Argo, and deep Argo).

Some delayed-mode PFL O_2 measurements may show depth offsets that may be due to sensor drifting and other instrumental factors. The Argo community evaluates the Argo O_2 casts, and in many cases correct them with an adjustment (Thierry *et al.* 2016; Thierry *et al.* 2021). Since an oxygen content bias may exist in some of the real-time adjusted data, we have decided to only use delayed-mode Argo dissolved oxygen data in the WOA23F. The real-time, real-time adjusted, and delayed-mode oxygen data are all available in the WOD23 if users would like to use them in their analysis. Since the release of the WOD23, the WOD Team continues to add data from available observing systems including Argo/BGC-Argo. All of the new and updated data added to the WOD are made available online on a quarterly basis.

2.2.8 Matchup comparison between CTD and OSD O_2 datasets

The WOD23 oxygen observations obtained by chemical Winkler titration methods are generally considered of higher science quality than sensor-based data. The sensor-based data from CTD and Argo are often compared to or calibrated using Winkler data. Only OSD and CTD data that passed all the QC checks are used in the matchup comparison. We conducted a matchup between OSD and CTD casts. Each CTD cast were searched for matched OSD casts(s) measured within the same month with the search criteria of 1° square and 5 years apart. If matched OSD casts are found, the average difference between OSD and CTD stations will be calculated for a selected depth range with minimum temperature and salinity variations following Wong *et al.* (2023). This method is used to minimize the effects of spatial and temporal variabilities of the water masses by using isotherms with relatively uniform temperature/salinity.

The statistical histogram of $\Delta O_{CTD\text{-}OSD}$ provides a measure of the overall mean difference (Figure 1e). The mean and median of the distribution of $\Delta O_{CTD\text{-}OSD}$ are all very

small (mean, -0.27 μmol·kg^{-1} and median, -0.08 μmol·kg^{-1}). This suggests that the CTD oxygen data selected in this comparison agree relatively well with nearby reference OSD (Winkler) oxygen data. We note that some individual CTD O_2 profiles and even some research cruises have large depth offset differences compared to reference OSD stations. We examined CTD oxygen data cruise by cruise to identify data with obvious deviations and exclude from the oxygen climatology calculation.

2.2.9 Matchup comparison between PFL (Argo and BGC-Argo) and OSD/CTD data

A similar matchup comparison is conducted between PFL oxygen stations with an adjustment (delayed-mode or real-time adjusted, including 0.0 adjustment) and OSD/CTD stations. Only OSD/CTD oxygen data that passed all the QC checks from WOCE, CLIVAR and CLIVAR and Carbon Hydrographic Data Office (CCHDO) are used in this comparison. The statistical histogram (Figure 1f) of $\Delta O_{PFL\text{-}OSD/CTD}$ shows a negative difference between PFL adjusted stations and reference OSD/CTD stations even with the application of the Argo/BGC-Argo O_2 adjustments of -1.338 μmol·kg^{-1}. The PFL data are on average slightly lower than OSD/CTD matching pairs. We applied this adjustment to all delayed-mode Argo/BGC-Argo used in the analysis. We note that this is a global mean adjustment that may not reduce then differences between individual PFL and OSD/CTD profiles.

The magnitude of the adjustment is dependent on the available observational data used for comparison, which will likely change overtime as more floats and better calibrated sensors become available. We note that the quality of the measurements might not necessarily remain constant after deployment during the sampling life-time of each float (*i.e.* sensor drift and sensor-response time).

2.3 Calculation of AOU and O2S

The Apparent Oxygen Utilization (AOU, μmol·kg^{-1}) and percent dissolved oxygen saturation (O2S, %) parameters were calculated from the WOD23 when quality-controlled *in situ* dissolved oxygen (O_2, μmol·kg^{-1}), temperature (T, °C), and salinity (S, unitless) were all concurrently measured at the same location, time, and depth.

We note that there is a large number of O_2 observations in the WOD23 that do not include concurrent temperature and salinity measurements. In some cases, the temperature and/or salinity values were present and did not pass our quality-control tests or one or both values were unavailable. Thus, the total number of temperatures, salinity, and O_2 observations available for calculating AOU and O2S is smaller than the available number of O_2 observations.

The AOU parameter represents a rough estimate of the O_2 utilized due to biogeochemical sinks relative to a surface or near surface preformed value saturated with the atmosphere. As discussed below, AOU cannot be taken to represent the True Oxygen Utilization (TOU); hence the use of the word "Apparent". The AOU (μmol·kg^{-1}) was calculated as the difference between the O_2 solubility and the measured O_2 content,

$$AOU = P_a[O_2^*] - [O_2]$$

Where O_2^* is dissolved oxygen solubility content (μmol·kg^{-1}) calculated as a function of *in situ* temperature and salinity (Garcia and Gordon, 1992), and P_a is the atmospheric pressure correction factor. The atmospheric pressure correction P_a factor is 1.0 at 1.0 atmosphere of total pressure (Benson and Krause, 1984). We have used an atmospheric pressure correction P_a of 1.0. Thus, O2S in this atlas is calculated as a function of *in situ*

temperature and salinity assuming equilibrium with an atmosphere of standard composition saturated with water vapor at one atmosphere of total pressure.

The calculation of AOU assumes that the amount of O_2 used during local biochemical processes can be estimated by the difference in content between the observed O_2 and the preformed O_2 values taken as the solubility. AOU is affected by processes other than biochemical processes such as water mixing of waters of different preformed values, departures of O2S from full equilibration with the atmosphere, bubble gas injection, skin temperature effects, and other factors (*e.g.* Broecker and Peng, 1982; Redfield *et al.* 1963; Garcia and Keeling, 2001; Ito, 2004). We assume that these natural processes balance out in the long-term.

The O_2 saturation (O2S, %) was estimated as:

$$\text{O2S (\%)} = 100 \left(\frac{[O_2]}{P_a[\, O_2^*]} \right)$$

The calculated AOU and O_2 solubility values were analyzed following the same QC methods outlined in Section 1.2. Furthermore, if any of the O_2, temperature or salinity values were flagged during the QC procedure, then AOU and O_2 solubility values were not used in the analysis.

3. DATA PROCESSING PROCEDURES

3.1. Vertical interpolation to 102 standard depth levels (0-5500 m)

Vertical interpolation of observed depth level data to standard depth levels followed procedures in Joint Panel on Oceanographic Tables and Standards Editorial Panel (JPOTS, 1991). These procedures are in part based on the work of Reiniger and Ross (1968). Four observed depth level values surrounding the standard depth level value were used, two values from above the standard level and two values from below the standard level. The pair of values furthest from the standard level is termed "exterior" points and the pair of values closest to the standard level are termed "interior" points. Paired parabolas were generated via Lagrangian interpolation. A reference curve was fitted to the four data points and used to define unacceptable interpolations caused by "overshooting" in the interpolation. When there were too few data points above or below the standard level to apply the Reiniger and Ross technique, we used a three-point Lagrangian interpolation. If three points were not available (either two above and one below or vice-versa), we used linear interpolation. In the event that an observation occurred exactly at the depth of a standard level, then a direct substitution was made. Table 3 provides the range of acceptable distances for which observed level data could be used for interpolation to a standard level.

Starting with the World Ocean Atlas 2013 (WOA13), the number of standard depth levels were increased from 33 to 102, allowing for greater vertical resolution (0-5500 m depth). The WOA18 and WOA23 also use 102 standard depth levels. The method for interpolating data to standard levels remains the same as in previous analysis.

3.2. Methods of analysis

3.2.1. Overview

An objective analysis (OA) scheme of the type described by Barnes (1964) was used to produce the fields shown in this atlas. This scheme had its origins in the work of Cressman (1959). In the World Ocean Atlas 1994 (WOA94), the Barnes (1973) scheme was used. This required only one "correction" to the first-guess field at each grid point in comparison to the successive correction method of Cressman (1959) and Barnes (1964). This was to minimize

computing time used in the processing. Barnes (1964) recommends a return to a multi-pass analysis when computing time is not an issue. Based on our own experience we agree with this assessment. The single pass analysis, used in the WOA94, caused an artificial front in the Southeastern Pacific Ocean in a data sparse area (Anne Marie Treguier, personal communication). The analysis scheme used in generating the WOA98, WOA01, WOA05, WOA13, WOA18, and WOA23 analyses uses a three-pass "correction" which does not result in the creation of this artificial front. The WOA23 uses the same data analysis process as used in the WOA18.

Inputs to the analysis scheme were one-degree square means of data values at standard levels (for time period and variable being analyzed), and a first-guess value for each square. For instance, one-degree square means for our annual analysis were computed using all available data regardless of date of observation. For July, we used all historical July data regardless of year of observation.

Analysis was the same for all standard depth levels. Each one-degree latitude-longitude square value was defined as being representative of its square. The 360×180 grid points are located at the intersection of half-degree lines of latitude and longitude. An influence radius was then specified. At those grid points where there was an observed mean value, the difference between the mean and the first-guess field was computed. Next, a correction to the first-guess value at all grid points was computed as a distance-weighted mean of all grid point difference values that lie within the area around the grid point defined by the influence radius. Mathematically, the correction factor derived by Barnes (1964) is given by Equation 1:

$$C_{i,j} = \frac{\sum_{s=1}^{n} W_s Q_s}{\sum_{s=1}^{n} W_s} \qquad (1)$$

in which:

(i,j) - coordinates of a grid point in the east-west and north-south directions respectively;

$C_{i,j}$ - the correction factor at grid point coordinates (i,j);

n - the number of observations that fall within the area around the point i,j defined by the influence radius;

Q_s - the difference between the observed mean and the first-guess at the S^{th} point in the influence area;

$W_s = e^{-\frac{Er^2}{R^2}}$ (for $r \le R$; $W_s = 0$ for $r > R$);

r - distance of the observation from the grid point;

R - influence radius;

$E = 4$.

The derivation of the weight function, W_s, will be presented in the following section. At each grid point we computed an analyzed value $G_{i,j}$ as the sum of the first-guess, $F_{i,j}$, and the correction $C_{i,j}$. The expression for this is

$$G_{i,j} = F_{i,j} + C_{i,j} \qquad (2)$$

If there were no data points within the area defined by the influence radius, then the correction was zero, the first-guess field was left unchanged, and the analyzed value was simply the first-guess value. This correction procedure was applied at all grid points to produce an analyzed field. The resulting field was first smoothed with a median filter (Tukey, 1974; Rabiner *et al.* 1975) and then smoothed with a five-point smoother of the

type described by Shuman (1957) (hereafter referred to as five-point Shuman smoother). The choice of first-guess fields is important and we discuss our procedures in Section 1.3.2.5.

The analysis scheme is set up so that the influence radius, and the number of five-point smoothing passes can be varied with each iteration. The strategy used is to begin the analysis with a large influence radius and decrease it with each iteration. This technique allows us to analyze progressively smaller scale phenomena with each iteration.

The analysis scheme is based on the work of several researchers analyzing meteorological data. Bergthorsson and Doos (1955) computed corrections to a first-guess field using various techniques: one assumed that the difference between a first-guess value and an analyzed value at a grid point was the same as the difference between an observation and a first-guess value at a nearby observing station. All the observed differences in an area surrounding the grid point were then averaged and added to the grid point first-guess value to produce an analyzed value. Cressman (1959) applied a distance-related weight function to each observation used in the correction in order to give more weight to observations that occur closest to the grid point. In addition, Cressman introduced the method of performing several iterations of the analysis scheme using the analysis produced in each iteration as the first-guess field for the next iteration. He also suggested starting the analysis with a relatively large influence radius and decreasing it with successive iterations so as to analyze smaller scale phenomena with each pass.

Sasaki (1960) introduced a weight function that was specifically related to the density of observations, and Barnes (1964, 1973) extended the work of Sasaki. The weight function of Barnes (1964) has been used here. The OA scheme we used is in common use by the mesoscale meteorological community. Several studies of OA techniques have been made. Achtemeier (1987) examined the "concept of varying influence radii for a successive corrections objective analysis scheme." Seaman (1983) compared the "objective analysis accuracies of statistical interpolation and successive correction schemes." Smith and Leslie (1984) performed an "error determination of a successive correction type objective analysis scheme." Smith *et al.* (1986) made "a comparison of errors in objectively analyzed fields for uniform and non-uniform station distribution."

3.2.2. Derivation of Barnes (1964) weight function

The principle upon which the Barnes (1964) weight function is derived is that "the two-dimensional distribution of an atmospheric variable can be represented by the summation of an infinite number of independent harmonic waves, that is, by a Fourier integral representation". If $f(x,y)$ is the variable, then in polar coordinates (r,θ), a smoothed or filtered function $g(x,y)$ can be defined:

$$g(x,y) = \frac{1}{2\pi} \int_0^{2\pi} \int_0^{\infty} \eta f(x + r\cos\theta, y + r\sin\theta) \, d\left(\frac{r^2}{4K}\right) d\theta \qquad (3)$$

in which r is the radial distance from a grid point whose coordinates are (x,y). The weight function is defined as

$$\eta = e^{-\frac{r^2}{4K}} \qquad (4)$$

which resembles the Gaussian distribution. The shape of the weight function is determined by the value of K, which relates

to the distribution of data. The determination of K follows. The weight function has the property that

$$\frac{1}{2\pi}\int_0^{2\pi}\int_0^{\infty}\eta d\left(\frac{r^2}{4K}\right)d\theta = 1 \qquad (5)$$

This property is desirable because in the continuous case (3) the application of the weight function to the distribution *f(x,y)* will not change the mean of the distribution. However, in the discrete case (1), we only sum the contributions to within the distance R. This introduces an error in the evaluation of the filtered function, because the condition given by (5) does not apply. The error can be pre-determined and set to a reasonably small value in the following manner. If one carries out the integration in (5) with respect to θ, the remaining integral can be rewritten as

$$\int_0^{R}\eta d\left(\frac{r^2}{4K}\right)+\int_R^{\infty}\eta d\left(\frac{r^2}{4K}\right)=1 \qquad (6)$$

Defining the second integral as ε yields

$$\int_0^{R} e^{-\frac{r^2}{4K}} d\left(\frac{r^2}{4K}\right)=1-\varepsilon \qquad (7)$$

Integrating (7), we obtain

$$\varepsilon = e^{-\frac{R^2}{4K}} \qquad (7a)$$

Taking the natural logarithm of both sides of (7a) leads to an expression for K,

$$K = R^2 / 4E \qquad (7b)$$

where $E \equiv -\ln \varepsilon$

Rewriting (4) using (7b) leads to the form of weight function used in the evaluation of (1). Thus, choice of E and the specification of R determine the shape of the weight function. Levitus (1982) chose E=4 which corresponds to a value of ε of approximately 0.02. This choice implies with respect to (7) the representation of more than 98 percent of the influence of any data around the grid point in the area defined by the influence radius R. This analysis (WOA23) and previous analyses (WOA94, WOA98, WOA01, WOA05, WOA13, WOA18) used E=4.

Barnes (1964) proposed using this scheme in an iterative fashion similar to Cressman (1959). Levitus (1982) used a four-iteration scheme with a variable influence radius for each pass. WOA94 used a one-iteration scheme. WOA98, WOA01, WOA05, WOA13, WOA18 and WOA23 employed a three-iteration scheme with a variable influence radius.

3.2.3. Derivation of Barnes (1964) response function

It is desirable to know the response of a data set to the interpolation procedure applied to it. Following Barnes (1964) and reducing to a one-dimensional case we let

$$f(x) = A\sin(\alpha x) \qquad (8)$$

in which $\alpha = 2\pi/\lambda$ with λ being the wavelength of a particular Fourier component, and substitute this function into Equation (3) along with the expression for η in equation (4). Then

$$g(x) = D\left[A\sin(\alpha x)\right] = Df(x) \qquad (9)$$

in which D is the response function for one application of the analysis and defined as

$$D = e^{-\left(\frac{\alpha R}{4}\right)^2} = e^{-\left(\frac{\pi R}{2\lambda}\right)^2}$$

The phase of each Fourier component is not changed by the interpolation procedure. The results of an analysis pass are used as the first-guess for the next analysis pass in an iterative fashion. The relationship between

the filtered function *g(x)* and the response function after *N* iterations as derived by Barnes (1964) is

$$g_N(x) = f(x)D\sum_{n=1}^{N}(1-D)^{n-1} \qquad (10)$$

Equation (10) differs trivially from that given by Barnes. The difference is due to our first-guess field being defined as a zonal average, annual mean, seasonal mean, or monthly mean, whereas Barnes used the first application of the analysis as a first-guess. Barnes (1964) also showed that applying the analysis scheme in an iterative fashion will result in convergence of the analyzed field to the observed data field. However, it is not desirable to approach the observed data too closely, because at least seven or eight grid points are needed to represent a Fourier component.

The response function given in (Equation 10) is useful in two ways: it is informative to know what Fourier components make up the analyses, and the computer programs used in generating the analyses can be checked for correctness by comparison with (Equation 10).

3.2.4. Choice of response function

The distribution of O_2 observations (see appendices) at different depths and for the different averaging periods, are not regular in space or time. At one extreme, regions exist in which every one-degree square contains data and no interpolation needs to be performed. At the other extreme are regions in which few if any data exist. Thus, with variable data spacing the average separation distance between grid points containing data is a function of geographical position and averaging period. However, if we computed and used a different average separation distance for each variable at each depth and each averaging period, we would be generating analyses in which the wavelengths of observed phenomena might differ from one depth level to another and from one season to another. In the WOA94, a fixed influence radius of 555 kilometers was used to allow uniformity in the analysis of all variables. For the present WOA23 analyses (as well as for the WOA18, WOA13, WOA09, WOA04, and WOA01), a three-pass analysis, based on Barnes (1964), with influence radii of 892, 669 and 446 km was used for the 1° analysis.

Inspection of Equation 1 shows that the difference between the analyzed field and the first-guess field values at any grid point is proportional to the sum of the weighted-differences between the observed mean and first-guess at all grid points containing data within the influence area.

The reason for using the five-point Shuman smoother and the median smoother is that our data are not evenly distributed in space. As the analysis moves from regions containing data to regions devoid of data, small-scale discontinuities may develop. The five-point Shuman and median smoothers are used to eliminate these discontinuities. The five-point Shuman smoother does not affect the phase of the Fourier components that comprise an analyzed field.

The response function for the analyses presented in the WOA23 series is given in Table 4 and in Figure 2. For comparison purposes, the response function used by Levitus (1982), WOA94, and others are also presented. The response function represents the smoothing inherent in the OA described above plus the effects of one application of the five-point Shuman smoother and one application of a five-point median smoother. The effect of varying the amount of smoothing in North Atlantic sea surface temperature (SST) fields has been quantified by Levitus (1982) for a particular case. In a region of strong SST gradient such as the Gulf Stream, the effect of smoothing can

easily be responsible for differences between analyses exceeding 1.0°C.

To avoid the problem of the influence region extending across land or sills to adjacent basins, the OA routine employs basin "identifiers" to preclude the use of data from adjacent basins. Table 5 lists these basins and the depth at which no exchange of information between basins is allowed during the objective analysis of data, *i.e.* "depths of mutual exclusion." Some regions are nearly, but not completely, isolated topographically. Because some of these nearly isolated basins have water mass properties that are different from surrounding basins, we have chosen to treat these as isolated basins as well. Not all such basins have been identified because of the complicated structure of the sea floor. In Table 5, a region marked with an (*) can interact with adjacent basins except for special areas such as the Isthmus of Panama.

3.2.5. First-guess field determination

There are gaps in the data coverage and, in some parts of the world ocean, there exist adjacent basins whose water mass properties are individually nearly homogeneous but have distinct basin-to-basin differences. Spurious features can be created when an influence area extends over two basins of this nature (basins are listed in Table 5). Our choice of first-guess field attempts to minimize the creation of such features. To maximize data coverage and best represent global variability, a set of "time-indeterminant" climatologies were produced as a first-guess for each set of decadal climatologies. The time-indeterminant climatologies used the first-guess field procedures developed for earlier versions of the WOA: To provide a first-guess field for the "all-data" annual analysis at any standard level, we first zonally averaged the observed data in each one-degree latitude belt by individual ocean basins. The annual analysis was then used as the first-guess for each seasonal analysis and each seasonal analysis was used as a first-guess for the appropriate monthly analysis if computed.

We then reanalyzed the oxygen data using the newly produced analyses as first-guess fields described as follows. A new annual mean was computed as the mean of the twelve-monthly analyses for the upper 1500 m, and the mean of the four seasons below 1500 m depth. This new annual mean was used as the first-guess field for new seasonal analyses. These new seasonal analyses in turn were used to produce new monthly analyses. This procedure produces slightly smoother means.

These time-indeterminant monthly mean oxygen OA fields were used as the first-guess fields for each "decadal" monthly climatology. Likewise, time-indeterminant seasonal and annual climatologies were used as first-guess fields for the seasonal and annual decadal climatologies.

We recognize that fairly large data-void regions exist, in some cases to such an extent that a seasonal or monthly analysis in these regions is not meaningful. Geographic distribution of observations for the "all-data" annual periods (see appendices) is excellent for the upper layers of the ocean. By using an "all-data" annual mean, first-guess field regions where data exist for only one season or month will show no contribution to the annual cycle. By contrast, if we used a zonal average for each season or month, then, in those latitudes where gaps exist, the first-guess field would be heavily biased by the few data points that exist. If these were anomalous data in some way, an entire basin-wide belt might be affected.

One advantage of producing "global" fields for a particular compositing period (even though some regions are data void) is that such analyses can be modified by investigators for use in modeling studies.

3.3. Choice of objective analysis procedures

Optimum interpolation (Gandin, 1963) has been used by some investigators to objectively analyze oceanographic data. We recognize the power of this technique but have not used it to produce analyzed fields. As described by Gandin (1963), optimum interpolation is used to analyze synoptic data using statistics based on historical data. In particular, second-order statistics such as correlation functions are used to estimate the distribution of first order parameters such as means. We attempt to map most fields in this atlas based on relatively sparse data sets. By necessity we must composite all data regardless of year of observation, to have enough data to produce a global, hemispheric, or regional analysis for a particular month, season, or even yearly. Because of the paucity of data, we prefer not to use an analysis scheme that is based on second order statistics. In addition, as Gandin, 1963 noted, there are two limiting cases associated with optimum interpolation. The first is when a data distribution is dense. In this case, the choice of interpolation scheme makes little difference. The second case is when data are sparse. In this case, an analysis scheme based on second order statistics is of questionable value. For additional information on OA procedures see Thiebaux and Pedder (1987) and Daley (1991).

3.4. Choice of spatial grid

The analyses that comprise the WOA23 have been computed using the ETOPO2 (Earth Topography 2 arc minute) land-sea topography to define ocean depths at each grid point. From the ETOPO2 land mask, a quarter-degree land mask was created based on ocean bottom depth and land criteria. If sixteen or more 2-minute square values out of a possible forty-nine in a one-quarter-degree box were defined as land, then the quarter-degree grid box was defined to be land. If no more than two of the 2-minute squares had the same depth value in a quarter-degree box, then the average value of the 2-minute ocean depths in that box was defined to be the depth of the quarter-degree grid box. If ten or more 2-minute squares out of the forty-nine had a common bottom depth, then the depth of the quarter-degree box was set to the most common depth value. The same method was used to go from a quarter-degree to a one-degree resolution. In the one-degree resolution case, at least four points out of a possible sixteen (in a one-degree square) had to be land in order for the one-degree square to remain land and three out of sixteen had to have the same depth for the ocean depth to be set. These criteria yielded a mask that was then modified by:

1. Connecting the Isthmus of Panama;
2. Maintaining an opening in the Straits of Gibraltar and in the English Channel;
3. Connecting the Kamchatka Peninsula and the Baja Peninsula to their respective continents.

The one-degree mask was created from the quarter-degree mask instead of directly from ETOPO2 in order to maintain consistency between the quarter-degree and one-degree masks.

The WOA23 and all previous climatologies use 1-degree longitude × 1-degree latitude at 102 depth levels (360×180×102). Increasing the spatial resolution from 1-dgree to ¼-degree resolution would enable resolving O_2 content distribution to be better represented in the higher-resolution analysis. We find that at present, there many ocean areas away from coastal areas without observations within the radius of influence. We are encouraged that Argo and BGC Argo O_2 data collection could help mitigate O_2 4-D (time, depth, latitude, and longitude) data

coverage in all seasons.

4. RESULTS

The on-line figures for this atlas include several types of horizontal maps representing annual, seasonal, and monthly spatial distribution of analyzed data and data statistics as a function of selected standard depth levels for dissolved O_2, AOU, and O2S at one-degree latitude-longitude grid (Table 6). In addition, the figures include selected meridional and zonal sections along WOCE lines (Figure 8c). The figures include:

a) Objectively analyzed climatology fields. Grid boxes for which there were less than three values available in the objective analysis defined by the influence radius are denoted by a white "+" symbol shade.

b) Statistical mean one-degree fields. Grid boxes for which there were less than three values available in the objective analysis defined by the influence radius are denoted by a white "+" symbol shade.

c) Data distribution fields for the number of observations in each grid box used in the objective analysis binned into 1 to 2, 3-5, 6-10, 11-30, 31-50 and greater than 51 observations.

d) Standard deviation of the mean fields is binned into several ranges depending on the depth level. The maximum value of the standard deviation is shown on the map.

e) Standard error of the mean fields binned into several ranges depending on the depth level.

f) Difference between observed and analyzed fields binned into several ranges depending on the depth level.

g) Difference between seasonal and monthly temperature fields and the annual mean field.

h) The number of mean values within the radius of influence for each grid box was also calculated. This is not represented as stand-alone maps, but the results are used on a) and b) maps (see above) to mark the grid boxes with less than three mean values within the radius of influence. These calculations are available as data files.

The WOA23 maps presented were arranged by composite time periods (annual, seasonal, month) for O_2, AOU, and O2S, respectively. Table 6 describes all available O_2, AOU, and O2S maps and data fields. Figures 4a-s show horizontal distribution maps for O_2, AOU, and O2S at selected depth levels. Figures 4t-v show selected meridional sections of O_2 content in the Atlantic (near WOCE A16 line), Indian (near WOCE I8), and Pacific (near WOCE P15) basins (Figure 8c, WOCE Atlas figures). Figures 4w-z show the annual O_2 content statistical mean of the observations minus analyzed values at selected depths. We note that the complete set of all climatological maps (in PNG format), objectively analyzed data fields, and associated statistical fields at all standard depth levels shown in Table 6, are available on-line at NOAA NCEI from the WOA webpage.

All of the map figures use consistent symbols and notations for displaying information. Continents are displayed as light-gray areas. Coastal and open ocean areas shallower than the standard depth level being displayed are shown as solid gray areas. The objectively analyzed fields include the nominal contour interval used. In addition, these maps may include in some cases additional contour lines displayed as dashed black lines. All of the maps were drafted using PyGMT, a python program based on the Generic Mapping Tools (GMT, Wessel and Smith, 1998).

We describe next the computation of annual and seasonal fields (Section 4.1) and

available objective and statistical fields (Section 4.2).

4.1. Computation of annual, seasonal, and monthly fields

After completion of all of our analyses, we define a final annual analysis as the average of our twelve-monthly mean fields in the upper 1500 m of the ocean. Below 1500 m depth we define an annual analysis as the mean of the four seasonal analyses. Our final seasonal analyses are defined as the average of monthly analyses in the upper 1500 m of the ocean (Figure 3). We note that the seasonal field values below about 1500 m generally approximate the annual field value with noted exceptions where variability might be larger (*i.e.* convectively formed waters). As noted before, the volume of O_2 observations with global coverage below about 1500 m depth decreases.

4.2. Available objective and statistical data fields

Table 6 lists all objective and statistical fields calculated as part of the WOA23. Climatologies of oceanographic variables and associated statistics described in this document, as well as global figures of the same can be obtained on-line.

The sample standard deviation in a grid box was computed using:

$$s = \sqrt{\frac{\sum_{n=1}^{N}(x_n - \overline{x})^2}{N-1}} \qquad (11)$$

in which x_n= the n^{th} data value in the grid box, $\bar{x}$ = mean of all data values in the grid box, and N= total number of data values in the grid box. The standard error of the mean was computed by dividing the standard deviation by the square root of the number of observations in each grid box.

In addition to statistical fields, the land/ocean bottom mask and basin definition mask are available online. A user could take the standard depth level data from the WOD23 with flags and these masks, and recreate the WOA23 fields following the procedures outlined in this document. Explanations and data formats for the data files are found under documentation on the WOA webpage.

4.3. Obtaining WOA23 data fields and figures on-line

The objective and statistical data fields can be obtained on-line in different digital formats and maps at the WOA webpage, which has WOA23 and earlier versions of WOA. WOA23 data are FAIR-compliant and available online in different digital formats including ASCII comma separated value (CSV) and Network Common Data Form (NetCDF). The NetCDF data use the Climate and Forecast (CF) Metadata Conventions. Figures 4a-w provide selected horizontal maps and sections for distribution of O_2, AOU, and O2S. Figures 4w-z provide statistical mean of the observations minus the objectively analyzed values at selected depths.

For users interested in specific geographic areas, the World Ocean Atlas Select (WOAselect) selection tool can be used to designate a subset geographic area, depth, and oceanographic variable to view, and optionally download, climatological means or related statistics in shapefile format which is compatible with GIS software such as ESRI ArcMap. WOA23 includes a digital collection of "PNG" images of the objective and statistical fields. In addition, WOA23 can be obtained in Ocean Data View (ODV) format. ODV (Schlitzer, 2023) is a data analysis and visualization product developed by Dr. Reiner Schlitzer, Alfred Wegener Institute for Polar and Marine Research. WOA23 will be available through other on-line locations as well. including the IOC

IODE project office. Earlier WOA version (WOA98, WOA01, WOA05, WOA09, WOA13, WOA18) are still available and sometimes served in different online locations (*i.e.* IRI/LDEO Climate Data Library with access to statistical and objectively analyzed fields in a variety of digital formats).

4.4. WOA23F basin-scale O_2, AOU, O2S mean and O_2 inventory

4.4.1 WOAF23 depth averaged means

The objectively analyzed fields enable estimation of basin-scale mean values as a function of depth for different ocean locations and composite time periods (*i.e.* annual, seasonal, and monthly).

The global annual mean and standard deviation of the mean are about 189.3 ± 17.2 μmol·kg^{-1}, 116.4 ± 52.0 μmol·kg^{-1}, and 65.1 ± 16.7 % for O_2, AOU, and O2S, respectively. Figure 5 shows the annual objectively analyzed annual mean for different ocean basins. The Arctic has the largest mean O_2 content and O2S and lowest AOU as a function of depth.

4.4.2 WOAF23 global ocean O_2 inventory estimate

The O_2 inventory (O2I) can be estimated by vertically integrating as a function of depth the objectively analyzed annual mean O_2 content values using equation 12:

$$O2I = \rho A \int_0^h O_2 dz \qquad (12)$$

Where ρ is seawater density (assumed constant at 1025 kg·m^{-3}), O_2 is the measured dissolved oxygen content (μmol·kg^{-1}), A is the area in m^2 of each 1°×1° latitude-longitude grid box, dz is half the distance (m) between the next shallowest level and the current level plus half the distance between the next deepest level and the current level in the WOA23 (*i.e.* thickness of each depth layer), and *h* is depth (0-5500m depth). The ocean areas (m^2) were calculated as a function of latitude assuming a mean earth radius of 6371008.7714 m (World Geodetic System 1984 datum, WGS84).

Based on the WOA23F (0-5500 m), we estimate the global ocean O2I to be about 238.2 ± 0.1 Pmol (1 Pmol= 1 × 10^{15} moles, Figure 5d, Table 11). We can roughly estimate the global mean O_2 content. Suppose that the O2I is homogeneously distributed in the global ocean volume (~1.3554 × 10^{18} m^3) then the global ocean mean O_2 content would be ~171.5 μmol·kg^{-1} (assuming a constant seawater density of 1025 kg·m^{-3}). We note that the O_2 content in the ocean is not homogeneous over time, depth, and location. For comparison, the WOA23N O2I is about 239.1 ± 0.1 Pmol corresponding to an estimated global O_2 content mean of ~172.0 μmol·kg^{-1}. The differences in inventory and content are small between the WOA23F and the WOA23N at global scales.

The ocean volume computed from the WOA23 may be slightly different than volumes estimated using higher spatial and vertical (bathymetry) resolution. This is because WOA23 uses a mean standard depth level to represent the bottom depth each 1×1-degree grid point. Charette and Smith (2010) estimated a global ocean volume of 1.3324 × 10^{18} m^3 which is about 3% lower than our ocean volume estimate. Scaling our estimate of 238.2 Pmol from 1.3554 × 10^{18} m^3 to 1.3324 × 10^{18} m^3 results in an O2I of approximately 237.7 Pmol. For comparison, Schmidtko *et al. (*2017) indicated a smaller O2I of 227.4 ± 1.1 Pmol and an ocean volume of ~1.3011 × 10^{18} m^3. Volumetrically scaling this O2I estimate from 1.3011 × 10^{18} m^3 to 1.3324 × 10^{18} m^3 results in an O_2 inventory of ~232.9 Pmol; or about 4.8 Pmol lower than our estimate (*i.e.* 238.2 minus 232.9 = 4.8 Pmol).

It is interesting to estimate the impact of the deoxygenation trends in the global O2I. Assuming a constant deoxygenation rate of -0.96 Pmol·decade^{-1} (from Schmidtko *et al.* 2017) then after 50 years, the O2I decrease is ~4.8 Pmol and the O_2 content by ~3.4 µmol/kg from the WOA23 baseline values (~238.2 Pmol and ~171.5 µmol·kg^{-1}). For comparison, the 1998-2018 global ocean Gross Primary Production (GPP) is estimated to be in the range of 48.7 to 52.5 Gt C·year^{-1}; or about 4.1 to 4.4 Pmol C·year^{-1} (Kulk *et al.* 2020). Assuming a molar ratio of 106 C: 138 O_2 (Redfield *et al.* 1963), the estimated biologically-mediated O_2 production is in the range of about 53.4 to 57.3 Pmol·decade^{-1}. While these are rough estimates, the GPP-based O_2 production values are much larger than the reported global ocean deoxygenation changes over the same time period. This helps illustrates in part the difficulty in estimating ocean deoxygenation trends apart from natural and man-made variability and uncertainties.

What is the impact of global ocean deoxygenation to the O_2 content in the atmosphere? Earth's atmosphere contains ~20.95% oxygen by volume and ~23.14 % by mass. Trenberth and Smith (2005) indicated a dry mass of air of about 5.1352 ± 0.0003 × 10^{18} kg. Using an O_2 molar mass of ~31.999 gr·mol^{-1} (Laeter J. *et al.* 2003), the O2I in the atmosphere is roughly 37135 Pmol (*i.e.* 0.2314 × 5.1352 × 10^6 / 31.999 ~ 37135 Pmol). Since the atmosphere O2I is 156:1 larger than the ocean (*i.e.* 37135/238.2= 156), ocean deoxygenation changes of about 1 Pmol·decade^{-1} would have little net contribution if hypothetically exported to the atmosphere.

4.5 Observed minus objectively analyzed fields

The WOA23 analysis includes a number of statistical and objectively analyzed fields (Table 6). The statistical fields include calculations of the standard deviation from statistical mean of the observations, standard error of the statistical mean of the observations, the number of observations of the mean, and the statistical mean minus objectively analyzed climatology at each 1° square and at each standard depth with observations that passed our QC checks. The statistical mean minus objectively analyzed fields provides a quantitative measure of deviation between the mean of the observations and the objectively analyzed values. Figures 4w-z show the O_2 content (µmol·kg^{-1}) annual statistical mean minus objectively analyzed fields at each 1-degree box at selected depths.

The deviations may reflect various errors including representative 4-D (time, depth, latitude, and longitude) data coverage, depth interpolation, smoothing by the response function, data errors (Table 4, Figure 2). Figures 4f-I shown the objectively analyzed standard deviation of the annual statistical climatological mean. The deviation is expected to be generally smaller in the open ocean than in coastal regions, frontal zones, and western boundary currents where short-term variability is generally higher.

Table 10 shows the WOA23F depth averaged global mean deviation of the observed (statistical mean) and the objectively analyzed values for O_2, AOU, and O2S in different ocean basins. The global annual mean deviations are relatively small, about 0.20 ± 0.28 µmol·kg^{-1} for O_2; 0.46 ± 0.93 µmol·kg^{-1} for AOU; and 0.12 ± 0.21 % for O2S. Figures 6a-c show the annual mean deviation as a function of depth. The relatively small deviations at all depth levels is encouraging. This suggest that the objective analyses represented well the statistical mean of the observations at basin-scales. Some ocean regions reveal higher deviations. Figure 7 shows histograms of the mean deviation at selected depths. The

mean values are all centered near zero. Figure 8a,b shows the geographic coverage used to represent the global ocean and different basins.

We note that the mean O_2 deviation values are slightly positive. This suggests that the objectively analyzed fields tend to slightly underestimate the statistical mean fields. On average, these values are smaller than or comparable to the precision of Winkler O_2 measurements (0.5-1 µmol·kg^{-1}; Saunders, 1986; Langdon, 2010, GOOS EOV Oxygen, 2017). The relatively small mean deviation values in all basins is encouraging.

4.6 Comparison to other mapped data products

In Sections 4.6.1 and 4.6.2, we compare the WOA23F global annual mean O_2, AOU, O2S values as a function of depth to those in the WOA23N and WOA18. In Sections 4.6.3 and 4.6.4, we compare the WOA23F to Global Ocean Data Analysis Project version 2.2016b (GLODAPv2.2016b downloaded November 2023, Olsen *et al.* 2016, Lauvset *et al.* 2022, GLODAP for short) and the Gridded Ocean Biogeochemistry from Artificial Intelligence for O_2 (GOBAI-O_2, Sharp *et al.* 2022, Sharp *et al.* 2023; GOBAI for short). The GOBAI data is available. Table 9 provides a summary of global mean O_2 content differences. The global mean differences between the WOAF23 and other O_2 mapped products are shown in Figure 9.

4.6.1 WOA23F comparison to WOA18

Table 7a shows depth averaged (0-5500m) of the WOA23F minus WOA18 annual mean differences for different ocean basins. The global depth averaged differences are about -1.03 ± 0.98 µmol·kg^{-1} for O_2; -0.45 ± 0.35 µmol·kg^{-1} for AOU; and for 1.51 ± 1.04 % O2S. While the WOA23F-WOA18 O_2 content mean differences decrease as a function of depth, the WOA18 underestimates the WOA23F by about -1.55 ± 0.81 µmol·kg^{-1} in the upper 2 km (Table 9). WOA18 is based on a smaller set of Winkler-based O_2 measurements collected between 1965 and 2018 than in the WOA23F which uses OSD, CTD, and PFL data (1965-2022). The WOA18 statistical means do not include O_2 solubility adjustments as was done in the WOA23.

4.6.2 WOA23F comparison to WOA23N.

Table 7b shows depth averaged (0-5500 m) WOA23F minus WOA23N annual mean differences for different ocean basins. The global mean differences are about -1.02 ± 0.73 µmol·kg^{-1} for O_2; µmol·kg^{-1} for AOU, and for O2S (Figure 9). The magnitude of global mean difference is relatively small. We note that the O_2 content differences are not solely attributed to solubility decreases between years because of global ocean warming. All of the observational O_2 data used in the objective analysis have been adjusted to help account for solubility changes between years due to ocean warming (Table 13).

4.6.3 WOA23F comparison to GLODAP

We matched the WOA23F 102 depth levels to the corresponding 33 standard depth levels in GLODAP based on data collected between 1972 and 2021. The depth averaged annual O_2 content difference of the WOA23F minus GLODAP is small, about -0.41 ± 0.48 µmol·kg^{-1} for the 0-5500 m depth layer (Table 8, Figure 9). The basin-scale mean content differences are approximately less than 0.80 µmol·kg^{-1}, except in the Arctic basin where the mean difference is largest, ~2.67 ± 2.63 µmol·kg^{-1}. The GLODAP mapped product has sparse data coverage in the Arctic and perhaps this might be in part the reason for the relatively larger difference. We note that most of the observational O_2 data used in the GLODAP are also available in the WOD23 and used in the WOA23.

4.6.4 WOA23F comparison to GOBAI

The GOBAI data product spans the years 2004-2022 and depths 0-2000 m at 58 depth levels different from the WOA23. The GOBAI fields were derived using machine learning (ML) algorithms trained on O_2 observations from Argo/BGC Argo and discrete measurements from ship-based surveys (Sharp *et al.* 2022, Sharp *et al.* 2023). We note that some of observational O_2 data used in both GLODAP and GOBAI are available in the WOD23.

The GOBAI and WOA23F data products use different depth levels and grid points locations. We interpolated the WOA23F depth levels to those in GOBAI. We then re-gridded the GOBAI fields with data to match the WOA23F. The global ocean mean difference WOA23F minus GOBAI is ~3.14 ± 1.08 µmol·kg^{-1} (Table 9). The global mean GOBAI underestimates those of the WOA23F and WOA23N at all depths < 2000 m depth (Figure 9)

4.6.5 WOA23F differences with other O_2 mapped products in context.

Differences are expected between the WOA23F, WOA23N, WOA18, GLODAP, and GOBAI data products. Their differences can be attributed to a combination of several factors. We describe a few potential factors.

The products use different types of O_2 measurements. WOA23F uses quality-controlled O_2 data from three observing systems: OSD (1965-2022), CTD (1987-2022), and Argo/BGC-Argo (2005-2022). This results in a larger 4-D data coverage in all months, seasons, and depths than WOA23N, WOA18, GLODAP, and GOBAI. The WOA23F is based on ~1.0 million profiles (~27.4 million observations at standard depths) collected between 1965 and 2022 (Table 1b). GLODAP and to some extent GOBAI use measurements that were largely collected during the summer months. GOBAI also used Argo/BGC-Argo data. The WOA23 includes the WOD18 data used in WOA18 after additional QC.

Each of the mapped products is centered on different baseline time periods and datasets than the WOA23. For example, the WOA18 is based on OSD Winkler data (1965-2017), GLODAP Winkler data (1972-2021), WOA23N OSD and CTD (1971-2000), and GOBAI OSD and Argo/BGC-Argo (2004-2022). Except for the GOBAI, the global mean O_2 content difference between the WOA23F, WOA23N, WOA18, and GLODAP below about 2000 m depth are relatively small in magnitude (Table 9, Figure 9).

The delayed-mode Argo and BGC-Argo O_2 data used in the WOA23F were mostly collected in the upper 2 km depth layer. In our analysis, we include deep Argo/BGC-Argo. As described in Section 2.2.9, the PFL O_2 profiles were adjusted by adding 1.338 µmol·kg^{-1} for internal consistency with the ship board data from WOCE, CLIVAR, GO-SHIP (Figure 1f). The addition of the PFL data has significantly increased the 4-D O2 data coverage.

The observations used in WOA23 include a O_2 solubility adjustment (See Section 2.2.6). While this solubility adjustment was used in the WOA23F and WOA23N, it was not used in WOA18, GLODAP, or GOBAI. Each mapped product uses different QC procedures and metrics from each other with the exception of the WOA23 and WOA18. The 0-5500 m global mean O_2 content differences between the WOA23F and WOA18, WOA23N, and GLODAP; howver are relatively small (< 1.0 µmol·kg^{-1}), and larger for GOBAI by about 3.1 µmol·kg^{-1} (Table 9).

The GLODAP and GOBAI use different mapping tools. GLODAP, for example, uses the Data-Interpolating Variational Analysis software (DIVA) on a uniform 1°×1° grid for

33 standard depth surfaces. GLODAP's 33 depth levels are a subset of the WOA23 102 depth levels. Sharp *et al.* (2023) describes the data mapping done for GOBAI.

Without the benefit of a mapping inter-comparison using the same starting data conditions, it would be difficult to compare the data products.

5. SUMMARY AND DISCUSSION

In the preceding sections, we have described the results of a project to objectively analyze all historical quality-controlled O_2 data in the WOD23 for the 1965 to 2022 (WOA23F) and 1971-2000 (WOA23N) time periods. We desire to build a set of climatological analyses that are nearly identical in all respects for all variables in the WOA23 data product series including relatively data sparse variables such as dissolved inorganic nutrients (Garcia *et al.* 2024a). This provides investigators with an internally consistent set of analyses of known quality to work with.

One advantage of the analysis techniques used in this atlas is that we know the amount of smoothing by objective analyses as given by the response function (Table 4, Figure 2). We believe this to be an important function for constructing and describing a climatology of any variable or parameter. Particularly when computing anomalies from a standard climatology, it is important that the data field be smoothed to the same extent as the climatology, to prevent generation of spurious anomalies simply through differences in smoothing. A second reason is that purely diagnostic computations require a minimum of seven or eight grid points to represent any Fourier component with statistical confidence. Higher order derivatives will require more smoothing.

To our knowledge, the WOA23 is the most comprehensive and representative observation-based global ocean O_2, AOU, and O2S climatology to date of the past 57 years (1965-2022). The WOA23F is based on quality-controlled data (~27.3 million observations, ~1.0 million profiles) from NOAA's World Ocean Database 2023. In addition, we developed for the first time, a 30-year Climate Normal for O_2, AOU, and O2S (1971-2000) WOA23 Climate Normal (WOA23N).

All of the quality-controlled O_2 measurements used to calculate the WOA23 annual, seasonal, and monthly statistical mean fields were adjusted for O_2 solubility changes between years because of ocean warming. The delayed-mode Argo and BGC-Argo O_2 data were also adjusted to account for a relatively small global mean content depth offset underestimation when compared to nearby Winkler/CTD O_2 profiles.

The depth averaged (0-5500 m) global mean difference of the objectively analyzed fields for the WOA23 O_2, AOU, and O2S are relatively small, approximately 0.2 ± 0.3 $\mu mol \cdot kg^{-1}$, 0.6 ± 1.0 $\mu mol \cdot kg^{-1}$, and 0.1 ± 0.2 %, respectively (Figure 6). The mean deviations suggest that the objective analysis tends to slightly overestimate the observed mean fields. The deviation was estimated from the global deviations between the objectively analyzed and the statistical mean fields at all grids and depths. Some grids have larger number of observations than others. A more in-depth data error analysis is beyond the scope of this analysis.

Figure 9 shows the global mean O_2 content deviation estimates between the WOA23F and other mapped data products as a function of depth. The deviations from the WOA23F are generally within about ± 1 $\mu mol \cdot kg^{-1}$ with those in the WOA23N, WOA18, and GLODAP. In the case of GOBAI, the mean difference is about 3.1 ± 1.1 $\mu mol \cdot kg^{-1}$.

We have attempted to develop the most comprehensive and representative global

mean O_2 content climatology of the past 57 years (1965 to 2022). The WOA23 uses a number of objective QC procedures. The results are further analyzed by Subject Matter Experts (SME). Even after all the QC performed, some observations may have passed (not passed) the QC when they should not (should) haven been flagged as questionable. For those users who wish to make their own data QC choices, all the observational data used in our analyses are available both at standard depth levels as well as observed depth levels as part of the WOD23.

The WOA23 is reproducible from the quality-controlled data in the WOD23. The results presented in this atlas show some sub meso-scale ocean features that may be due to non-representative or low-quality data that were not flagged by the QC techniques used. Although we have attempted to identify as many of these features as possible by flagging and not using the data in the analysis, some obviously could remain. Some may eventually turn out not to be real ocean features, not yet capable of being described in a meaningful way by our analysis due to lack of uniform 4-D data coverage, grid resolution (360×180×102), and our QC procedures. The views, findings, and any errors in this document are those of the authors and do not reflect any position of the U.S. Government, the Department of Commerce, or National Oceanic and Atmospheric Administration (NOAA).

6. FUTURE WORK

The WOA23 O_2, AOU, and O2S analyses will be updated when justified by additional and updated observations. As more oceanographic data are received and archived at NCEI/WDS-Oceanography for inclusion in the World Ocean Database (WOD), we will also be able to produce higher 4-D resolution mean climatologies for O_2, AOU, and O2S of known science-quality.

We are encouraged by the significant amount and coverage of O_2 data being collected as part of the Argo and BGC-Argo effort. The data provides significantly higher 4-D coverage. On the other hand, there are still many global ocean profile O_2 and other EOV data not yet publicly and openly accessible. The IOC IODE is helping to facilitate open data sharing in these and other geographic regions (*e.g.* IOCARIBE, ODINAFRICA). There are also ocean profile data that may not be available yet in the WOD in other ocean databases, data repositories, and federated data services such as for example, the European Marine Observation and Data Network (EMODnet), SeaDataNet, Blue-Cloud 2026, IOC Ocean Data and Information System (ODIS). There are also citizen science efforts collecting valuable EOV data including O_2 such as for example, "The Ocean Race". The OCL Team is working to help ensure that the greatest and most comprehensive ocean profile data coverage are shared and made available to all data users.

To date, the Argo/BGC-Argo O_2 profilers provide the best 4-D coverage. At present, there are potential instrumental biases and further work is needed to recalibrate the historical PFL observational data using a common and reproducible analysis method. It would also be useful to carry out an inter-comparison data synthesis analysis of the PFL data to better assess the research-quality quality of the data.

Our analysis blends QC O_2 data collected by both chemical and sensor-based methods to develop a more representative and internally consistent statistical and objectively analyzed global gridded fields of known science quality. Figure 1a shows our roadmap for developing more comprehensive and representative O_2 climatologies. The addition of sensor-based data has improved the temporal and spatial coverage of O_2 data as well as the representativeness of the results

presented here. As more data are added, additional observational constraints on coastal and open ocean variability could be more reliably assessed.

Each ocean O_2 observing system adds additional 4-D data coverage (*e.g.* OSD, CTD, Argo, Gliders). At the same time, the research data quality of each O_2 observing system must be carefully quality-controlled before and after combining them into an internally consistent blended climatology. While we have taken great effort to QC the OSD, CTD, and PFL data used in the WOA23, some questionable data may remain in the WOD23.

As the 4-D coverage of the ocean observations increases, we may be able to create more representative climatological fields with finer grid resolution (*e.g.* ¼-degree or less). This would enable O_2 content distribution analysis along coastal regions, western and eastern boundary currents, Oxygen Minimum Zones (OMZ), and other geographic and depth locations.

We are encouraged by the acquisition of data through global projects such as the Global Ocean Observing System (GOOS) 2030 Strategy and the United Nations Decade of Ocean Science for Sustainable Development (2021-2030). GOOS is sponsored by the Intergovernmental Oceanographic Commission (IOC) of the United Nations Educational, Scientific and Cultural Organization (UNESCO), the World Meteorological Organization (WMO), the United Nations Environment Programme (UNEP), and the International Science Council (ISC). Expansion of the current global ocean observing system will enable the creation of more representative climatologies that span different climatological time-periods ranging from sub-seasonal, inter-annual, and decadal periods and with smaller grid size spatial resolution. The sustained collection overtime of research-quality O_2 measurements from research ships and Argo/BGC-Argo will help enable achieving this goal.

We note with concern the significant decrease in the number of OSD O_2 (Winkler shipboard measurements) profiles collected after about the year 2000 (Figure 1b, Figure 1c). The majority of the OSD O_2 observations were collected between 1965 and 2000 (Figure 1c). After the year 2000 approximately, the number of O_2 sensor-based measurements is much larger than for OSD data. At present, the Winkler-based O_2 measurements are nominally used as reference for comparison and QC of sensor-based data. In the absence of independent quality-controlled Winkler-based measurements, Certified Reference Standards, or other reliable O_2 reference data of known science quality, it would be difficult at present to assess and quantify the research-quality of sensor-based measurements over time and location (*e.g.* sensor-drift and adjustment factors). The ocean science community is investigating and correcting instrumental biases in the BCG-Argo and other sensor-based O_2 measurements (*e.g.* Bittig *et al.* 2015; Bittig *et al.* 2018).

One country cannot afford the observational system needed to monitor the entire ocean domain; and thus, open sharing, access and reuse of observations is critical for assessing ocean climate variability and for formulating informed science-based societal-relevant strategies for sustainable ocean use (*i.e.* blue economy). Global ocean deoxygenation can have significant impacts on the marine ecosystem worldwide (Giovannoni *et al.* 2021). It would also impact O_2 content in the deep ocean though ventilation as well as organic matter remineralization and chemical oxidation-reduction (redox) reactions.

The oceanographic observational data available in the WOD23 were collected at

great public funding cost and collected by many scientists, institutions, programs, and countries over many decades. The historical instrumental record data are of irreplaceable scientific value as the data are our only means to assess observation-based ocean climate variability and their impacts such as in global ocean deoxygenation. The WOA and WOD data are openly shared with the global ocean community as research-quality data products.

A critical gap is the absence of ocean community-adopted QC metrics for O_2 measurements collected over many years and by different O_2 observing systems. While the WOA23 QC process addresses the WOA23 data product fit-for-purpose quality control requirements, it would be useful to adopt common community use QC for each variable that the ocean community could adopt, use, and evolve for internal consistency. This would minimize the use of similar QC tests based on different quantifiable metrics.

We are encouraged by the emergence of Artificial Intelligence (AI) and Machine Learning (ML) research to help examine the 4-D O_2 data distribution patterns as well as for other applications (*e.g.* Sharp *et al.* 2023).

We welcome the ocean community comments that would improve the usefulness of this Atlas. We envision the WOD and WOA as data products accessible to all global data users with equity. While we have done extensive efforts to QC the data, ocean researchers and data users could help us to identify questionable data that we may have missed, data that we flagged erroneously, newer data set versions of what is in WOD, duplicate data, additional metadata, or new QC metrics and methods.

In the acknowledgement section of this atlas, we emphasize our deep and sincere gratitude to all of the worldwide researchers, technicians, data managers, projects, institutions, data centers, IOC IODE, WDS, and others who have collected and openly shared and continue to share oceanographic data to national, regional, global data centers, and the WDS-Oceanography. Documenting ocean climate variability and impacts relies on open access to global measurements. In the WOD23 metadata we acknowledge the investigators and data providers of every single dataset that is included. In all cases, the data in the WOD provides links to the NOAA NCEI long-term data archive where the original data provided are preserved exactly as received and where the provenance and attribution of the data are fully described including DOI's if the information is made available. The WOD aims to merge of the available oceanographic profile data in a uniform FAIR-compliant analysis-ready dataset that can be reliably used by the global ocean science community.

The WOA23 series includes several volumes for different variables and parameters (Table 12). The WOA23 is a NOAA NCEI Ocean Climate Laboratory Team effort by many individuals. The views, findings, and any errors in this document are those of the authors and do not reflect any position of the U.S. Government, DOC, or NOAA.

7. REFERENCES

Achtemeier, G.L. (1987). On the concept of varying influence radii for a successive corrections objective analysis. *Mon. Wea. Rev*., 11, 1761-1771. https://doi.org/10.1175/1520-0493(1987)115<1760:OTCOVI>2.0.CO;2

Barnes, S.L. (1964). A technique for maximizing details in numerical weather map analysis. *J. App. Meteor*., 3, 396-409. https://doi.org/10.1175/1520-0450(1964)003<0396:ATFMDI>2.0.CO;2

Barnes, S.L. (1973). Mesoscale objective map analysis using weighted time series observations. NOAA Technical Memorandum ERL NSSL-62, 60 pp. [PDF]

Barnes, S.L. (1994). Applications of the Barnes Objective Analysis Scheme, Part III: Tuning for Minimum Error. *J. Atmosph. and Oceanic Tech*., 11, 1459-1479.

https://doi.org/10.1175/1520-0426(1994)011%3C1459:AOTBOA%3E2.0.CO;2

Benson, B.B., and O. Krauss (1984). The concentration and isotopic fractionation of oxygen dissolved in freshwater and seawater in equilibrium with the atmosphere. *Limnol. Oceanogr.,* 10, 264-277. https://aslopubs.onlinelibrary.wiley.com/doi/10.4319/lo.1984.29.3.0620

Bergthorsson, P. and B. Doos (1955). Numerical Weather map analysis. Tellus, 7, 329-340. [PDF]

Bindoff, N.L. and T.J. McDougall (2000). Decadal changes along an Indian Ocean section at 32°S and their interpretation, *J. Phys. Oceanogr*., 30, 1207-1222. https://doi.org/10.1175/1520-0485(2000)030<1207:DCAAIO>2.0.CO;2

Bittig, H.C. and A. Kortzinger (2015). Tackling oxygen optode drift: Near-surface and in-air oxygen optode measurements on a float provide an accurate *in situ* reference. *J. Atmos. Ocean. Technol.* 32: 1536–1543. https://doi.org/10.1175/JTECH-D-14-00162.1

Bittig H.C., A. Körtzinger, C. Neill, E.V. Ooijen, J.N. Plant, J. Hahn, K. Johnson, B. Yang, and S.R. Emerson (2018). Oxygen Optode Sensors: Principle, Characterization, Calibration, and Application in the Ocean. *Front. Mar. Sci*., 24, https://doi.org/10.3389/fmars.2017.00429

Bopp, L. Bopp, L., Resplandy, L., Orr, J. C., Doney, S. C., Dunne, J. P., Gehlen, M., Halloran, P., Heinze, C., Ilyina, T., Séférian, R., Tjiputra, J., Vichi, M (2013) Multiple stressors of ocean ecosystems in the 21st century: projections with CMIP5 models. *Biogeosciences* 10, 6225–6245, https://bg.copernicus.org/articles/10/6225/2013/

Bopp, L., C. Le Quéré, M. Heimann, A. C. Manning, and P. Monfray (2002), Climate-induced oceanic oxygen fluxes: Implications for the contemporary carbon budget, *Global Biogeochem. Cycles*, 16(2), 1022, doi:10.1029/2001GB001445.

Boyer, T.P. and S. Levitus (1994). Quality control and processing of historical temperature, salinity and oxygen data. *NOAA Technical Report NESDIS 81*, 65 pp. [PDF]

Boyer, T., C.M. Domingues, S.A. Good, G.C. Johnson, J.M. Lyman, M. Ishii, V. Gouretski, J.K. Willis, J. Antonov, S. Wijffels, *et al.* (2016). Sensitivity of global upper-ocean heat content estimates to mapping methods, XBT bias corrections, and baseline climatologies. *J. Climate* 29(13) https://doi.org/10.1175/JCLI-D-15-0801.1

Broecker, W.S. and T.H. Peng (1982). Tracers in the Sea, *Eldigio Press*, Palisades, N.Y., 690 pp.

Bushinsky S.M., S.R. Emerson, S.C. Riser, D.D. Swift (2016). Accurate oxygen measurements on modified Argo floats using *in situ* air calibrations. *Limnol. Oceanogr.: Methods*, 14(8), 491-505. https://doi.org/10.1002/lom3.10107

Carpenter, J.H. (1965a). The Chesapeake Bay Institute technique for the Winkler dissolved oxygen titration, *Limnol. Oceanogr*., 10, 141-143. https://aslopubs.onlinelibrary.wiley.com/doi/10.4319/lo.1965.10.1.0141

Carpenter, J. H. (1965b). The accuracy of the Winkler method for dissolved oxygen analysis. *Limnol. Oceanogr*., 10(1), 135-140. https://aslopubs.onlinelibrary.wiley.com/doi/10.4319/lo.1965.10.1.0135

Charette, M.A., and W.H.F. Smith. 2010. The volume of Earth's ocean. *Oceanography* 23(2):112–114, https://doi.org/10.5670/oceanog.2010.51.

Craig, H., and T. Hayward (1987), Oxygen supersaturation in the ocean: Biological versus physical contributions, *Science*, 235, 199–202. https://www.science.org/doi/10.1126/science.235.4785.199

Cressman, G.P. (1959). An operational objective analysis scheme. *Mon. Wea. Rev.*, 87, 329-340.

Culberson, C.H. and S.L. Huang (1987). Automated amperometric oxygen titration, *Deep-Sea Res*., 34, 875-880. https://doi.org/10.1016/0198-0149(87)90042-2

Daley, R. (1991). Atmospheric Data Analysis. Cambridge University Press, Cambridge, 457 pp.

Deutsch, C., S. Emerson, and L. Thompson (2005). Fingerprints of climate change in North Pacific oxygen. *Geophys. Res. Lett*., 32, https://doi.org/10.1029/2005GL023190.

Dickson, A.G. (1994). Determination of dissolved oxygen in sea water by Winkler titration. WOCE Hydrographic Program, Operations and Methods Manual, Woods Hole, Mass., U.S.A. [PDF]

Emerson S., C. Stump, D. Wilbur, and P. Quay. (1999). Accurate measurement of O_2, N_2, and Ar gases in water and the solubility of N_2. *Marine Chemistry*, 64(4), 337-347. https://doi.org/10.1016/S0304-4203(98)00090-5

Emerson S., C. Stump, B. Johnson, and D.M. Karl (2002). *In situ* determination of oxygen and nitrogen dynamics in the upper ocean, *Deep-Sea Res.*, 49, 941-952. https://doi.org/10.1016/S0967-0637(02)00004-3

Forster, P., T. Storelvmo, K. Armour, *et al.* (2021). The Earth's Energy Budget, Climate Feedbacks, and Climate Sensitivity, in: Climate Change 2021: The Physical Science Basis. Contribution of Working Group I to the Sixth Assessment Report of the Intergovernmental Panel on Climate Change, edited by: V. Masson-Delmotte *et al.* Cambridge University Press, Cambridge, United Kingdom and New York, NY, USA, 923–1054. https://doi.org/10.1017/9781009157896.009.

Gandin, L.S. (1963). Objective Analysis of Meteorological fields. *GidrometIzdat*, Leningrad (translation by Israel program for Scientific Translations), Jerusalem, 1966, 242 pp.

Garcia, H.E. and L.I. Gordon (1992). Oxygen solubility in seawater: Better fitting equations. *Limnol. Oceanogr*., 37, 1307-1312, https://doi.org/10.4319/lo.1992.37.6.1307

Garcia, H.E., A. Cruzado, L.I. Gordon, and J. Escanez (1998). Decadal-scale chemical variability in the subtropical North Atlantic deduced from nutrient and oxygen data. *J. Geophys. Res*., 103, 2817–2830, https://doi.org/10.1029/97JC03037

Garcia, H.E. and R.E. Keeling (2001). On the global oxygen anomaly and air-sea flux. *J. Geophys. Res*., 106, https://doi.org/10.1029/1999JC000200

Garcia, H. E., K. Weathers, C. R. Paver, I. Smolyar, T. P. Boyer, R. A. Locarnini, M. M. Zweng, A. V. Mishonov, O. K. Baranova, D. Seidov, and J. R. Reagan, 2018. World Ocean Atlas 2018, Volume 3: Dissolved Oxygen, Apparent Oxygen Utilization, and Oxygen Saturation. A. Mishonov Technical Ed.; *NOAA Atlas NESDIS* 83, 38pp [PDF]

Garcia, H.E., T.P. Boyer, S. Levitus, R.A. Locarnini, and J.I. Antonov (2005a). Climatological annual cycle of upper ocean oxygen content, *Geophys. Res. Lett*., 32, https://doi.org/10.1029/2004GL021745.

Garcia, H.E., T.P. Boyer, S. Levitus, R.A. Locarnini, and J.I. Antonov (2005b). On the variability of dissolved oxygen and apparent oxygen utilization content for the upper world ocean: 1955 to 1998. *Geophysical Res. Lett.*, https://doi.org/10.1029/2004GL022286.

Garcia H.E., T.P. Boyer, O.K. Baranova, R.A. Locarnini, A.V. Mishonov, A. Grodsky, C.R. Paver, K.W. Weathers, I.V. Smolyar, J.R. Reagan, D. Seidov, M.M. Zweng (2019a). World Ocean Atlas 2018: Product Documentation. A. Mishonov, Tech. Editor. [PDF]

Garcia, H. E., K. Weathers, C. R. Paver, I. Smolyar, T. P. Boyer, R. A. Locarnini, M. M. Zweng, A. V. Mishonov, O. K. Baranova, D. Seidov, and J. R. Reagan (2019b). World Ocean Atlas 2018, Volume 3: Dissolved Oxygen, Apparent Oxygen Utilization, and Oxygen Saturation. A. Mishonov Tech. Ed.; *NOAA Atlas NESDIS 83*, 38pp. [PDF]

Garcia, H. E., K. Weathers, C. R. Paver, I. Smolyar, T. P. Boyer, R. A. Locarnini, M. M. Zweng, A. V. Mishonov, O. K. Baranova, D. Seidov, and J. R. Reagan (2019c). World Ocean Atlas 2018, Volume 4: Dissolved Inorganic Nutrients (phosphate, nitrate and nitrate + nitrite, silicate). A. Mishonov Tech. Ed.; *NOAA Atlas NESDIS 84*, 35pp. [PDF]

Garcia H.E., C. Bouchard, S.L. Cross, C.R. Paver, T.P. Boyer, J.R. Reagan, R.A. Locarnini, A.V. Mishonov, O.K. Baranova, D. Seidov, Z. Wang, and D. Dukhovskoy (2024a). World Ocean Atlas 2023, Volume 4: Dissolved Inorganic Nutrients (Phosphate, Nitrate, Silicate). A. Mishonov Technical Editor. NOAA Atlas NESDIS 92, 78pp. https://doi.org/10.25923/39qw-7j08

Garcia, H. E., T. P. Boyer, R. A. Locarnini, J.R. Reagan, A.V. Mishonov, O.K. Baranova, C.R. Paver (2024b). World Ocean Database 2023: User's Manual. A.V. Mishonov, Tech. Ed., *NOAA Atlas NESDIS 98*, pp 107. https://doi.org/10.25923/j8gq ee82 (*in preparation*)

Giovannoni S., F. Chan, E. Davis, II, C. Deutsch, and S. Wolf. (2021). Biochemical Barriers on the Path to Ocean Anoxia? Environmental Microbiology https://doi.org/10.1128/mbio.01332-21

Grégoire, M., V. Garçon, H. Garcia *et al.* (2021). A Global Ocean Oxygen Database and Atlas for Assessing and Predicting Deoxygenation and Ocean Health in the Open and Coastal Ocean. *Front. Mar. Sci.* 8, https://doi.org/10.3389/fmars.2021.724913

Helm, K. P., N.L. Bindoff, and J.A. Church (2011) Observed decreases in oxygen content of the global ocean. *Geophysical Res. Lett.* https://doi.org/10.1029/2011GL049513

Helm, I., G. Karina, L. Jalukse, T. Pagano, and I. Leito. (2018) Comparative validation of amperometric and optical analyzers of dissolved oxygen: a case study. Environ Monit Assess 190, 313. https://doi.org/10.1007/s10661-018-6692-5

Hofmann M. and H-J. Schellnhuber (2009). Oceanic acidification affects marine carbon pump and triggers extended marine oxygen holes. *Proc. U.S. Natl. Acad. Sci., 106*: 3017-3022. https://www.pnas.org/doi/10.1073/pnas.0813384106

Ito T., M. Follows, and E.A. Boyle (2004). Is AOU a good measure of respiration in the oceans? *Geophysical. Res. Lett*., 31, https://doi.org/10.1029/2004GL020900

Ito T., Minobe S., Long M. C., Deutsch C. (2017). Upper ocean O2 trends: 1958–2015. *Geophysical Res. Lett*. 44, 42024b214–4223. doi:10.1002/2017GL073613

Ito, T., (2022). Optimal interpolation of global dissolved oxygen: 1965–2015. *Geoscience Data Journal,* Vol. 9, https://doi.org/10.1002/gdj3.130

Ito T., H. Garcia, Z. Wang *et al.* (2023) Underestimation of global O_2 loss in optimally interpolated historical ocean observations. https://doi.org/10.5194/bg-2023-72

JPOTS (Joint Panel on Oceanographic Tables and Standards) Editorial Panel (1991). Processing of Oceanographic Station Data. *UNESCO*, Paris, 138 pp. [PDF]

Johnson K.S., J.N. Plant, S.C. Riser, and D. Gilbert (2015). Air Oxygen Calibration of Oxygen Optodes on a Profiling Float Array. *J. of Atmos. And Oceanic Tech.*, 32: 2160-2172, https://doi.org/10.1175/JTECH-D-15-0101.1

Johnson, G. C., Hosoda, S., Jayne, S. R., Oke, P. R., Riser, S. C., Roemmich, D., Suga, T., Thierry, V., Wijffels, S., and Xu, J. (2022). Argo – Two decades: Global oceanography, revolutionized, *Annu. Rev. Mar. Sci.,* 14, 379–403, https://doi.org/10.1146/annurev-marine-022521-102008

Knapp, G.P., M.C. Stalcup, and R.J. Stanley (1990). Automated oxygen titration and salinity determination, *Woods Hole Oceanographic Institution*, WHOI Ref. No. 90-35. [PDF]

Keeling, R. and H. Garcia (2002). The change in oceanic O_2 inventory associated with recent global warming, *Proc. U.S. Natl. Acad. Sci*., 99. https://doi.org/10.1073/pnas.122154899

Kulk G., T. Platt, J. Dingle *et al.* (2020). Primary Production, an Index of Climate Change in the Ocean: Satellite-Based Estimates over Two Decades. *Remote Sens.* 12(5). https://doi.org/10.3390/rs12050826

Kwiatkowski, L., Torres, O., Bopp, L., Aumont, O., Chamberlain, M., Christian, J., Dunne, J., Gehlen, M., Ilyina, T., John, J., Lenton, A., Li, H., Lovenduski, N., Orr, J., Palmieri, J., Schwinger, J., Séférian, R., Stock, C., Tagliabue, A., Takano, Y., Tjiputra, J., Toyama, K., Tsujino, H., Watanabe, M., Yamamoto, A., Yool, A., Ziehn, T. (2020). Twenty-first century ocean warming, acidification, deoxygenation, and upper ocean nutrient decline from CMIP6 model projections. *Biogeosciences* 17. https://doi.org/10.5194/bg-2020-16

Kwon, E. Y., Deutsch, C. A., Xie, S.-P., Schmidtko, S. and Cho, Y.-K. (2016) The North Pacific Oxygen uptake rates over the past half century. *J. Clim.* 29, 61–76. http://doi.org/10.1175/Jcli-D-14-00157.1

Körtzinger, A., J. Schimanski, U. Send, and D. Wallace (2004). The ocean takes a deep breath, *Science,* 306, 1337. DOI: 10.1126/science.1102557

Körtzinger, A., J. Schimanski and U. Send (2005). High Quality Oxygen Measurements from Profiling Floats: A Promising New Technique, *J. of Atmos. And Oceanic Tech.*, 22, https://doi.org/10.1175/JTECH1701.1.

Laeter J.R., J.K. Böhlke, P. De Bièvre, H. Hidaka, H.S. Peiser, K.J.R. Rosman, and P.D.P. Taylor. (2003). Atomic weights of the elements: Review 2000, IUPAC Technical Report. *Pure Appl. Chem*. 75, 683-800 [PDF]

Langdon, C.: Determination of Dissolved Oxygen in Seawater by Winkler Titration using Amperometric Technique, in: The GO-SHIP Repeat Hydrography Manual: A Collection of Expert Reports and Guidelines. Version 1, edited by: Hood, E. M., Sabine, C. L., and Sloyan, B. M., IOCCP Report no. 14, ICPO Publication Series no. 134, 18 pp. [PDF].

Lauvset, S. K., N. Lange, T. Tanhua, T., *et al.* (2022). GLODAPv2.2022: the latest version of the global interior ocean biogeochemical data product*, Earth Syst. Sci. Data,* 14, 5543–5572, https://doi.org/10.5194/essd-14-5543-2022.

Levitus, S. (1982). Climatological Atlas of the World Ocean*, NOAA Professional Paper No. 13*, U.S. Gov. Printing Office, 173 pp. (NTIS PB83-184093)

Levitus, S., and T.P. Boyer (1994a). World Ocean Atlas 1994. Vol. 2: Oxygen. *NOAA Atlas NESDIS 2*, U.S. Gov. Printing Office, Washington, D.C., 186 pp. [PDF]

Levitus, S., and T.P. Boyer (1994b). World Ocean Atlas 1994. Vol. 4: Temperature. *NOAA Atlas NESDIS 4*, U.S. Gov. Printing Office, Washington, D.C., 117 pp. [PDF]

Levitus, S., J.I. Antonov, T.P. Boyer, and C. Stephens. 2000. Warming of the world ocean. Science 287(5461):2,225–2,229. https://doi.org/10.1126/science.287.5461.2225

Levitus, S., J. I. Antonov, and T. P. Boyer (2005a), Warming of the world ocean, 1955-2003, *Geophys. Res. Lett.,* 32, L02604, https://doi.org/10.1029/2004GL021592

Levitus, S., S. Sato, C. Maillard, N. Mikhailov, P. Caldwell, H. Dooley (2005b). Building Ocean Profile-Plankton Databases for Climate and Ecosystem Research, *NOAA Technical Report NESDIS 117*, U.S. Gov. Printing Office, Washington, D.C., 29 pp. [PDF]

Levitus, S., J. I. Antonov, T.P. Boyer, O.K. Baranova, H.E. Garcia, R.A .Locarnini, A.V. Mishonov, J.R. Reagan, D. Seidov, E.S. Yarosh, and M.M. Zwen (2012). World ocean heat content and thermosteric sea level change(0–2000m), 1955–2010, *Geophys. Res. Lett.*, 39, L10603. https://doi.org/10.1029/2012GL051106

Locarnini, R.A., A.V. Mishonov, O.K. Baranova, J.R. Reagan, T.P. Boyer, D. Seidov, Z. Wang, H.E. Garcia, C. Bouchard, S.L. Cross, C.R. Paver, and D. Dukhovskoy (2024). World Ocean Atlas 2023, Volume 1: Temperature. A. Mishonov Tech. Ed. *NOAA Atlas NESDIS* 89, 51 pp, https://doi.org/10.25923/54bh-1613

Maurer T.L., J.N. Plant, and K.S. Johnson (2021). Delayed-Mode Quality Control of Oxygen, Nitrate, and pH Data on SOCCOM Biogeochemical Profiling Floats. *Front. Mar. Sci.*, https://doi.org/10.3389/fmars.2021.683207

Matear, R.J. and A.C. Hirst (2003). Long-term changes in dissolved oxygen concentrations in the ocean caused by protracted global warming. *Glob. Biogeochem. Cycles,* 17(4), 1125, https://doi.org/10.1029/2002GB001997.

Mignot, A. F. D'Ortenzio, V. Taillandier, G. Cossarini, S. Salon (2019) Quantifying Observational Errors in Biogeochemical-Argo Oxygen, Nitrate, and Chlorophyll a Concentrations. *Geophys. Res. Letter* https://doi.org/10.1029/2018GL080541

Mishonov, A.V., T.P. Boyer, O.K. Baranova, C.N. Bouchard, S.L. Cross, H.E. Garcia, R.A. Locarnini, C.R. Paver, J.R. Reagan, Z. Wang, D. Seidov, A.I. Grodsky, J. Beauchamp (2024). World Ocean Database 2023. C. Bouchard, Tech. Ed. *NOAA Atlas NESDIS 97*, https://doi.org/10.25923/z885-h264 (in preparation)

Morée, A. L., Clarke, T. M., Cheung, W. W. L., and Frölicher, T. L. (2023) Impact of deoxygenation and warming on global marine species in the 21st century, *Biogeosciences*, 20, 2425–2454, https://doi.org/10.5194/bg-20-2425-2023.

Nicholson, D. P., and Feen, M. L. (2017). Air calibration of an oxygen optode on an underwater glider. Limnol. Oceanogr.: Methods, 15, 495–502. https://doi.org/10.1002/lom3.10177

Oschlies A., P. Brandt, L. Stramma & S. Schmidtko (2018). Drivers and mechanisms of ocean deoxygenation. Nature Geosci 11, 467–473 (2018). https://www.nature.com/articles/s41561-018-0152-2

Olsen, A., R. M. Key, S. van Heuven, S. K. Lauvset, A. Velo, X. Lin, C. Schirnick, A. Kozyr, T. Tanhua, M. Hoppema, S. Jutterström, R. Steinfeldt, E. Jeansson, M. Ishii, F. F. Pérez and T. Suzuki (2016). The Global Ocean Data Analysis Project version 2 (GLODAPv2) - an internally consistent data product for the world ocean, *Earth System Science Data*, 8, 297-323, https://doi.org/10.5194/essd-8-297-2016.

Pavlov A., D. Faller, M. Erfurt, T. Lane, J. Hasdell and J. E. Collins (2024) Growing demand for environmental science expertise in the corporate sector. *Nat Rev Earth Environ*. https://doi.org/10.1038/s43017-024-00526-0

Rabiner, L.R., M.R. Sambur, and C.E. Schmidt (1975). Applications of a non-linear smoothing algorithm to speech processing, *IEEE Trans. on Acoustics, Speech and Signal Processing*, 23, 552-557. [PDF]

Reagan, J. R.; T.P. Boyer, H.G. García, R. Locarnini, O.K. Baranova, C. Bouchard, S.L. Cross, A.V. Mishonov, C.R. Paver, D. Seidov, Z. Wang, and Dukhovskoy (2023). World Ocean Atlas 2023. [indicate subset used]. NOAA National Centers for Environmental Information. Dataset. https://doi.org/10.25921/va26-hv25

Reagan, J.R., D. Seidov, Z. Wang, D. Dukhovskoy, T.P. Boyer, R.A. Locarnini, O.K. Baranova, A.V. Mishonov, H.E. Garcia, C. Bouchard, S.L. Cross, and C.R. Paver. (2024a). World Ocean Atlas 2023, Volume 2: Salinity. A. Mishonov, Tech. Ed., *NOAA Atlas NESDIS 90*, 51pp. https://doi.org/10.25923/70qt-9574

Reagan, J.R., D. Seidov, Z. Wang, T.P. Boyer, R.A. Locarnini, O.K. Baranova, A.V. Mishonov, H.E. Garcia, C. Bouchard, S.L. Cross, C.R. Paver, and D. Dukhovskoy (2024b). World Ocean Atlas 2023, Volume 6: Conductivity. A. Mishonov Tech. Ed. *NOAA Atlas NESDIS 94*, https://doi.org/10.25923/wz4d-6x65

Redfield A., B. Ketchum, and F. Richards (1963). The influence of organisms on the composition of seawater*, In The Sea*, *Vol. 2*, pp 224-228, N. Hill, Ed. Inter-science, New York.

Reiniger, R.F. and C.F. Ross (1968). A method of interpolation with application to oceanographic data. *Deep-Sea Res*., 9, 185-193. https://doi.org/10.1016/0011-7471(68)90040-5

Riebesell U., A. Körtzinger, and A. Oschlies (2009). Sensitivities of marine carbon fluxes to ocean change. *Proc. U.S. Natl. Acad. Sci*., 106:20602-20609. https://doi.org/10.1073/pnas.0813291106

Sarmiento J.L., Kenneth S. Johnson, Lionel A. Arteaga, Seth M. Bushinsky, Heidi M. Cullen, Alison R. Gray, Roberta M. Hotinski, Tanya L. Maurer, Matthew R. Mazloff, Stephen C. Riser,

Joellen L. Russell, Oscar M. Schofield, Lynne D. Talley (2023) The Southern Ocean carbon and climate observations and modeling (SOCCOM) project: A review. *Progress in Oceanography*, https://doi.org/10.1016/j.pocean.2023.

Sasaki, Y. (1960). An objective analysis for determining initial conditions for the primitive equations. Ref. 60-1 6T, Atmospheric Research Lab., *Univ. of Oklahoma Research Institute*, Norman, 23 pp.

Saunders, P. M. (1986). The accuracy of measurement of salinity, oxygen and temperature in the deep ocean. *J. Phys. Oceanography* 16(1):189-195. https://doi.org/10.1175/1520-0485(1986)016<0189:TAOMOS>2.0.CO;2

Schmidtko, S., L. Stramma, and M. Visbeck (2017). Decline in global oceanic oxygen content during the past five decades. *Nature* 542: 335-339, https://doi.org/10.1038/nature21399.

Schuckmann K. *et al.* (2020) Heat stored in the Earth system: where does the energy go*? Earth Syst. Sci. Data,* 12, 2013–2041, https://doi.org/10.5194/essd-12-2013-2020

Schuckmann K. *et al.* (2023) Heat stored in the Earth system 1960–2020: where does the energy go? *Earth Syst. Sci. Data*, https://doi.org/10.5194/essd-15-1675-2023

Schudlich, R., and Emerson, S. (1996). Gas supersaturation in the surface ocean: The roles of heat flux, gas exchange, and bubbles. *Deep Sea Research Part II: Topical Studies in Oceanography*, 43(2-3), 569-589. https://doi.org/10.1016/0967-0645(95)00098-4

Seaman, R.S. (1983). Objective Analysis accuracies of statistical interpolation and successive correction schemes. *Australian Meteor. Mag*., 31, 225-240.

Shaffer G., S.M. Olsen, and J.O.P. Pedersen (2009). Long-term ocean oxygen depletion in response to carbon dioxide emissions from fossil fuels. *Nature geoscience*, https://doi.org/10.1038/ngeo420.

Sharp, J. D. Fassbender, A. J. Carter, B. R., Johnson, G. C., Schultz, C., Dunne, J. P. (2022). GOBAI-O2: A Global Gridded Monthly Dataset of Ocean Interior Dissolved Oxygen Concentrations Based on Shipboard and Autonomous Observations (NCEI Accession 0259304). v1.0. NOAA National Centers for Environmental Information. Dataset. https://doi.org/10.25921/z72m-yz67

Sharp, J. D., Fassbender, A. J., Carter, B. R., Johnson, G. C., Schultz, C., and Dunne, J. P. (2023) GOBAI-O_2: temporally and spatially resolved fields of ocean interior dissolved oxygen over nearly 2 decades, *Earth Syst. Sci. Data*, 15, 4481–4518, https://doi.org/10.5194/essd-15-4481-2023

Shuman, F.G. (1957). Numerical methods in weather prediction: II. Smoothing and filtering. *Mon. Wea. Rev.*, 85, 357-361. https://doi.org/10.1175/1520-0493(1957)085%3C0357:NMIWPI%3E2.0.CO;2

Schlitzer, R., Ocean Data View, odv.awi.de, (2023).

Smith, D.R. and F. Leslie (1984). Error determination of a successive correction type objective analysis scheme. *J Atm. and Oceanic Tech*., 1, 121-130. https://doi.org/10.1175/1520-0426(1984)001<0120:EDOASC>2.0.CO;2

Smith, D.R., M.E. Pumphrey, and J.T. Snow (1986). A comparison of errors in objectively analyzed fields for uniform and nonuniform station distribution, *J. Atm. Oceanic Tech*., 3, 84-97. https://doi.org/10.1175/1520-0426(1986)003<0084:ACOEIO>2.0.CO;2

Stramma, L., G.C. Johnson, J. Sprintall, and V. Mohrholz (2008). Expanding Oxygen-Minimum Zones in the Tropical Oceans. *Science*, 320(5876):655–658. doi:10.1126/science.115384.

Stramma, L., E. D. Prince, S. Schmidtko, J. Luo, J. P. Hoolihan, M. Visbeck, D. W. Wallace, P. Brandt, and A. Körtzinger (2012). Expansion of oxygen minimum zones may reduce available habitat for tropical pelagic fishes. *Nature Climate Change* 2:33-37, https://doi.org/10.1038/nclimate1304.

Sverdrup, H.U., M.W. Johnson, and R.H. Fleming (1942). The Oceans: Their physics, chemistry, and general biology. *Prentice Hall*, 1060 pp.

Takano Y, T. Ilyina J. Tjiputra, YA Eddebbar, *et al.* (2023) Simulations of ocean deoxygenation in the historical era: insights from forced and coupled models. *Front. Mar. Sci.* 10:1139917. https://doi.org/10.3389/fmars.2023.1139917

Thiebaux, H.J. and M.A. Pedder (1987). Spatial Objective Analysis: with applications in atmospheric science. *Academic Press*, 299 pp.

Thierry V., H. Bittig, and the BGC-ARGO Team (2016). Argo quality control manual for dissolved oxygen concentration. http://doi.org/10.13155/46542

Thierry V., H. Bittig, and the BGC-ARGO team (2021). Argo Quality Control Manual for Dissolved Oxygen Concentration, v2.1 http://dx.doi.org/10.13155/46542

Trenberth, K. E., and L. Smith. (2005). The Mass of the Atmosphere: A Constraint on Global Analyses. *Journal of Climate*, 18(6), 864–875. http://www.jstor.org/stable/26253433

Tukey, J.W. (1974). Non-linear (non-superposable) methods for smoothing data, in "Cong. Rec.", 1974 *EASCON*, 673 pp.

Uchida, H., G.C. Johnson, and K.E. McTaggart. (2010). "CTD oxygen sensor calibration procedures," in The GO-SHIP Repeat Hydrography Manual: A Collection of Expert Reports and Guidelines, IOCCP Report Number 14. ICPO Publication Series Number 134, eds E. M. Hood, C. L. Sabine, and B. M. Sloyan. Available online at: http://www.go-ship.org/HydroMan.html

Wang, Z., Garcia, H. E., Boyer, T. P., Reagan, J., and Cebrian, J. (2022). Controlling factors of the climatological annual cycle of the surface mixed layer oxygen content: A global view. *Front. Mar. Sci.*, https://doi.org/10.3389/fmars.2022.1001095

Wilkinson, M., Dumontier, M., Aalbersberg, I. *et al. (*2016). The FAIR Guiding Principles for scientific data management and stewardship. *Sci Data* 3, 160018. https://doi.org/10.1038/sdata.2016.18

Winkler, L.W. (1888). Die Bestimmung des in Wasser gelösten Sauerstoffen. *Berichte der Deutschen Chemischen Gesellschaft*, 21, 2843–2855. https://doi.org/10.1002/cber.188802102122

Wishner K.F., B. A. Seibel, C. Roman, *et al.* (2018). Ocean deoxygenation and zooplankton: Very small oxygen differences matter. *Science Advances*, Vol 4, Issue 12, doi:10.1126/sciadv.aau5180

Wessel, P., and W.H.F. Smith. (1998). New, improved version of Generic Mapping Tools released, *EOS Trans*. Amer. Geophys. U., 79, 579. https://doi.org/10.1029/98EO00426

Wong, A. P., Gilson, J., and Cabanes, C. (2023). Argo salinity: bias and uncertainty evaluation. *Earth System Science Data*, 15(1), 383-393. https://doi.org/10.5194/essd-15-383-2023

8. TABLES

Table 1a. Number of available O_2 profiles and observations at standard depth levels in the WOD23 spanning the 1965-2022 time period before quality control.
Notes: About 92% of the available profiles were collected on or after 1965 and 2022. Table 1e provides definitions for each dataset in the WOD23. Prior to 1965, there are 177,779 O_2 profiles in the OSD dataset.

Dataset	Number of profiles	Number of observations
OSD	794,191	24,405,895
CTD	214,674	7,583,972
PFL	234,519	4,271,208
GLD	1,050,877	18,048,720
DRB	38,989	1,029,882
UOR	361	10,452
Total	2,333,611	55,350,129

Table 1b. Number of O_2 profiles and observations at standard depth levels in the WOD23 datasets for the 1965-2022 time period after quality control and used in the WOA23.
Notes: Table 1e defines the WOD23 datasets. Garcia *et al.* (2024b) provides a technical manual of the WOD23 (Mishonov *et al.* 2024).

WOD23 Dataset	Number of profiles	Number of observations
OSD	678,837	14,178,451
CTD	178,530	5,715,648
PFL	135,649	7,468,426
Total	993,016	27,362,525

Table 1c. Datasets in the WOD23 with O_2 measurements.

Datasets	Description	WOA23F (year span)	WOA23N (year span)
OSD	Ocean Station Data, Low-resolution CTD	√ 1965-2022	√ 1971-2000
CTD	High-resolution Conductivity-Temperature-Depth	√ 1987-2022	√ 1987-2000
PFL	Profiling float data (Argo/BGC-Argo)	√ 2005-2022	
DRB	Drifting buoy data	Dissolved O_2 data from DRB, MRB, SUR, and UOR will be added to future WOA O_2 as schematically shown in Figure 1a.	
MRB	Moored buoy data		
SUR	Surface-only data		
UOR	Undulating Oceanographic Recorder data		

Table 1d. Depth-dependent measured variables present in the WOD23.

Variable (abbreviations)	Standard unit (abbreviation)	Dataset(s) where variable(s) is/are stored
Temperature	Degrees Celsius (°C)	OSD, CTD, MBT, XBT, SUR, APB, MRB, PFL, UOR, DRB, GLD
Salinity	Dimensionless	OSD, CTD, SUR, MRB, PFL, UOR, DRB, GLD
Oxygen	Micro-mol kilogram^{-1} (μmol·kg^{-1})	OSD, CTD, PFL, UOR, DRB
Phosphate	Micro-mol kilogram^{-1} (μmol·kg^{-1})	OSD
Silicate	Micro-mol kilogram^{-1} (μmol·kg^{-1})	OSD
Nitrate, Nitrate + Nitrite	Micro-mol kilogram^{-1} (μmol·kg^{-1})	OSD, PFL
pH	Dimensionless	OSD, SUR
Chlorophyll	Micro-gram per liter (μg·l^{-1})	OSD, CTD, SUR, UOR, DRB
Alkalinity	Milli-mole liter^{-1} (mmol·l^{-1})	OSD, SUR
Partial pressure of carbon dioxide	Micro-atmosphere (μatm)	OSD, SUR
Dissolved Inorganic carbon	Milli-mole liter^{-1} (mmol·l^{-1})	OSD
Transmissivity (Beam Attenuation Coefficient)	Per meter (m^{-1})	CTD
Pressure	Deci-bar	OSD, CTD, UOR, GLD, PFL, DRB
Air temperature	Degree Celsius (°C)	SUR
xCO_2atmosphere	Parts per million (ppm)	SUR
Air pressure	Milli-bar (mbar)	SUR
Latitude	Degrees	SUR, APB, UOR
Longitude	Degrees	SUR, APB, UOR
Julian year-day[1]	Day	SUR, APB, UOR
Tritium [^{3}H]	Tritium Unit (TU)	OSD
Helium [He]	Nano-mol kilogram^{-1} (nmol·kg^{-1})	OSD
Delta Helium-3 [Δ^3He]	Percent (%)	OSD
Delta Carbon-14 [Δ^{14}C]	Per mille (‰); parts per thousand	OSD
Delta Carbon-13 [Δ^{13}C]	Per mille (‰); parts per thousand	OSD
Argon	Nano-mol kilogram^{-1} (nmol·kg^{-1})	OSD
Neon	Nano-mol kilogram^{-1} (nmol·kg^{-1})	OSD
Chlorofluorocarbon 11	Pico-mol kilogram^{-1} (pmol·kg^{-1})	OSD
Chlorofluorocarbon 12	Pico-mol kilogram^{-1} (pmol·kg^{-1})	OSD
Chlorofluorocarbon 113	Pico-mol kilogram^{-1} (pmol·kg^{-1})	OSD
Delta Oxygen-18 [Δ^{18}O]	Per mille (‰); parts per thousand	OSD

[1] Julian year-day is the decimal day for the year in which the observations were made

Table 1e. Dataset definitions in the WOD23

DATASETS	DATASETS INCLUDES	WOA23F	WOA23N
OSD	Ocean Station Data, Low-resolution CTD/XCTD, Plankton data	√ 1965-2022	√ 1965-2000
CTD	High-resolution Conductivity-Temperature-Depth / XCTD data	√ 1987-2022	√ 1987-2000
PFL	Profiling float data such as Argo and BGC-Argo	√ 2005-2022	
MBT	Mechanical / Digital / Micro Bathythermograph data		
XBT	Expendable Bathythermograph data		
SUR	Surface-only data		
APB	Autonomous Pinniped data		
MRB	Moored buoy data		
DRB	Drifting buoy data		
UOR	Undulating Oceanographic Recorder data		
GLD	Glider data		

Table 2. Descriptions of climatologies for dissolved oxygen (O_2), Apparent Oxygen Utilization (AOU), and oxygen saturation (%) in the WOA23.

Variable	Depths for Annual Climatology	Depths for Seasonal Climatology	Depths for Monthly Climatology
O_2, AOU, and O2S	0-5500 m (102 levels)	0-1500 m (57 levels)	0-1500 m (57 levels)

Table 3. Acceptable distances (m) for defining interior (A) and exterior (B) values used in the Reiniger-Ross scheme for interpolating observed level data to standard levels used in the WOD23.

Standard Level #	Standard Depths (m)	A	B	Standard Level #	Standard Depths (m)	A	B
1	0	50	200	52	1250	200	400
2	5	50	200	53	1300	200	1000
3	10	50	200	54	1350	200	1000
4	15	50	200	55	1400	200	1000
5	20	50	200	56	1450	200	1000
6	25	50	200	57	1500	200	1000
7	30	50	200	58	1550	200	1000
8	35	50	200	59	1600	200	1000
9	40	50	200	60	1650	200	1000
10	45	50	200	61	1700	200	1000
11	50	50	200	62	1750	200	1000
12	55	50	200	63	1800	200	1000
13	60	50	200	64	1850	200	1000
14	65	50	200	65	1900	200	1000
15	70	50	200	66	1950	200	1000
16	75	50	200	67	2000	1000	1000
17	80	50	200	68	2100	1000	1000
18	85	50	200	69	2200	1000	1000
19	90	50	200	70	2300	1000	1000
20	95	50	200	71	2400	1000	1000
21	100	50	200	72	2500	1000	1000
22	125	50	200	73	2600	1000	1000
23	150	50	200	74	2700	1000	1000

Standard Level #	Standard Depths (m)	A	B	Standard Level #	Standard Depths (m)	A	B
24	175	50	200	75	2800	1000	1000
25	200	50	200	76	2900	1000	1000
26	225	50	200	77	3000	1000	1000
27	250	100	200	78	3100	1000	1000
28	275	100	200	79	3200	1000	1000
29	300	100	200	80	3300	1000	1000
30	325	100	200	81	3400	1000	1000
31	350	100	200	82	3500	1000	1000
32	375	100	200	83	3600	1000	1000
33	400	100	200	84	3700	1000	1000
34	425	100	200	85	3800	1000	1000
35	450	100	200	86	3900	1000	1000
36	475	100	200	87	4000	1000	1000
37	500	100	400	88	4100	1000	1000
38	550	100	400	89	4200	1000	1000
39	600	100	400	90	4300	1000	1000
40	650	100	400	91	4400	1000	1000
41	700	100	400	92	4500	1000	1000
42	750	100	400	93	4600	1000	1000
43	800	100	400	94	4700	1000	1000
44	850	100	400	95	4800	1000	1000
45	900	200	400	96	4900	1000	1000
46	950	200	400	97	5000	1000	1000
47	1000	200	400	98	5100	1000	1000
48	1050	200	400	99	5200	1000	1000
49	1100	200	400	100	5300	1000	1000
50	1150	200	400	101	5400	1000	1000
51	1200	200	400	102	5500	1000	1000

Table 4. Response function of the objective analysis scheme as a function of wavelength for the WOA23 and earlier WOA analyses. The response function is normalized to 1.0.

Wavelength[1]	**Levitus (1982)**	**WOA94**	**WOA98, 01, 05, 09, 13, 18, 23**
360ΔX	1.000	0.999	1.000
180ΔX	1.000	0.997	0.999
120ΔX	1.000	0.994	0.999
90ΔX	1.000	0.989	0.998
72ΔX	1.000	0.983	0.997
60ΔX	1.000	0.976	0.995
45ΔX	1.000	0.957	0.992
40ΔX	0.999	0.946	0.990
36ΔX	0.999	0.934	0.987
30ΔX	0.996	0.907	0.981
24ΔX	0.983	0.857	0.969
20ΔX	0.955	0.801	0.952
18ΔX	0.923	0.759	0.937
15ΔX	0.828	0.671	0.898
12ΔX	0.626	0.532	0.813
10ΔX	0.417	0.397	0.698
9ΔX	0.299	0.315	0.611
8ΔX	0.186	0.226	0.500
6ΔX	3.75×10^{-2}	0.059	0.229
5ΔX	1.34×10^{-2}	0.019	0.105
4ΔX	1.32×10^{-3}	2.23×10^{-3}	2.75×10^{-2}
3ΔX	2.51×10^{-3}	1.90×10^{-4}	5.41×10^{-3}
2ΔX	5.61×10^{-7}	5.30×10^{-7}	1.36×10^{-6}

[1]For ΔX = 111 km, the meridional separation at the Equator.

Table 5. Basins defined for objective analysis and the shallowest standard depth level for which each ocean basin is defined.

#	Basin[1]	Standard Depth Level	#	Basin[1]	Standard Depth Level
1	Atlantic Ocean	1*	31	West European Basin	82
2	Pacific Ocean	1*	32	Southeast Indian Basin	82
3	Indian Ocean	1*	33	Coral Sea	82
4	Mediterranean Sea	1*	34	East Indian Basin	82
5	Baltic Sea	1	35	Central Indian Basin	82
6	Black Sea	1	36	Southwest Atlantic Basin	82
7	Red Sea	1	37	Southeast Atlantic Basin	82
8	Persian Gulf	1	38	Southeast Pacific Basin	82
9	Hudson Bay	1	39	Guatemala Basin	82
10	Southern Ocean	1*	40	East Caroline Basin	87
11	Arctic Ocean	1	41	Marianas Basin	87
12	Sea of Japan	1	42	Philippine Sea	87
13	Kara Sea	22	43	Arabian Sea	87
14	Sulu Sea	25	44	Chile Basin	87
15	Baffin Bay	37	45	Somali Basin	87
16	East Mediterranean	41	46	Mascarene Basin	87
17	West Mediterranean	47	47	Crozet Basin	87
18	Sea of Okhotsk	47	48	Guinea Basin	87
19	Banda Sea	55	49	Brazil Basin	92
20	Caribbean Sea	55	50	Argentine Basin	92
21	Andaman Basin	62	51	Tasman Sea	87
22	North Caribbean	67	52	Atlantic Indian Basin	92
23	Gulf of Mexico	67	53	Caspian Sea	1
24	Beaufort Sea	77	54	Sulu Sea II	37
25	South China Sea	77	55	Venezuela Basin	37
26	Barents Sea	77	56	Bay of Bengal	1*
27	Celebes Sea	62	57	Java Sea	16
28	Aleutian Basin	77	58	East Indian Atlantic Basin	97
29	Fiji Basin	82	59	Chiloe	1
30	North American Basin	82	60	Bransfield Strait	37

[1]Basins marked with a "*" can interact with adjacent basins in the objective analysis.

Table 6. Statistical and objectively analyzed fields calculated for the WOA23F and WOA23N.

Statistical field	One-degree Field Calculated	Five-degree Statistics calculated
Objectively analyzed climatology - Annual	√	
Objectively analyzed climatology - Seasonal		
Objectively analyzed climatology - Monthly		
Statistical mean[1]	√	√
Number of observations	√	√
Seasonal (monthly) climatology minus annual climatology	√	
Standard deviation from statistical mean[1]	√	√
Standard error of the statistical mean	√	√
Statistical mean minus objectively analyzed climatology[1]	√	
Number of mean values within radius of influence	√	
Objectively analyzed climatology: Standard deviation from statistical mean	√	

[1]Statistical fields are only available when the objectively analyzed fields are available for one-degree fields.

Table 7a. Depth averaged difference and standard deviation of the mean for the WOA23F minus WOA18 for O_2, AOU, and O2S in different ocean basins.

Basin	WOA23F minus WOA18 mean ± standard deviation (0-5500 m depth)		
	O_2 (µmol·kg^{-1})	AOU (µmol·kg^{-1})	O2S (%)
Global	-1.03 ± 0.98	1.51 ± 1.04	-0.45 ± 0.35
Atlantic	-1.25 ± 0.96	1.67 ± 1.07	-0.51 ± 0.36
Pacific	-0.79 ± 1.03	1.64 ± 1.23	-0.49 ± 0.44
Indian	-1.14 ± 1.01	1.82 ± 1.46	-0.52 ± 0.36
Arctic	-1.47 ± 1.24	0.58 ± 1.46	-0.14 ± 0.42

Table 7b. Depth averaged difference and standard deviation of the mean WOA23F minus WOA23N for O_2, AOU, and O2S in different ocean basins.

Ocean Basin	WOA23F minus WOA23N depth averaged difference ± standard deviation (0-5500 m depth)		
	O_2 (µmol·kg^{-1})	**O2S (%)**	**AOU (µmol·kg^{-1})**
Global	-1.02 ± 0.73	-0.30 ± 0.25	0.86 ± 0.68
Atlantic	-1.34 ± 0.94	-0.44 ± 0.30	1.29 ± 0.86
Pacific	-1.01 ± 0.86	-0.33 ± 0.29	0.95 ± 0.81
Indian	-1.20 ± 0.83	-0.34 ± 0.31	1.04 ± 0.87
Arctic	-0.11 ± 0.42	0.17 ± 0.26	-0.60 ± 0.91

Table 8. Depth averaged difference and standard deviation of the mean for the WOA23F minus GLODAP in different ocean basins (0-5500 m).

Basin	WOA23F minus GLODAP depth averaged difference ± standard deviation (µmol·kg^{-1}; 0-5500 m depth)
Global	-0.41 ± 0.48
Atlantic	-0.78 ± 0.72
Pacific	0.20 ± 0.42
Indian	-0.57 ± 0.82
Arctic	-2.67 ± 2.63

Table 9. WOA23F global mean O_2 content difference (μmol·kg^{-1}) from GOBAI, WOA23N, WOA18, and GLODAP for selected depth ranges.

	Depth averaged global O_2 differences ± standard deviation (μmol·kg^{-1}) for different depths.		
Mapped Products	**0-2000 m**	**2000-5500 m**	**0-5500 m**
WOA23F - GOBAI	3.14 ± 1.08	No data > 2000 m	No data > 2000 m
WOA23F - WOA23N	-1.43 ± 0.58	-0.25 ± 0.06	-1.02 ± 0.73
WOA23F - WOA18	-1.55 ± 0.81	-0.02 ± 0.10	-1.03 ± 0.98
WOA23F - GLODAP	-0.59 ± 0.36	0.26 ± 0.13	-0.41 ± 0.48

Table 10. WOA23F depth averaged global mean difference between the annual statistical mean of the observations and the objectively analyzed values for O_2, AOU, and O2S**.**

	Mean and standard deviation of the statistical annual mean of the observations minus the objectively analyzed climatological values		
Basin	**O_2 (μmol·kg^{-1})**	**O2S (%)**	**AOU (μmol·kg^{-1})**
Global	0.20 ± 0.28	-0.46 ± 0.93	0.12 ± 0.21
Atlantic	0.20 ± 0.19	-0.41 ± 0.73	0.10 ± 0.16
Pacific	0.16 ± 0.28	-0.48 ± 0.88	0.13 ± 0.22
Indian	0.12 ± 0.39	-0.34 ± 0.84	0.11 ± 0.24
Arctic	0.89 ± 1.05	-0.96 ± 2.68	0.16 ± 0.44

Table 11. WOA23F O_2 and AOU content inventory (Pmol) in different ocean basins (0-5500 m).

		Basin-scale content inventory (Pmol) for the 0-5500 m depth layer	
Basin	**Volume ($\times 10^{18}$ m^3)**	**O_2**	**AOU**
Global	1.3554	238.2	210.9
Atlantic	0.3323	75.8	33.1
Pacific	0.7122	103.7	133.1
Indian	0.2871	51.9	43.2
Arctic	0.0187	5.7	1.1
Antarctic (50°S-90°S)	0.2950	38.1	22.7

Table 12. WOA23 data product series

World Ocean Atlas 2023 Products	Digital Object Identifier (DOI)
Volume 1: Temperature	https://doi.org/10.25923/54bh-1613
Volume 2: Salinity	https://doi.org/10.25923/70qt-9574
Volume 3: Dissolved Oxygen, Apparent Oxygen Utilization, Dissolved Oxygen Saturation, and 30-year Climate Normal (this atlas)	https://doi.org/10.25923/rb67-ns53
Volume 4: Dissolved Inorganic Nutrients (phosphate, nitrate and silicate)	https://doi.org/10.25923/39qw-7j08
Volume 5: Density	https://doi.org/10.25923/mcn4-d695
Volume 6: Conductivity	https://doi.org/10.25923/wz4d-6x65
Volume 7: Mixed Layer Depth	https://doi.org/10.25923/4adh-kq71
Volume 8: Bottom Temperature	https://doi.org/10.25923/s47b-gm86

Table 13. Global mean O_2 solubility content adjustment rate [$\mu mol/(kg \times decade)$] as a function of depth (m).

Depth (m)	**Adjustment rate** $\mu mol/(kg \times decade)$	**Depth (m)**	**Solubility adjustment rate** $\mu mol/(kg \times decade)$
0	-0.50	325	-0.23
5	-0.53	350	-0.22
10	-0.53	375	-0.19
15	-0.53	400	-0.19
20	-0.51	425	-0.19
25	-0.51	450	-0.19
30	-0.50	475	-0.19
35	-0.50	500	-0.18
40	-0.51	550	-0.19
45	-0.50	600	-0.19
50	-0.48	650	-0.20
55	-0.47	700	-0.20
60	-0.46	750	-0.21
65	-0.45	800	-0.16
70	-0.45	850	-0.15
75	-0.43	900	-0.14
80	-0.42	950	-0.14
85	-0.42	1000	-0.13
90	-0.42	1050	-0.13
95	-0.41	1100	-0.13
100	-0.40	1150	-0.13
125	-0.37	1200	-0.12
150	-0.35	1250	-0.11
175	-0.32	1300	-0.11
200	-0.31	1350	-0.10
225	-0.30	1400	-0.10
250	-0.29	1450	-0.09
275	-0.26	1500	-0.08
300	-0.25	> 1500	0.00

9. FIGURES

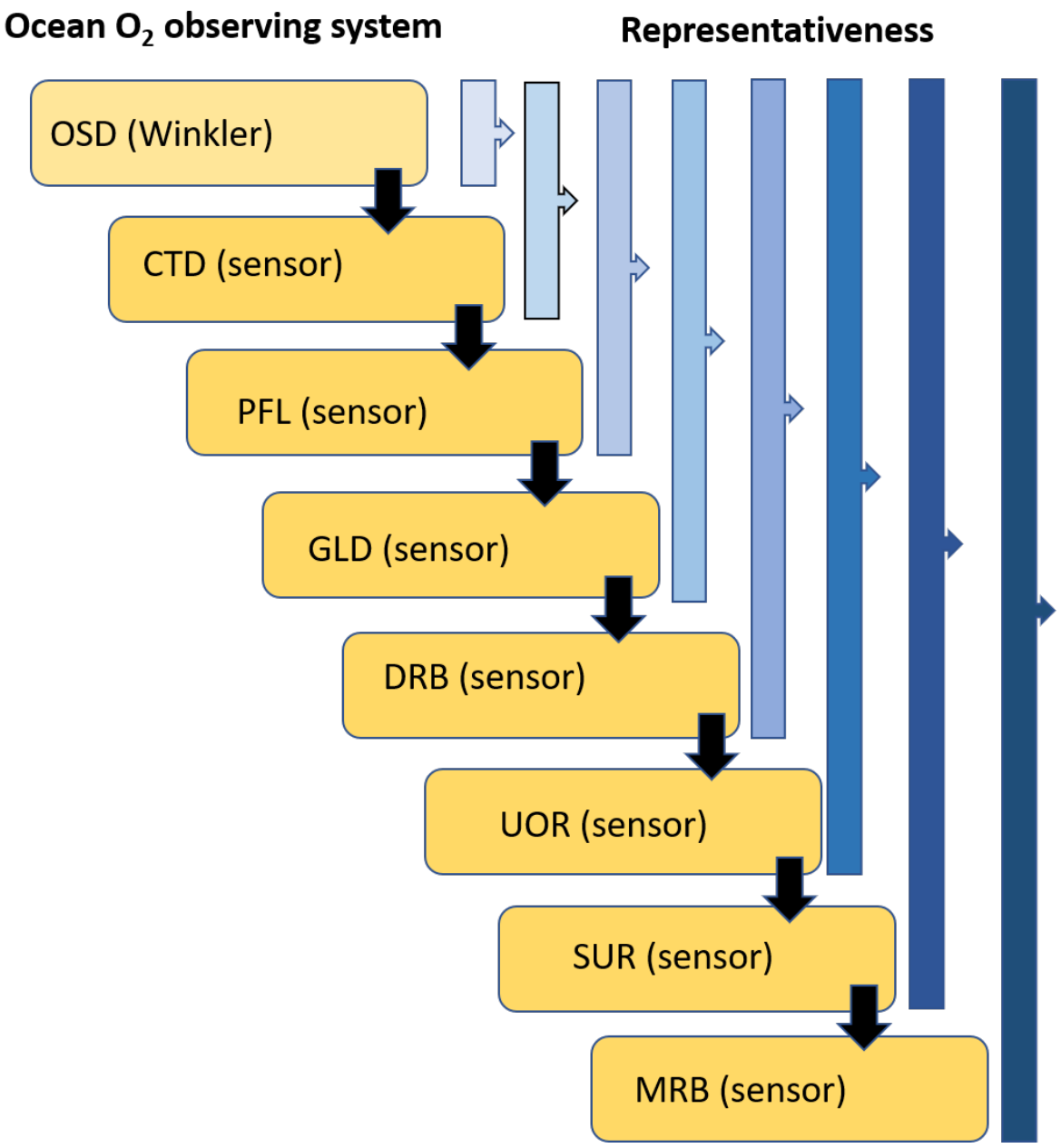

Figure 1a. NOAA's World Ocean Atlas strategic roadmap for developing more comprehensive, representative, and QC O_2 climatologies by blending data from different O_2 observing systems and instruments.
Notes: The WOA23F uses the OSD, CTD, PFL datasets in the WOD23 (See Table 1e for WOD dataset definitions). In future WOA O_2 data products we aim to incorporate additional data from other observing systems such as GLD, DRB, MRB, SUR, UOR.

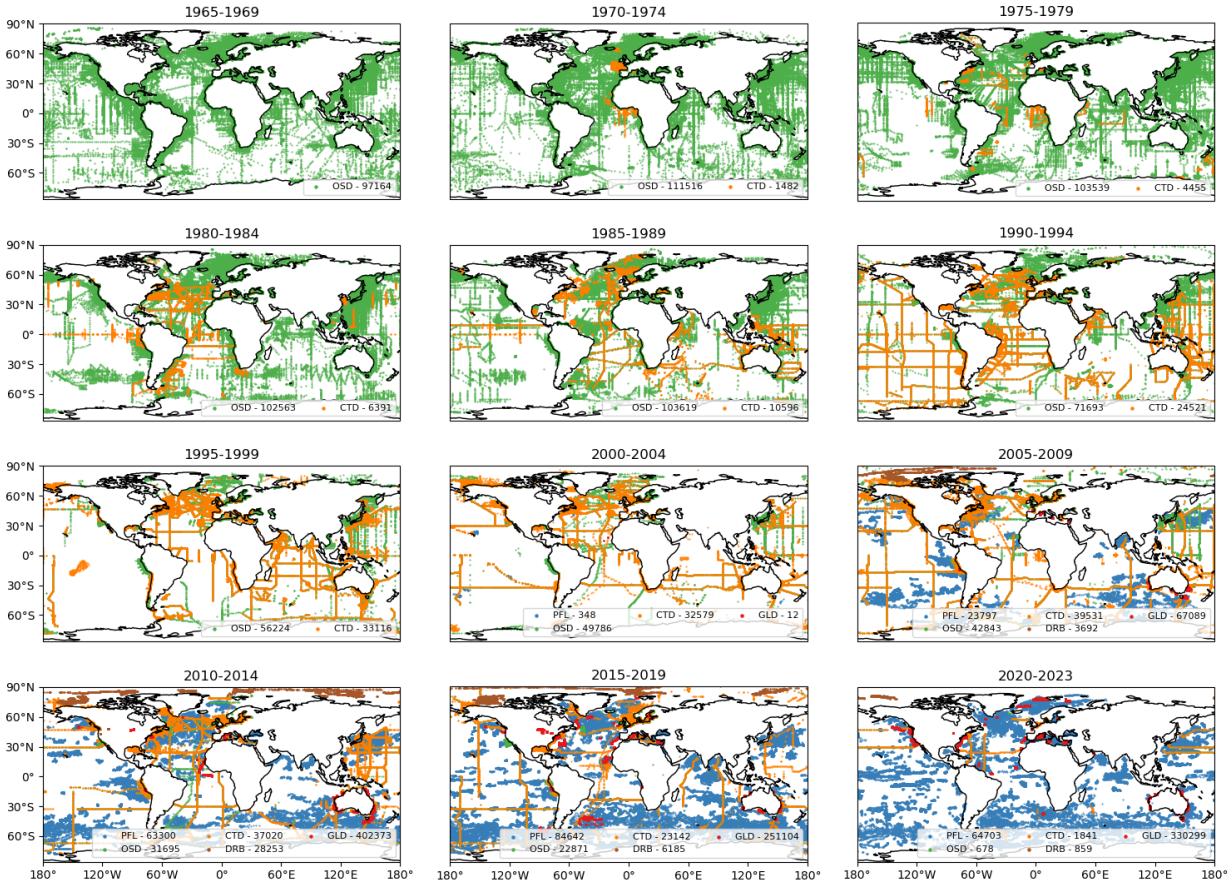

Figure 1b. Number of O_2 profiles after QC from different datasets in the WOD23 binned into 5-year time periods in the 1965 to 2022 time period.
Notes: The different colors represent the number of O_2 profiles in each dataset: OSD, CTD, PFL, DRB, and GLD (shown in Table 1a). Table 1e describes the WOD datasets. The WOA23F uses O_2 data in the OSD (1965-2022), CTD (1987-2022), and PFL (2005-2022) datasets. The WOA23N uses O_2 data in the OSD (1965-2022) and CTD (1987-2022) datasets. Future WOA O_2 climatologies will include data from other WOD datasets (Figure 1a).

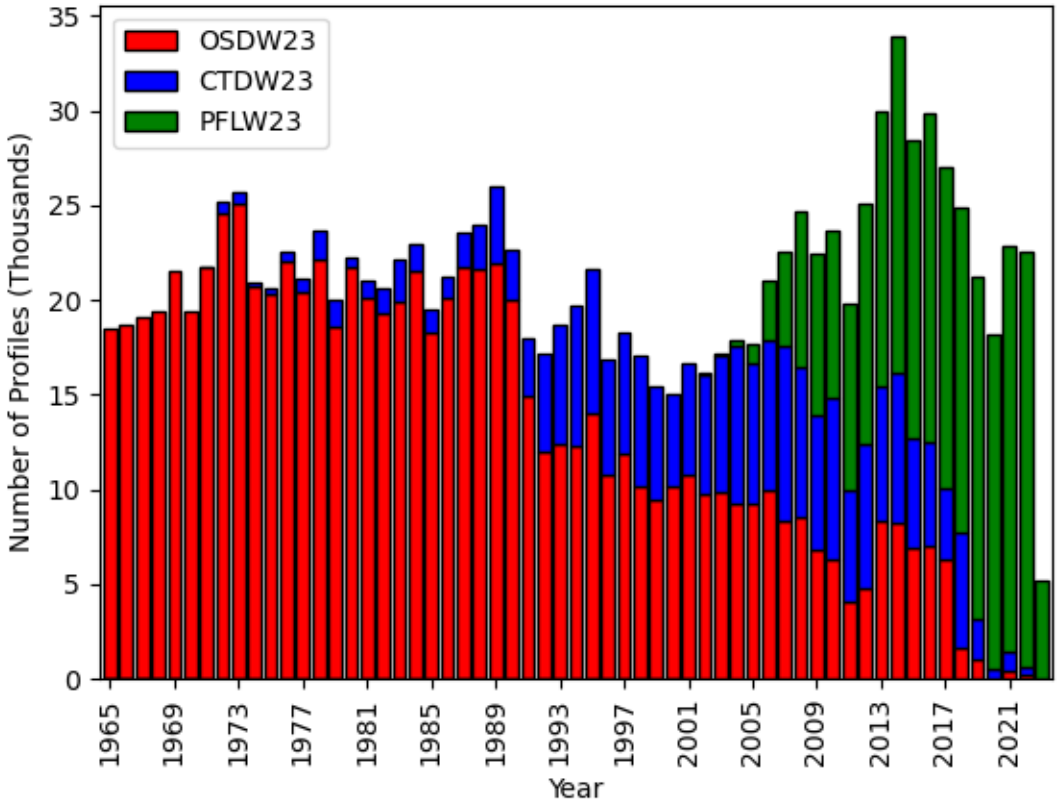

Figure 1c. Number of O_2 profiles per year (1965-2022) in the WOD23 OSD, CTD, and PFL datasets used in the WOA23.

Notes: The different colors represent the number of O_2 profiles from different observation systems. OSD (red bars): ocean station data obtained by Winkler chemical method; CTD (blue bars): data measured on conductivity-temperature-depth rosette; PFL (green bars): profiling float data, from Argo and from the BGC-Argo program. The WOA23F uses quality-controlled O_2 data from OSD (years 1965-2022), CTD (years 1987-2022), and PFL (years 2005-2022). The WOA23N uses quality-controlled O_2 data from OSD (years 1971-2000), CTD (years 1987-2000). The WOD23 has additional sensor-based O_2 measurements derived from gliders (GLD); drifters (DRB), moored buoys (MRB) that were not used in the WOA23 (Table 1c). Table 1b provides the total number of O_2 profiles.

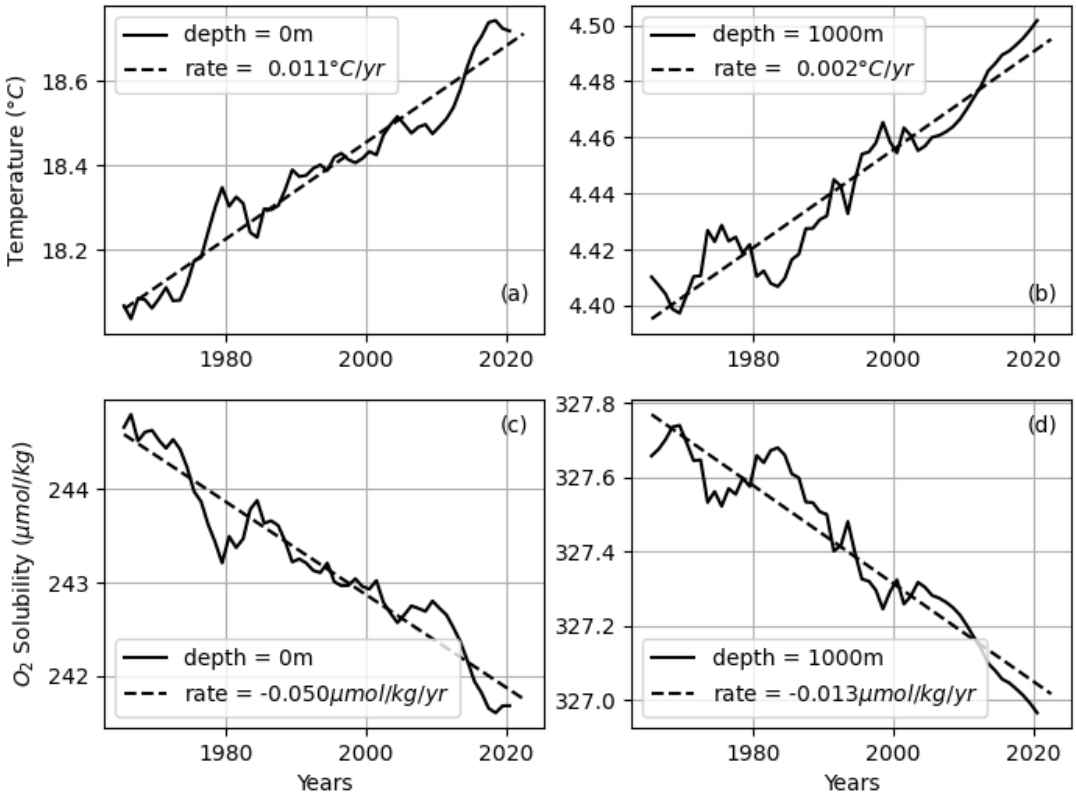

Figure 1d. Global mean temperature increase (°C) and estimated oxygen solubility content (µmol·kg^{-1}) variability and trends between 1965 and 2022 at constant salinity of 35.0.

Notes: (a) Global mean temperature increase at sea surface; (b) global mean temperature increase at 1000 m depth; (c) O_2 solubility content decrease at sea surface; and (d) O_2 solubility content decrease at 1000 m depth (Table 13). The temperature trends are derived from OHC data analysis (Levitus *et al.* 2012).

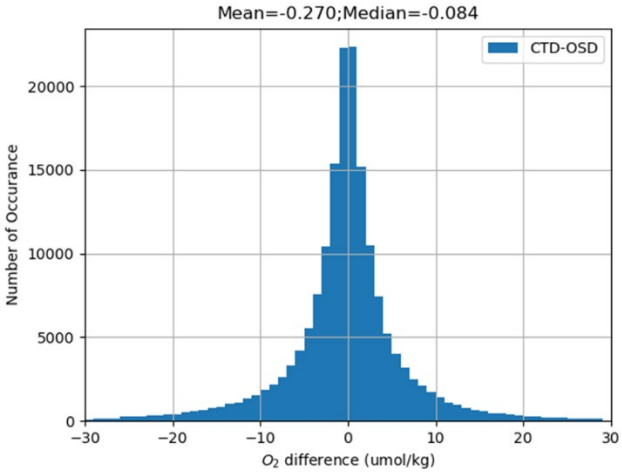

Figure 1e. Histogram of the O_2 content difference (µmol·kg^{-1}) between geographically and temporally matched CTD and OSD station pairs in the WOD23.
Notes: Match criteria: latitude/longitude ±1°; year ± 5; measured in the same month. The O_2 content difference of each matched pair is calculated as the mean in a depth range with minimum T/S variability in a 5° square (same method used in Wong *et al.* 2023). A. Wong (personal communication) provided the 5°×5° depth range for the matchup.

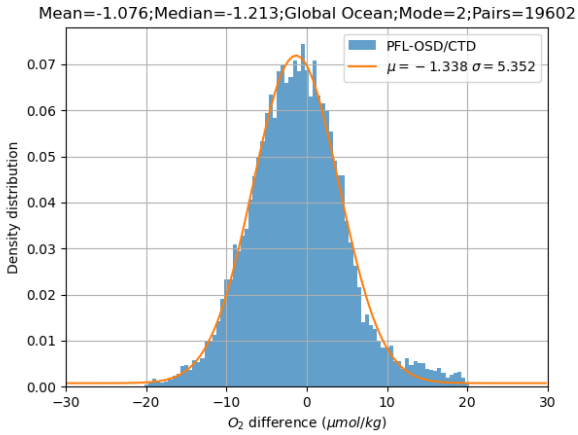

Figure 1f. Histogram of the O_2 content difference (µmol·kg^{-1}) between geographically and temporally matched PFL and OSD/CTD station pairs in the WOD23F.
Notes: Match criteria: latitude/longitude ±1°; year ± 5; measured in the same month. We applied the mean of the Gaussian curve (-1.338 µmol·kg^{-1}) as the global mean adjustment for all Argo and BGC Argo O_2 measurements used in the WOA23F. The O_2 difference of each matched pair is calculated as the mean in a depth range with minimum Temperature and salinity variability in a 5° square following Wong *et al.* (2023). A. Wong (personal communication) provided the 5°×5° depth range for the matchup.

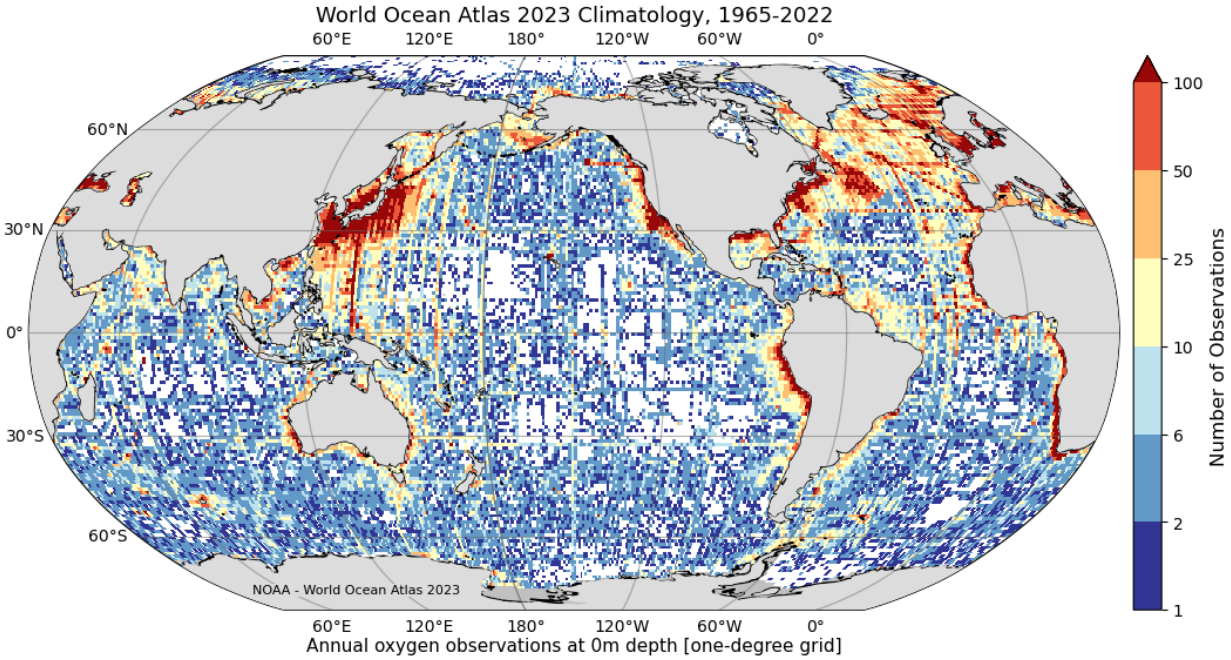

Figure 1g. Spatial distribution of O_2 profiles at the ocean surface.

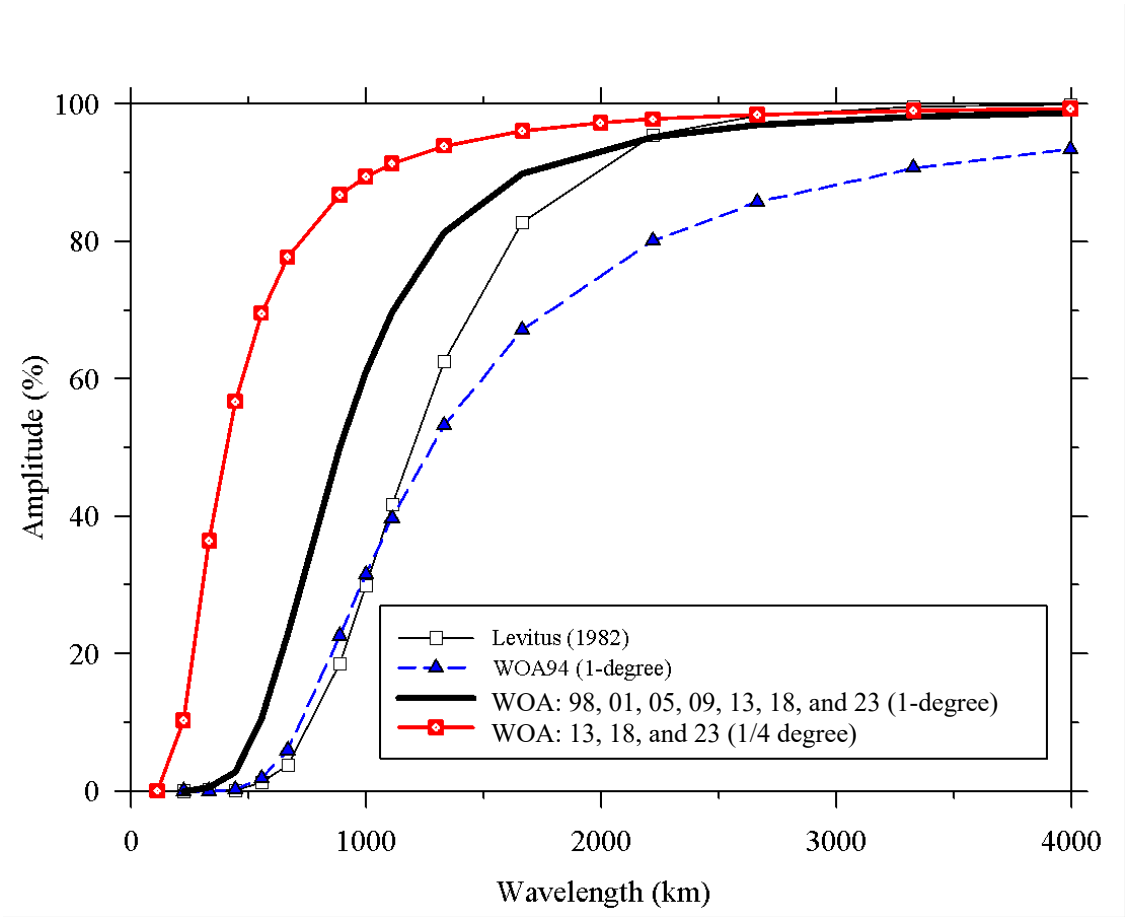

Figure 2. Response function of the WOA23, WOA18, WOA13, WOA05, WOA01, WOA98, WOA94, and Levitus (1982) objective analysis schemes.

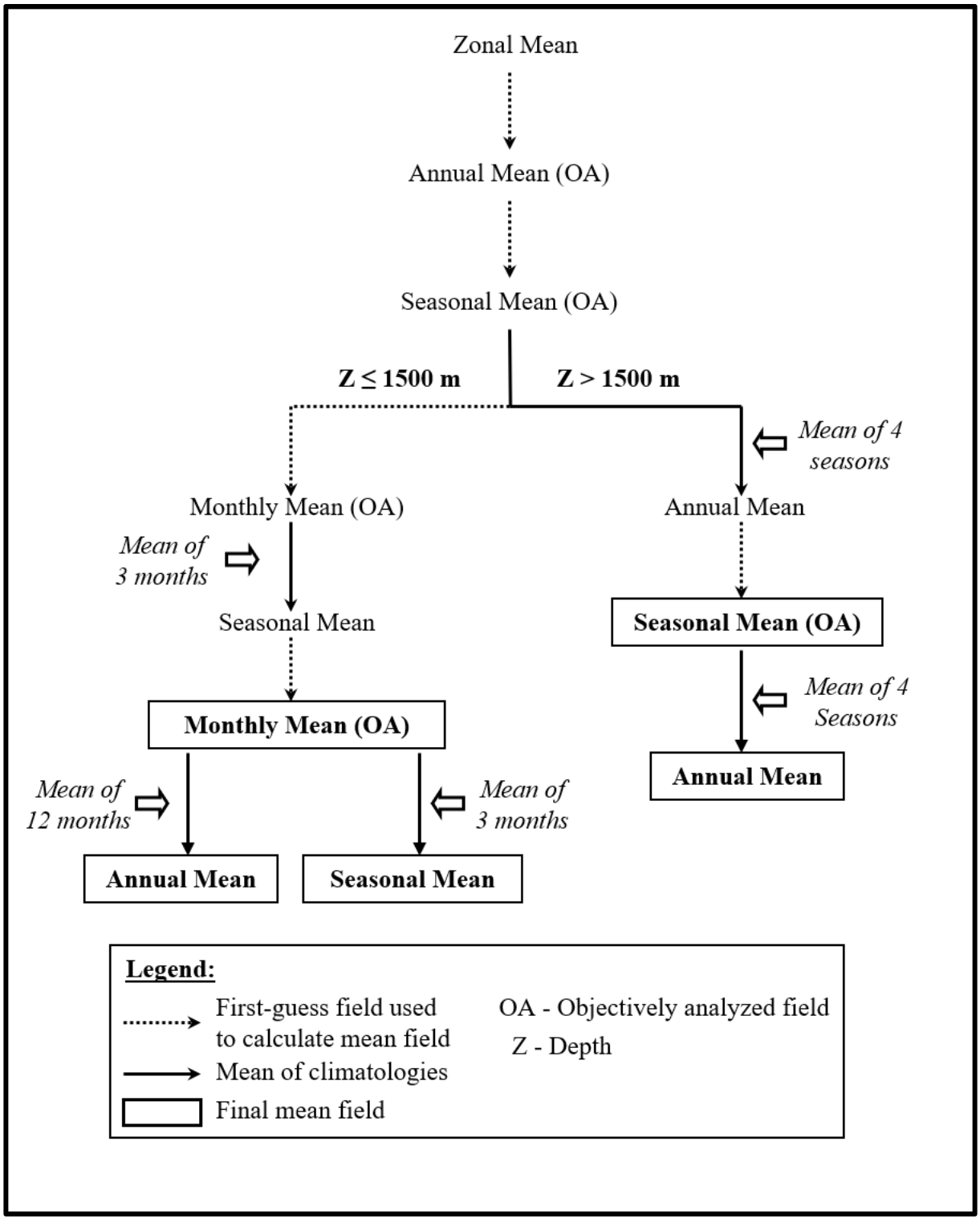

Figure 3. The WOA23 **s**cheme used in computing annual, seasonal, and monthly objectively analyzed means for dissolved oxygen (O_2, μmol·kg^{-1}), Apparent Oxygen Utilization (AOU, μmol·kg^{-1}), and Dissolved Oxygen Saturation (O2S, %).

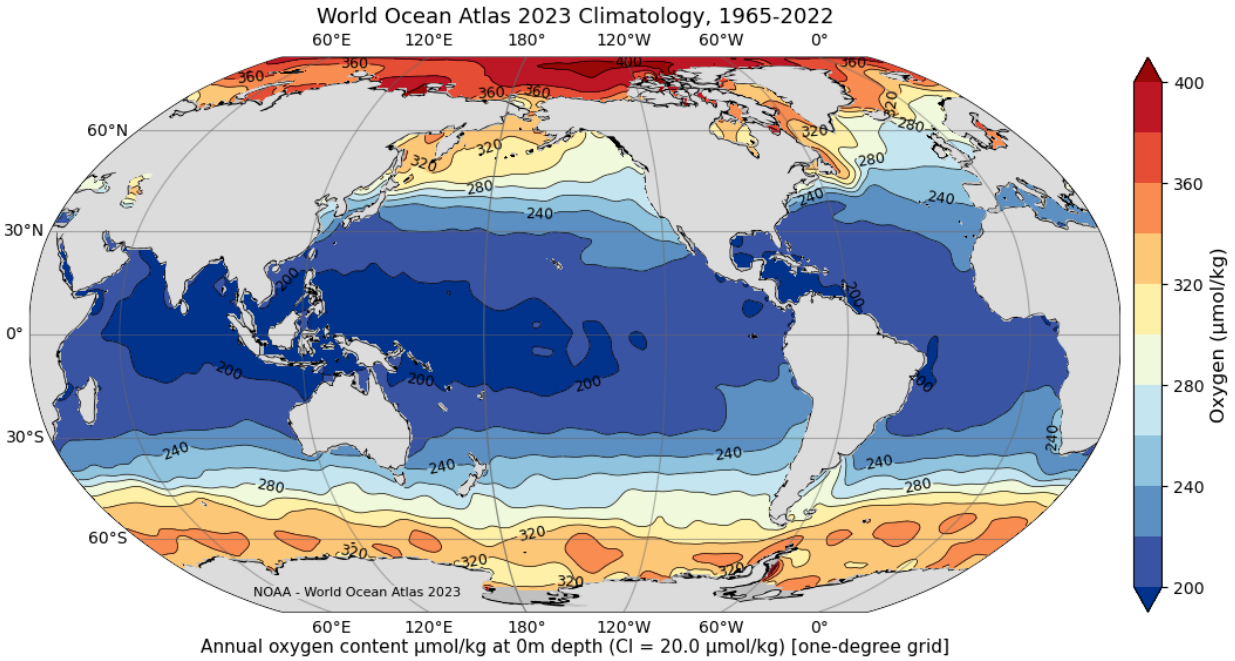

Figure 4a. WOA23F objectively analyzed annual mean O_2 content (µmol·kg^{-1}) at 0 m depth.

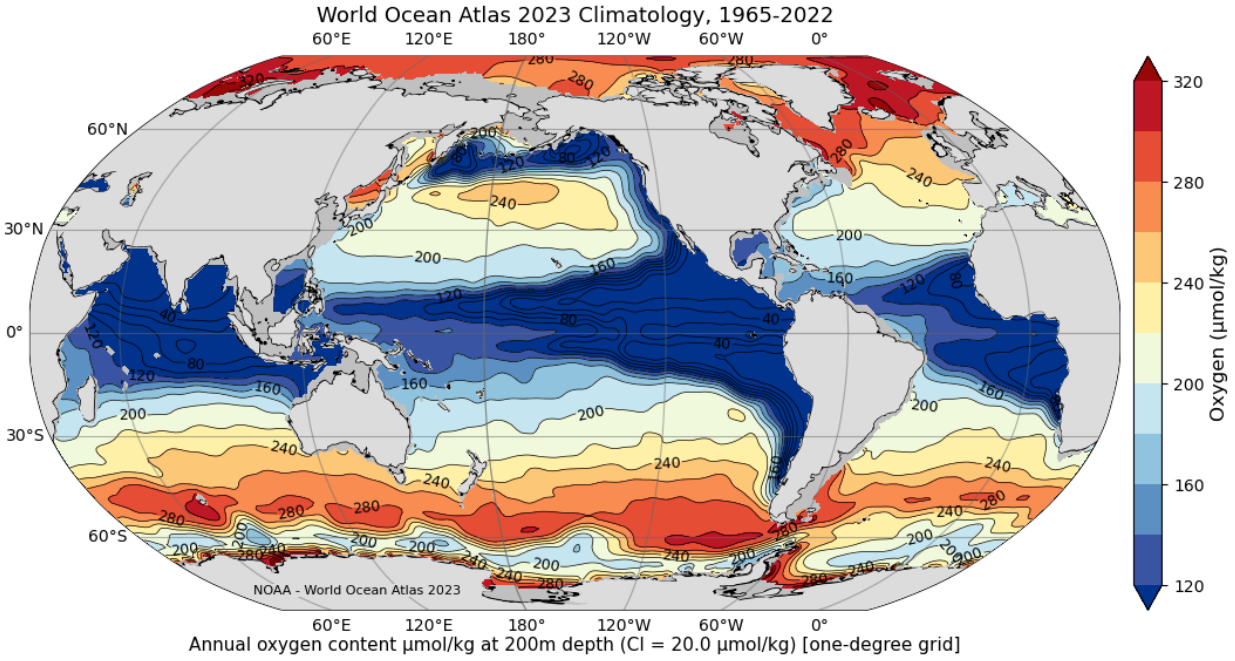

Figure 4b. WOA23F objectively analyzed annual mean O_2 content (µmol·kg^{-1}) at 200 m depth.

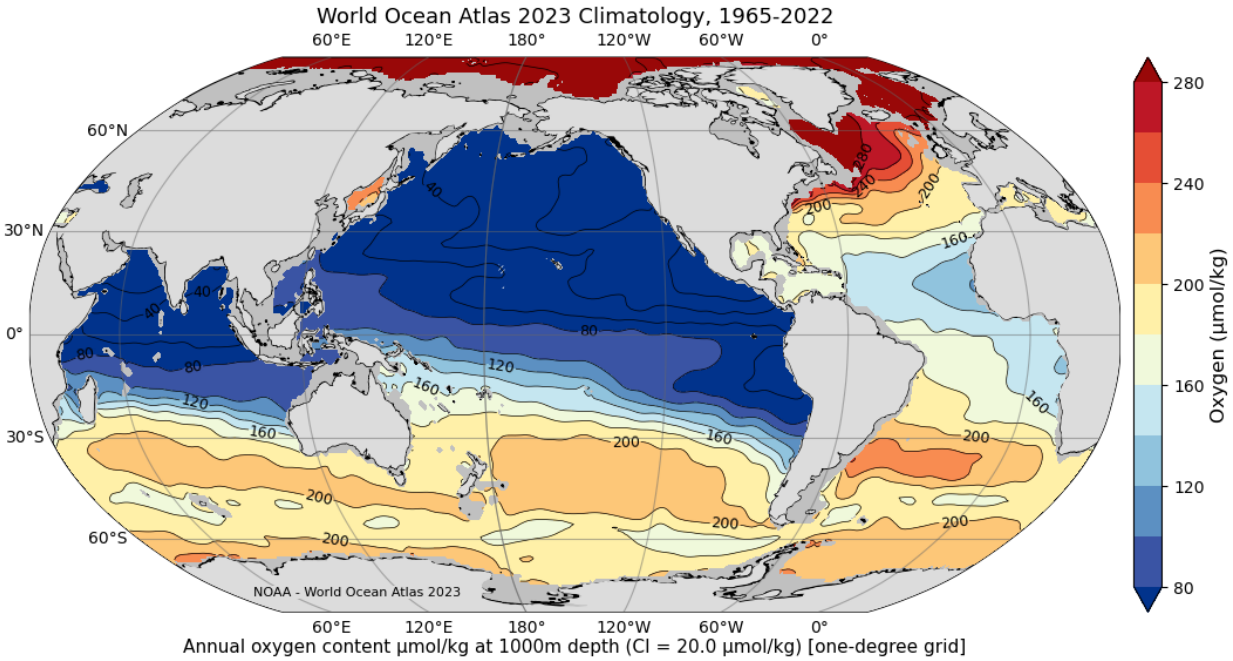

Figure 4c. WOA23F objectively analyzed annual mean O_2 content (µmol·kg^{-1}) at 1000 m depth.

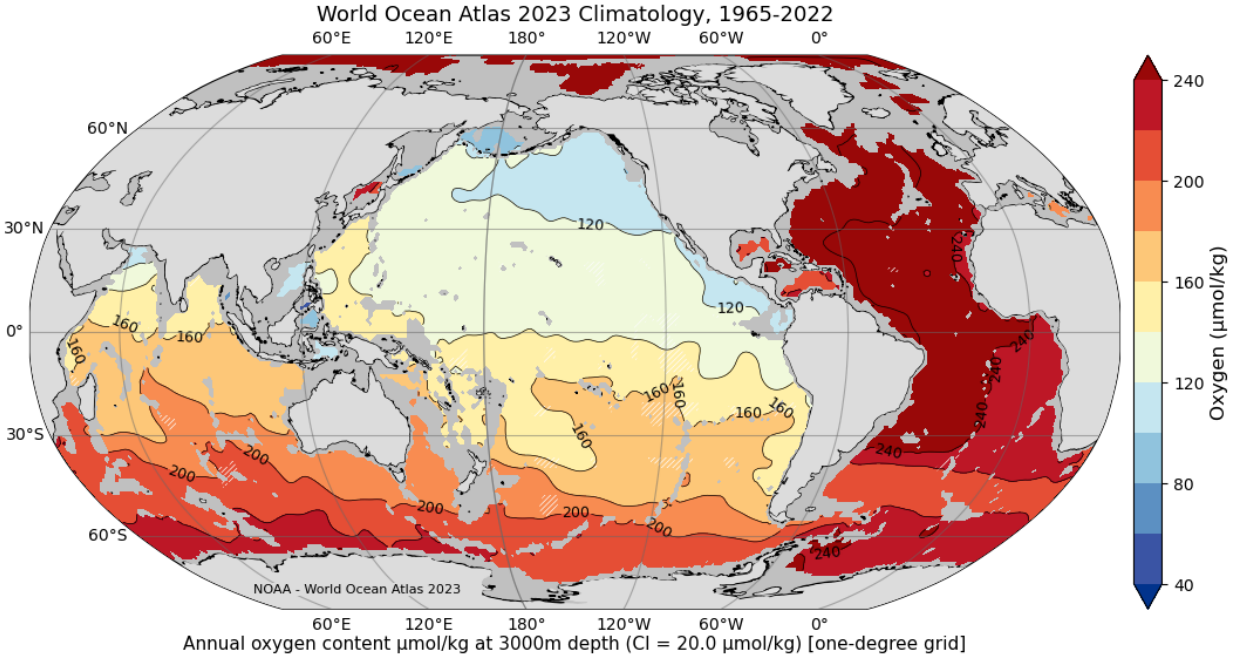

Figure 4d. WOA23F objectively analyzed annual mean O_2 content (µmol·kg^{-1}) at 3000 m depth.

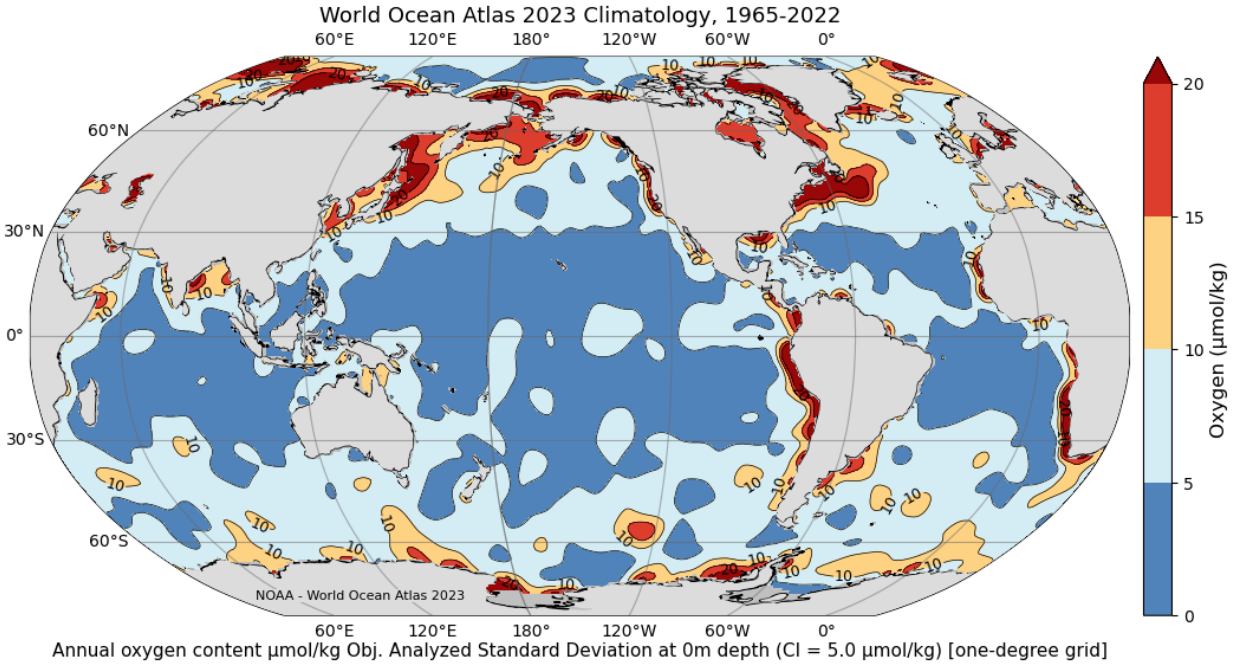

Figure 4e. WOA23F objectively analyzed standard deviation of the statistical annual mean O_2 content ($\mu mol \cdot kg^{-1}$) at 0 m depth .

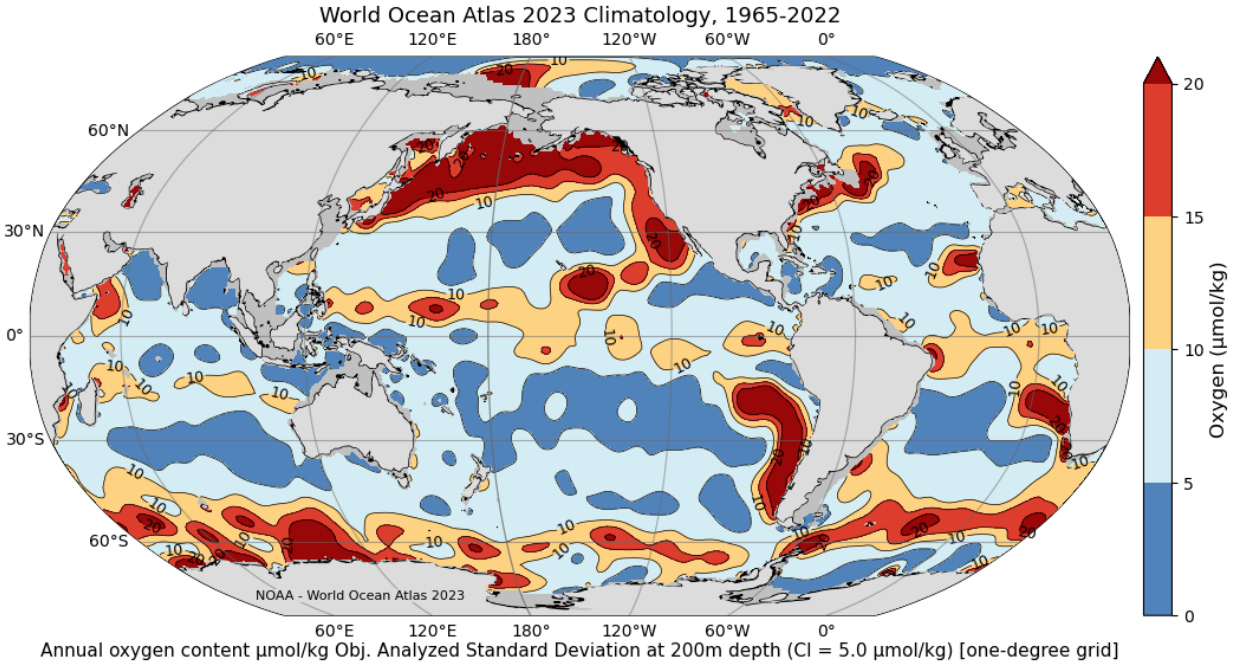

Figure 4f. WOA23F objectively analyzed standard deviation of the statistical annual mean O_2 content ($\mu mol \cdot kg^{-1}$) at 200 m depth.

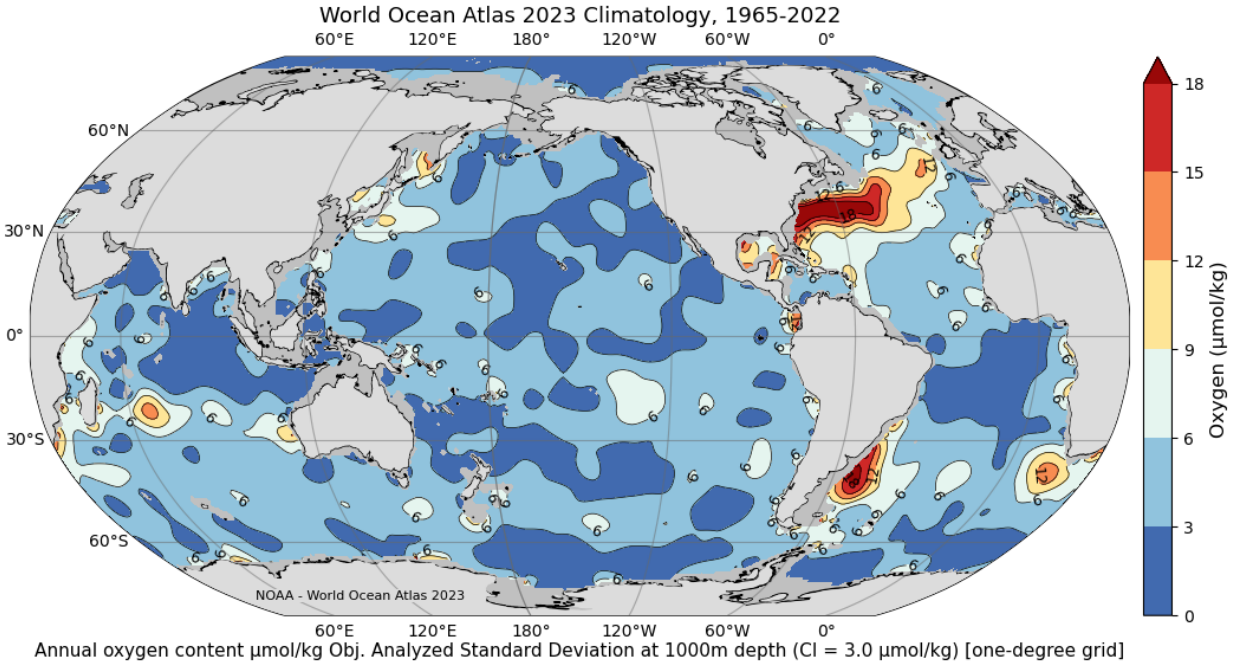

Figure 4g. WOA23F objectively analyzed standard deviation of the statistical annual mean O_2 content ($\mu mol \cdot kg^{-1}$) at 1000 m depth.

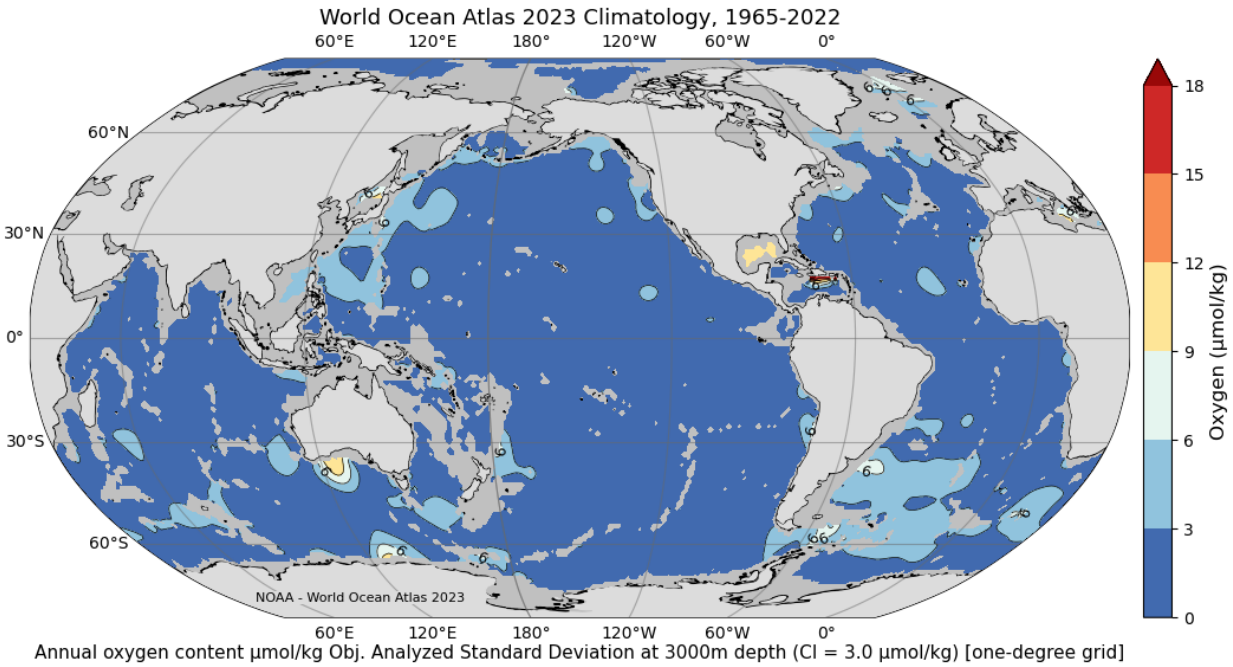

Figure 4h. WOA23F objectively analyzed standard deviation of the statistical annual mean O_2 content ($\mu mol \cdot kg^{-1}$) at 3000 m depth.

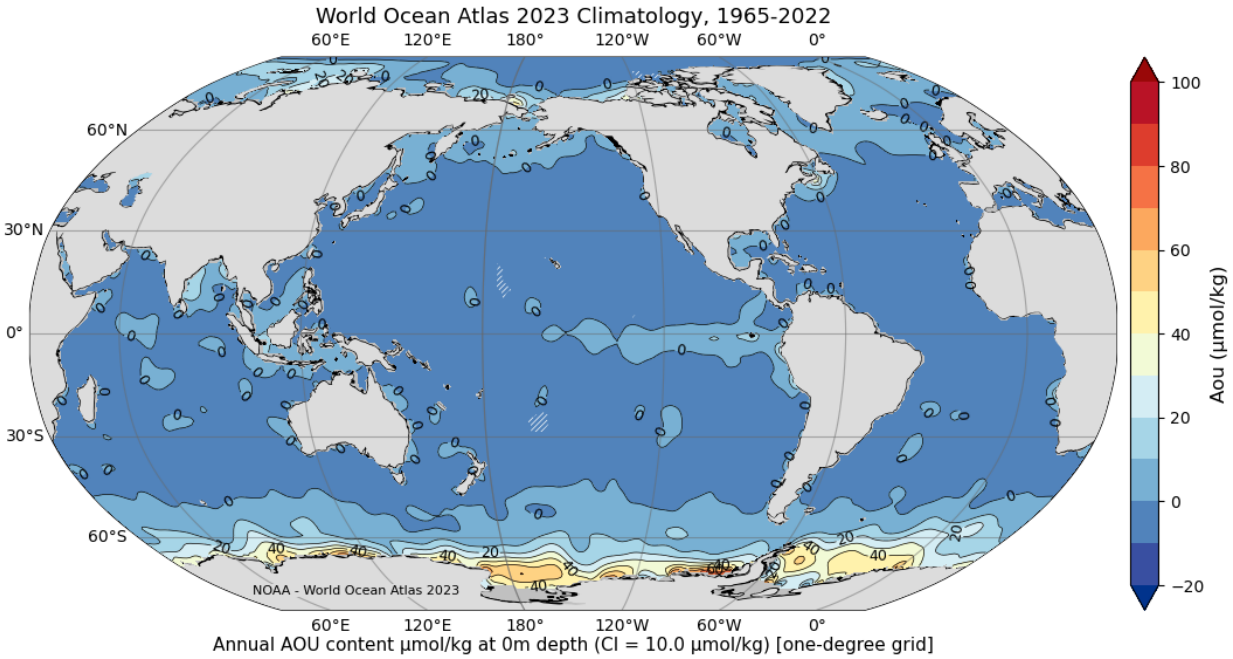

Figure 4i. WOA23F objectively analyzed annual mean AOU content (µmol·kg^{-1}) at 0 m depth .

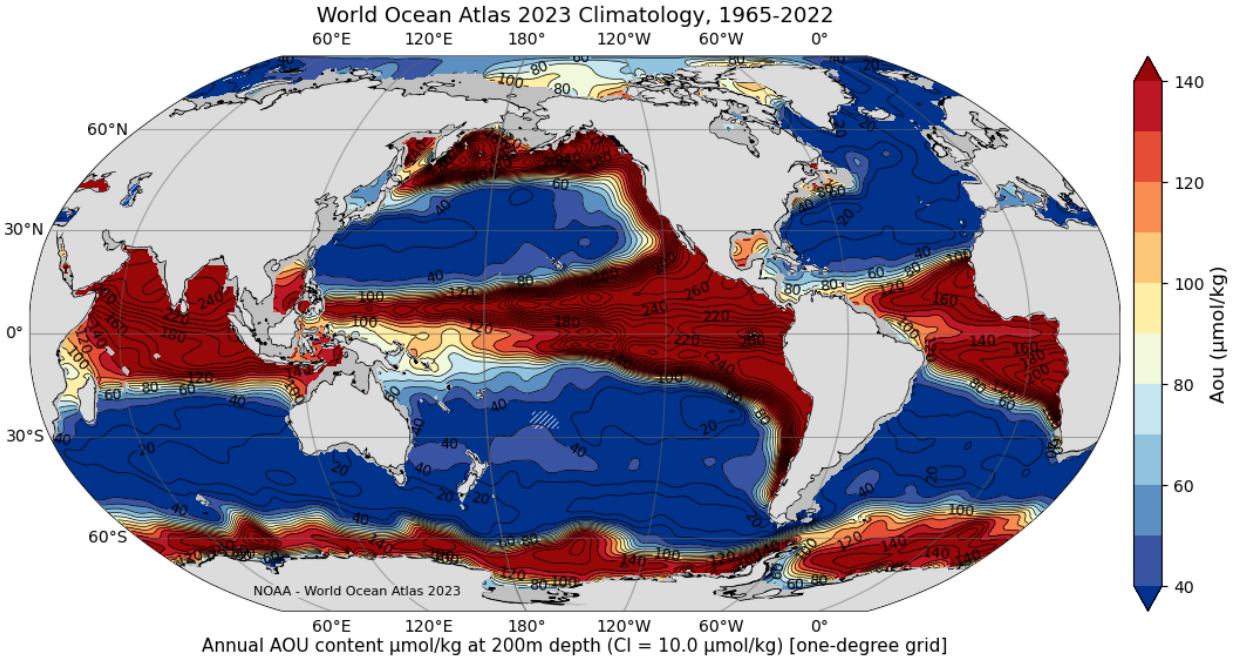

Figure 4j. WOA23F objectively analyzed annual mean AOU content (µmol·kg^{-1}) at 200 m depth.

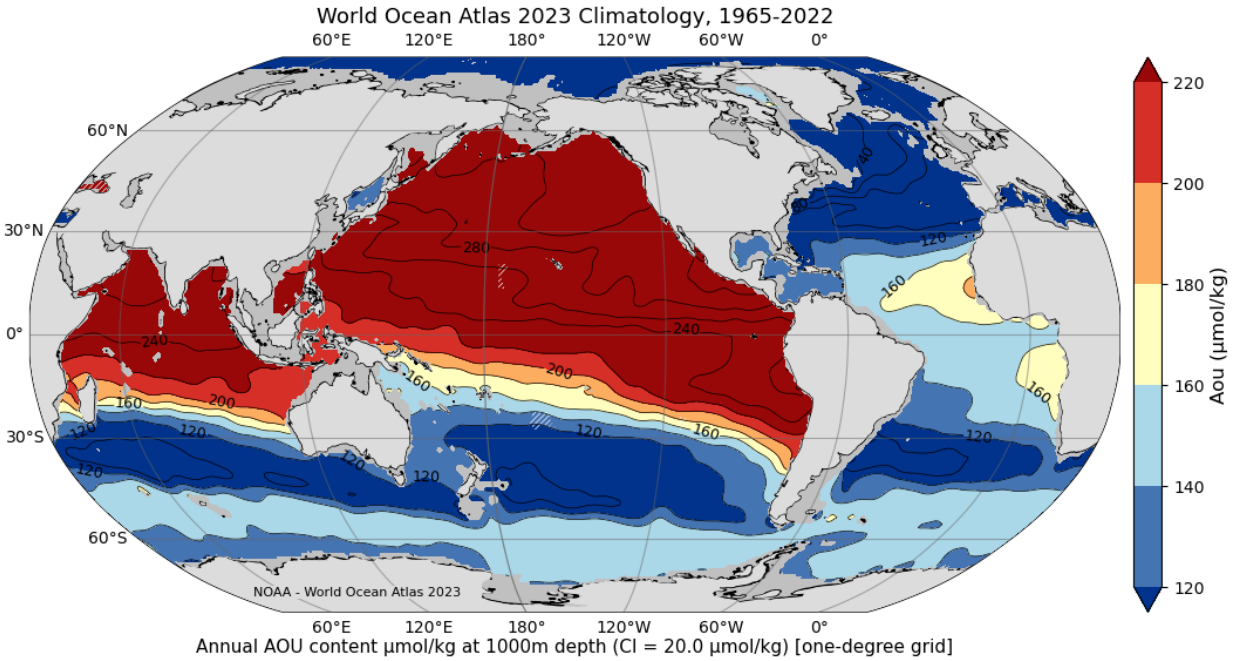

Figure 4k. WOA23F objectively analyzed annual mean AOU content (µmol·kg^{-1}) at 1000 m depth.

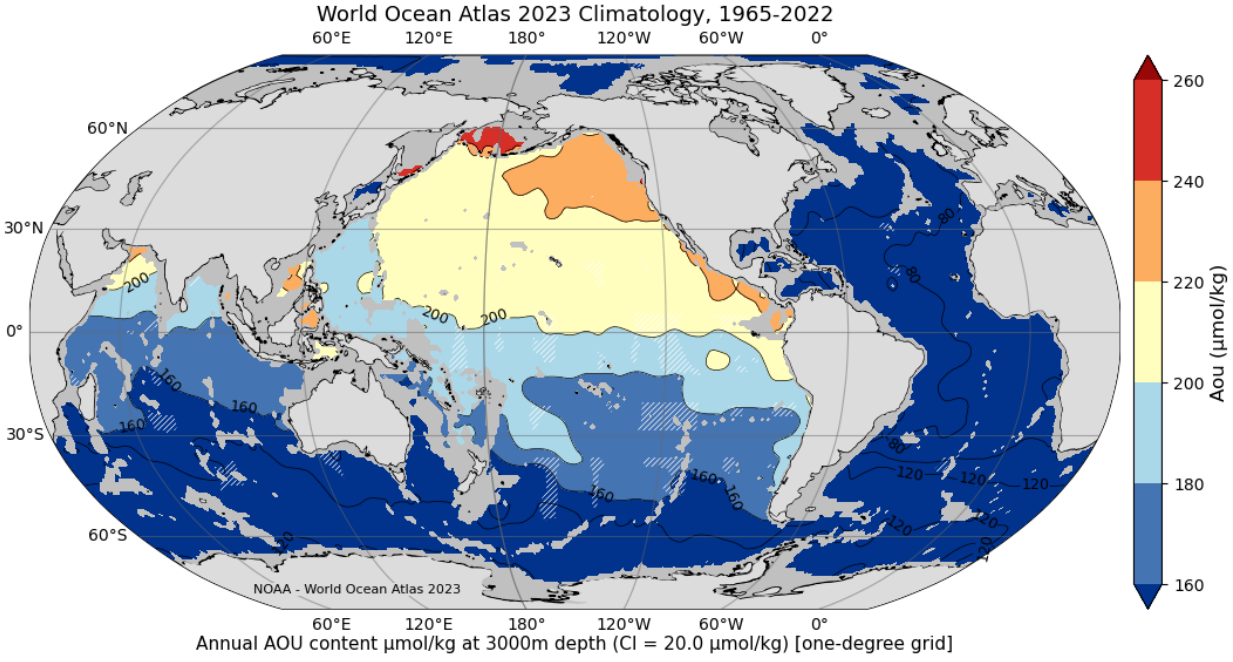

Figure 4l. WOA23F objectively analyzed annual mean AOU content (µmol·kg^{-1}) at 3000 m depth.

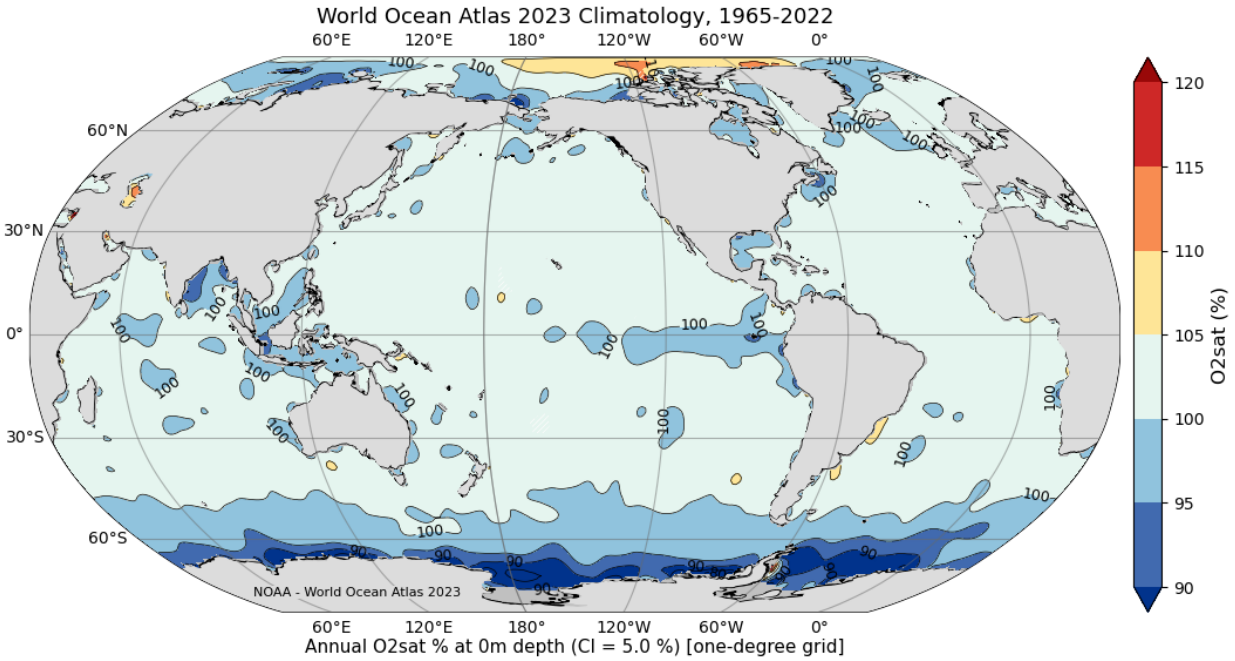

Figure 4m. WOA23F objectively analyzed annual mean O2S (%) at 0 m depth

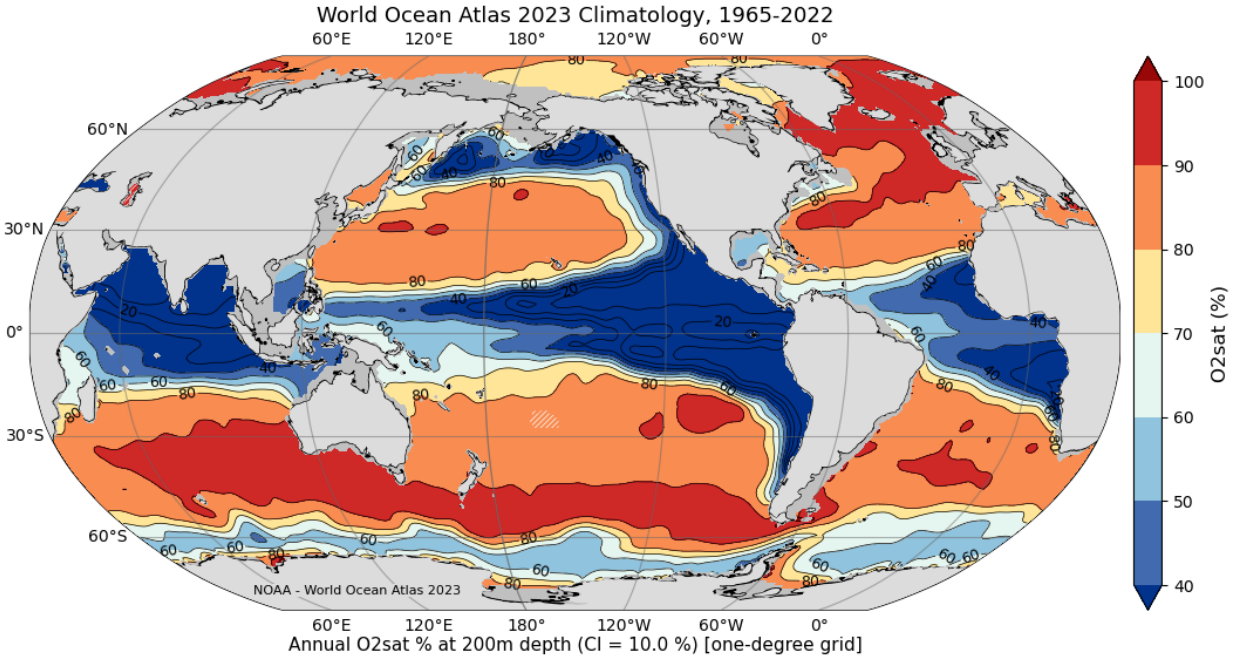

Figure 4n. WOA23F objectively analyzed annual mean O2S (%) at 200 m depth

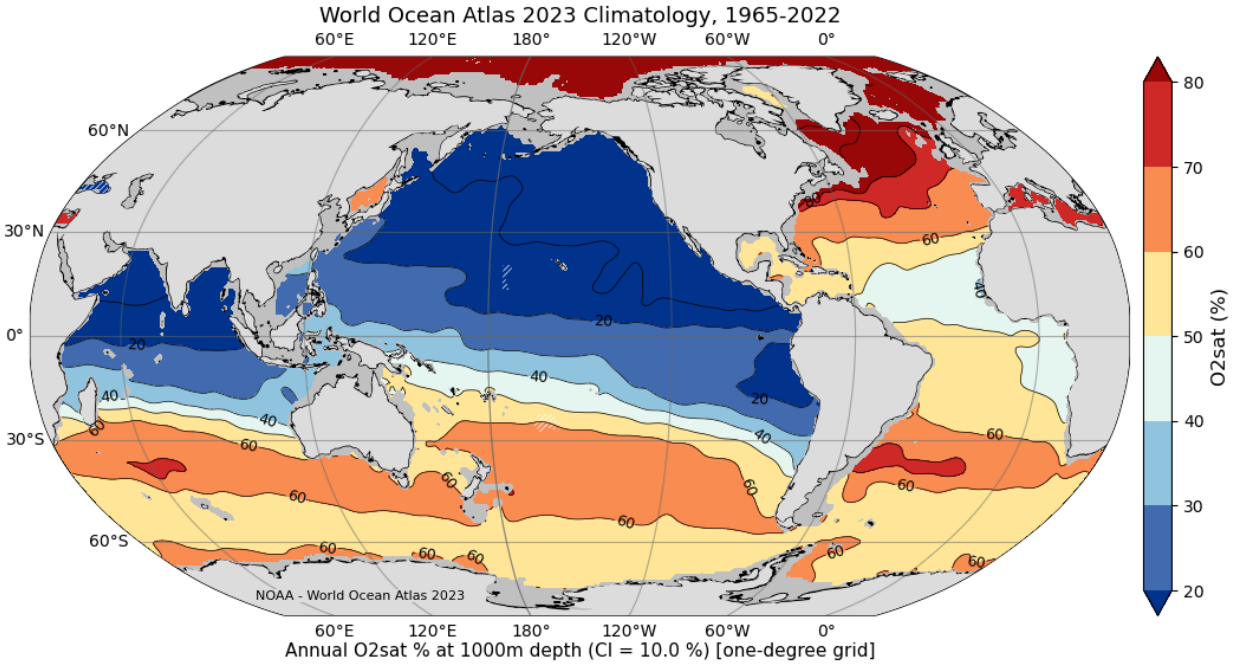

Figure 4o. WOA23F objectively analyzed annual mean O2S (%) at 1000 m depth

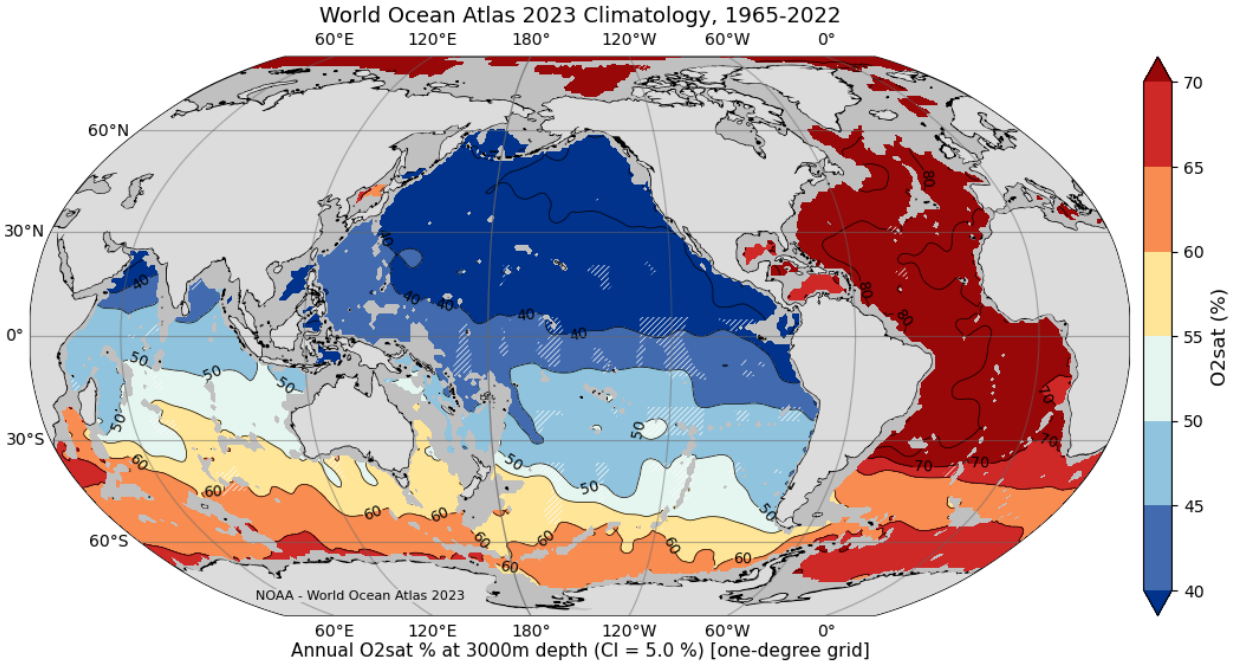

Figure 4p. WOA23F objectively analyzed annual mean O2S (%) at 3000 m depth

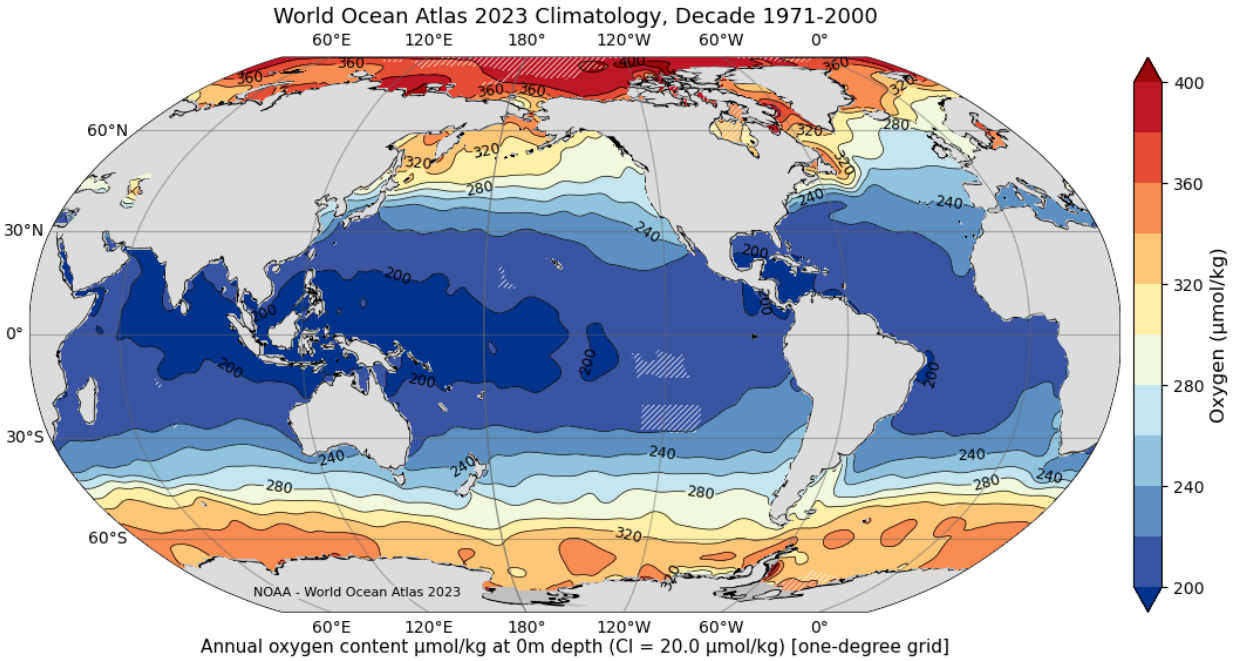

Figure 4q. WOA23N objectively analyzed annual mean O_2 content (µmol·kg^{-1}) at 0 m depth.

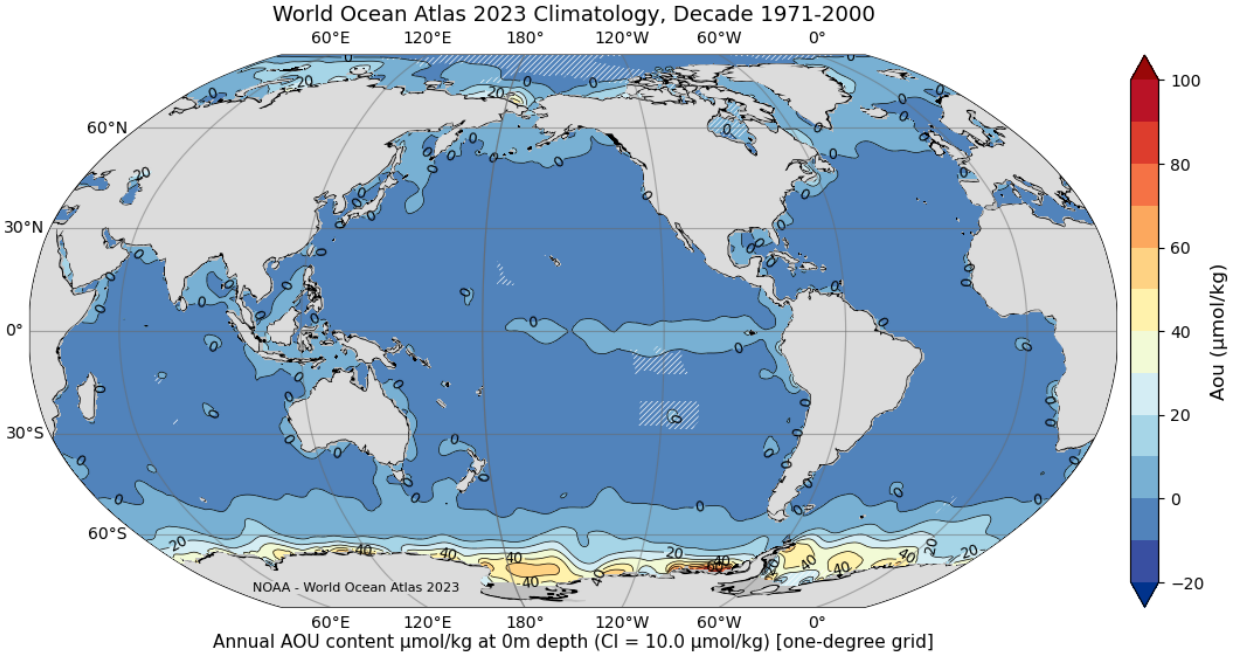

Figure 4r. WOA23N objectively analyzed annual mean AOU content (µmol·kg^{-1}) at 0 m depth.

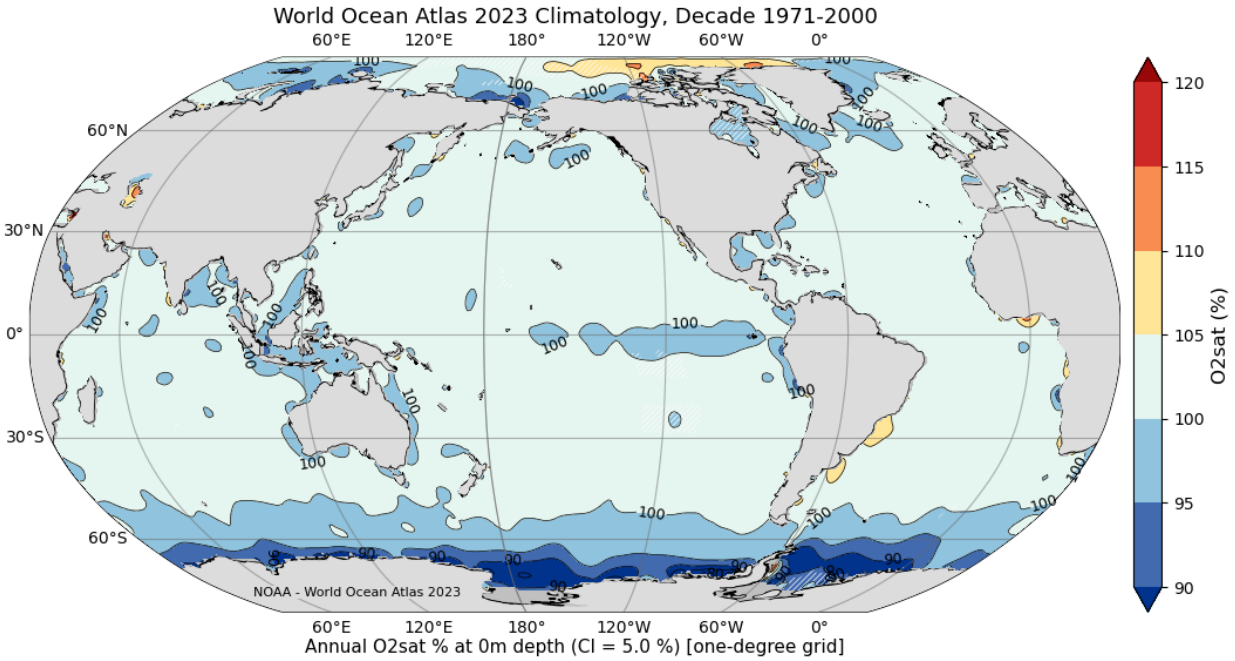

Figure 4s. WOA23N objectively analyzed annual mean O2S (%) at 0 m depth.

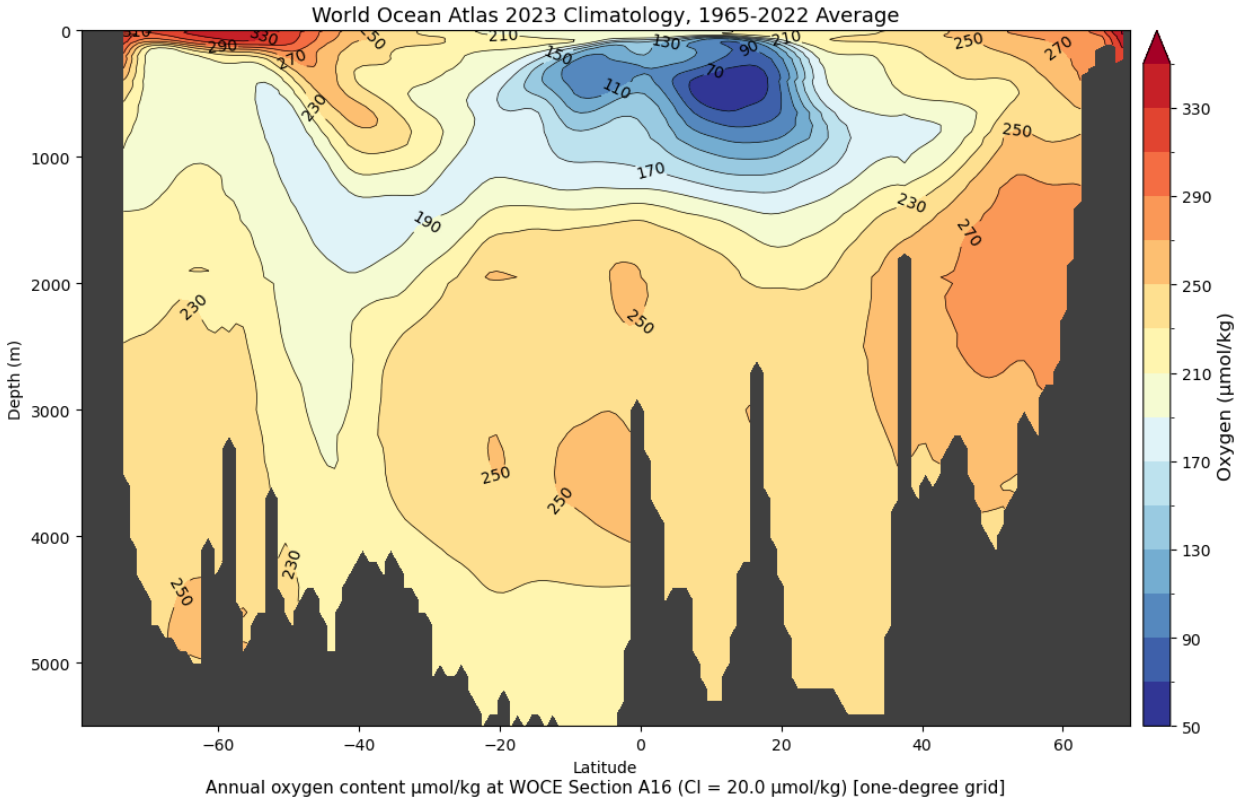

Figure 4t. WOA23F meridional cross section of climatological annual mean O_2 content ($\mu mol \cdot kg^{-1}$) in the Atlantic Ocean along 25°W; roughly the WOCE A16 line (Figure 8c).

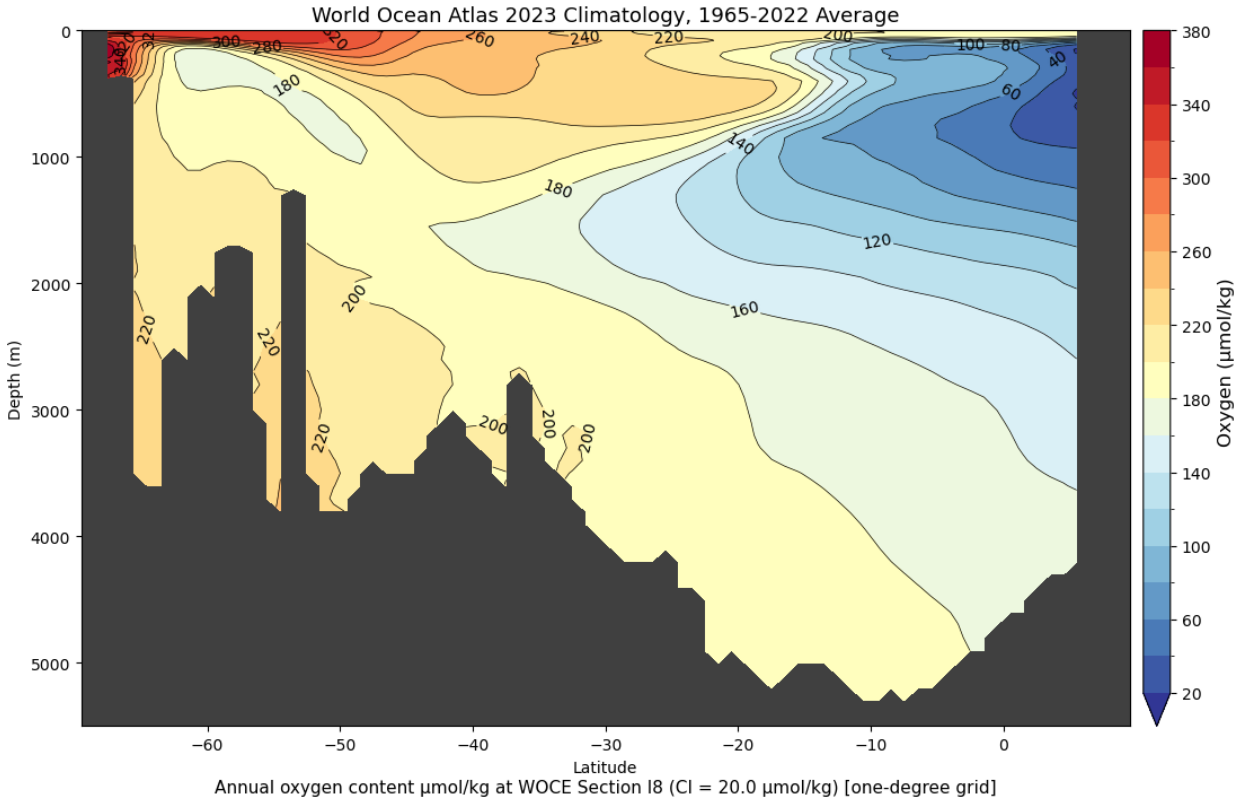

Figure 4u. WOA23F meridional cross section of climatological annual mean O_2 content (µmol·kg^{-1}) in the Indian Ocean at 80°E; roughly the WOCE I8 line (Figure 8c).

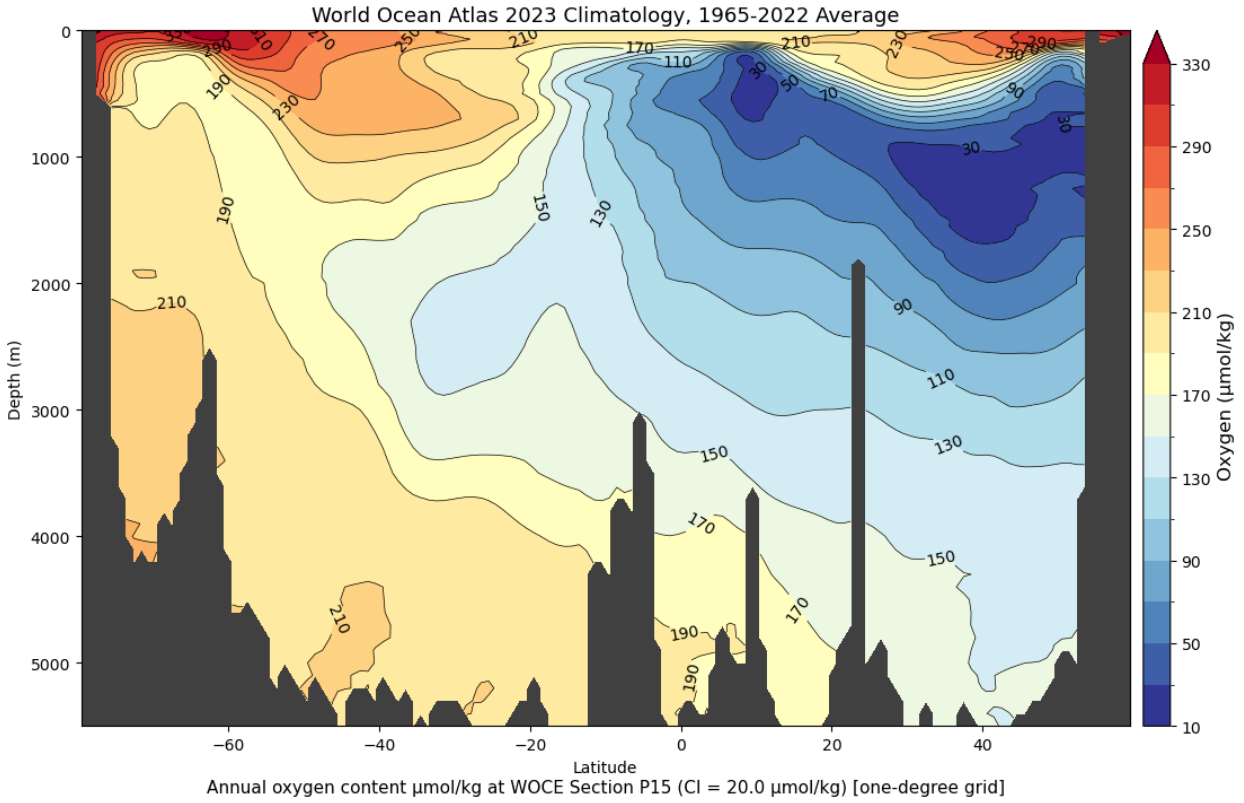

Figure 4v. WOA23F meridional cross section of climatological annual mean O_2 content ($\mu mol \cdot kg^{-1}$) in the Pacific Ocean at 165°W; roughly the WOCE P15 line (Figure 8c).

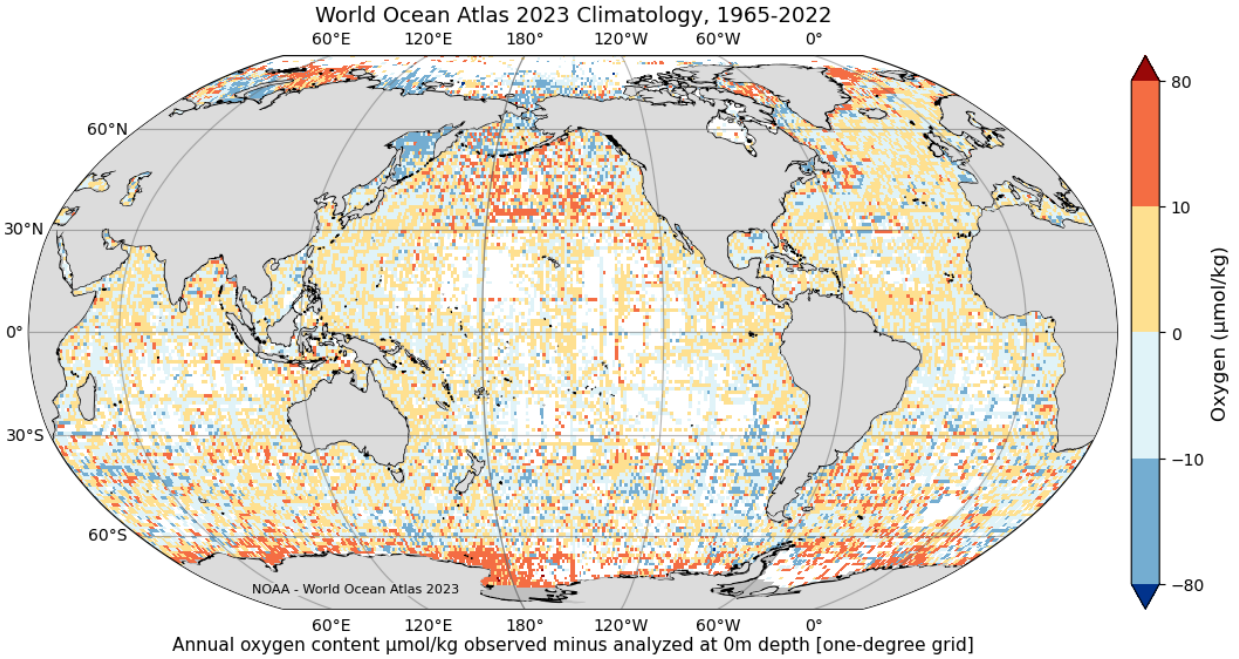

Figure 4w. WOA23F annual O_2 content ($\mu mol \cdot kg^{-1}$) statistical mean of the observations minus objectively analyzed at 0 m depth .

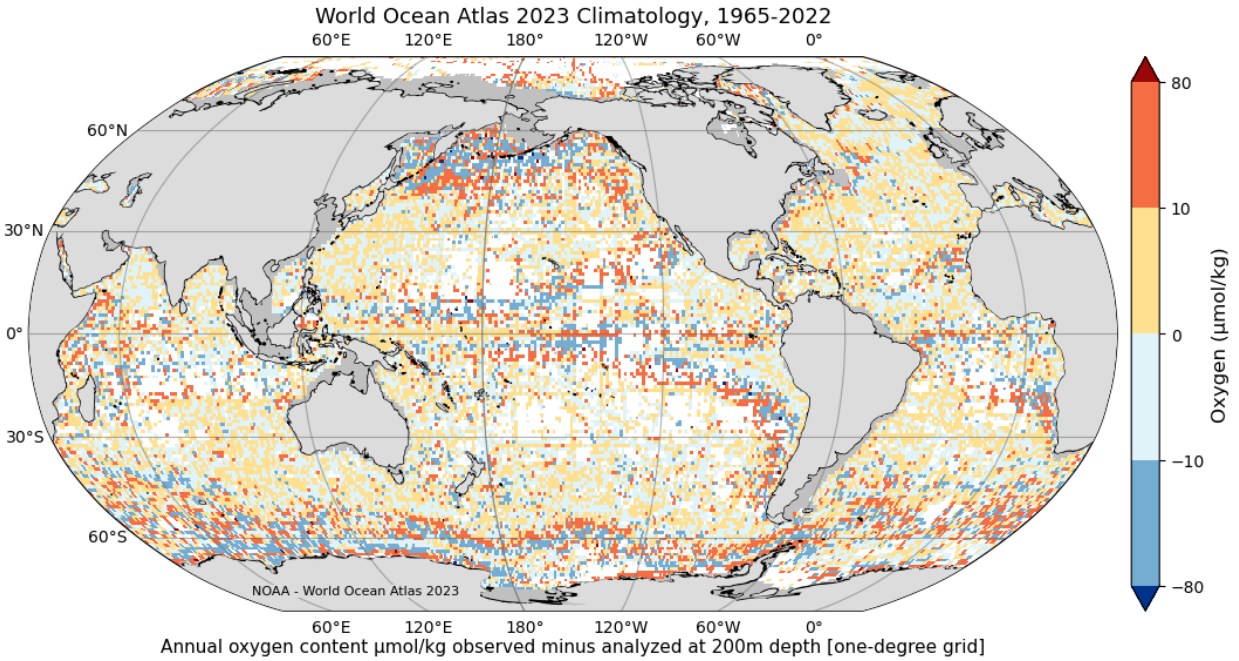

Figure 4x. WOA23F annual O_2 content ($\mu mol \cdot kg^{-1}$) statistical mean of the observations minus objectively analyzed at 200 m depth.

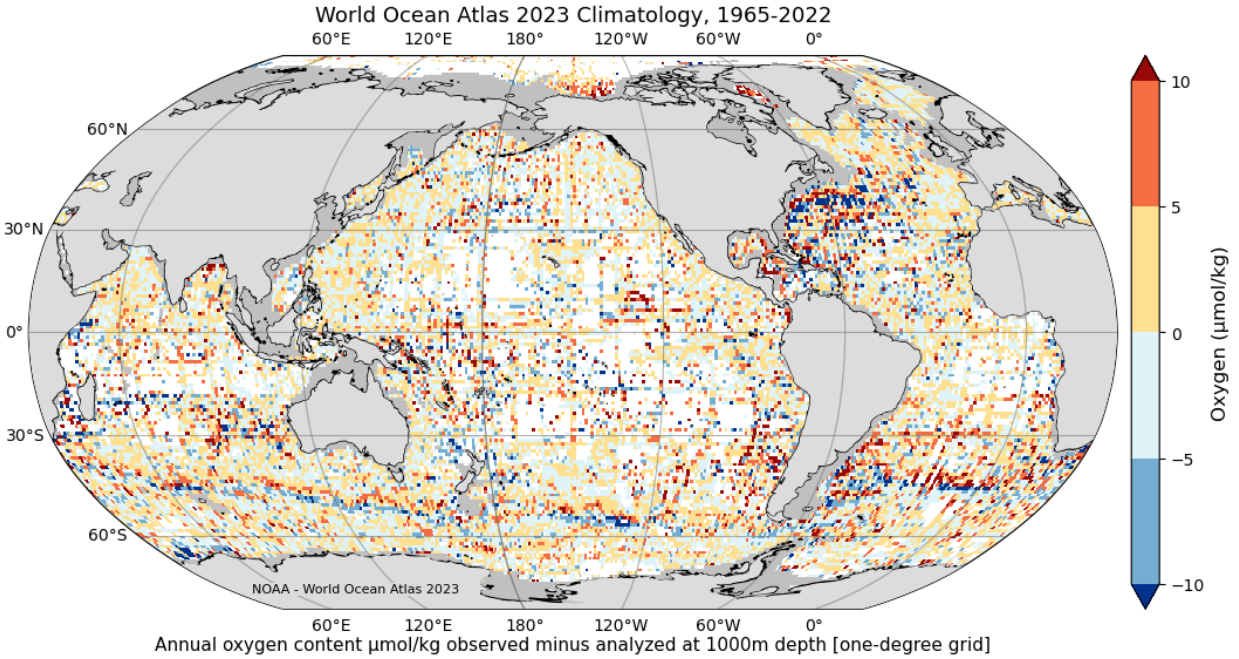

Figure 4y. WOA23F annual O_2 content ($\mu mol \cdot kg^{-1}$) statistical mean of the observations minus objectively analyzed at 1000 m depth.

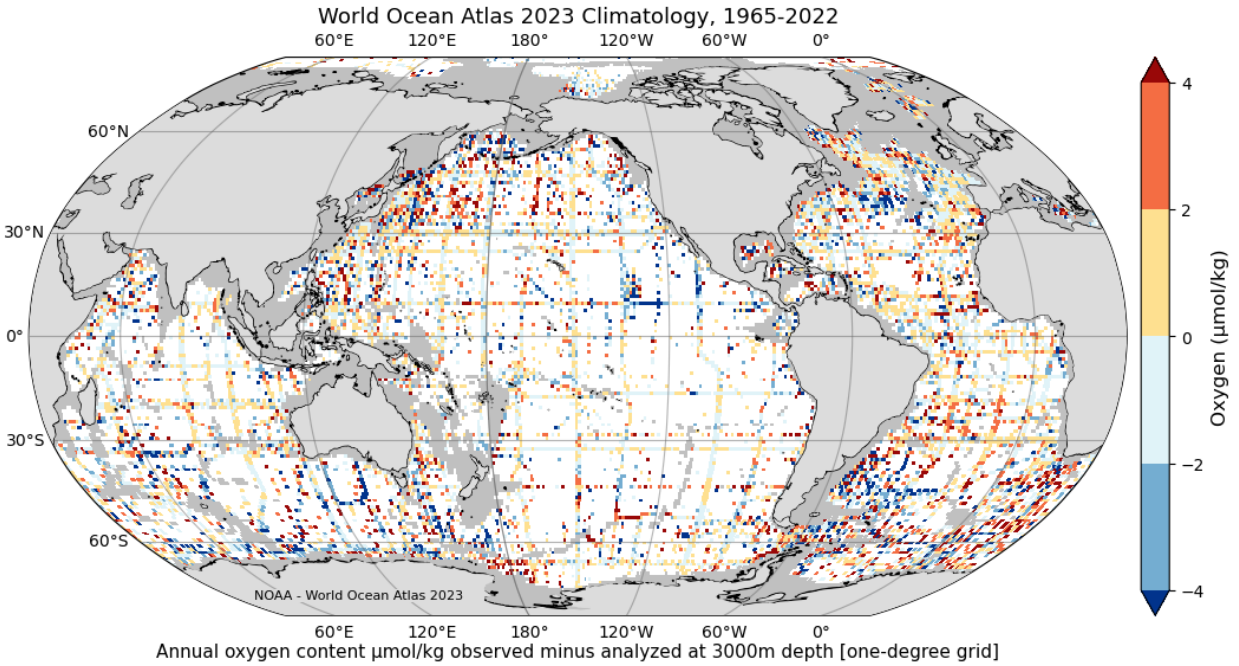

Figure 4z. WOA23F annual O_2 content ($\mu mol \cdot kg^{-1}$) statistical mean of the observations minus objectively analyzed at 3000 m depth.

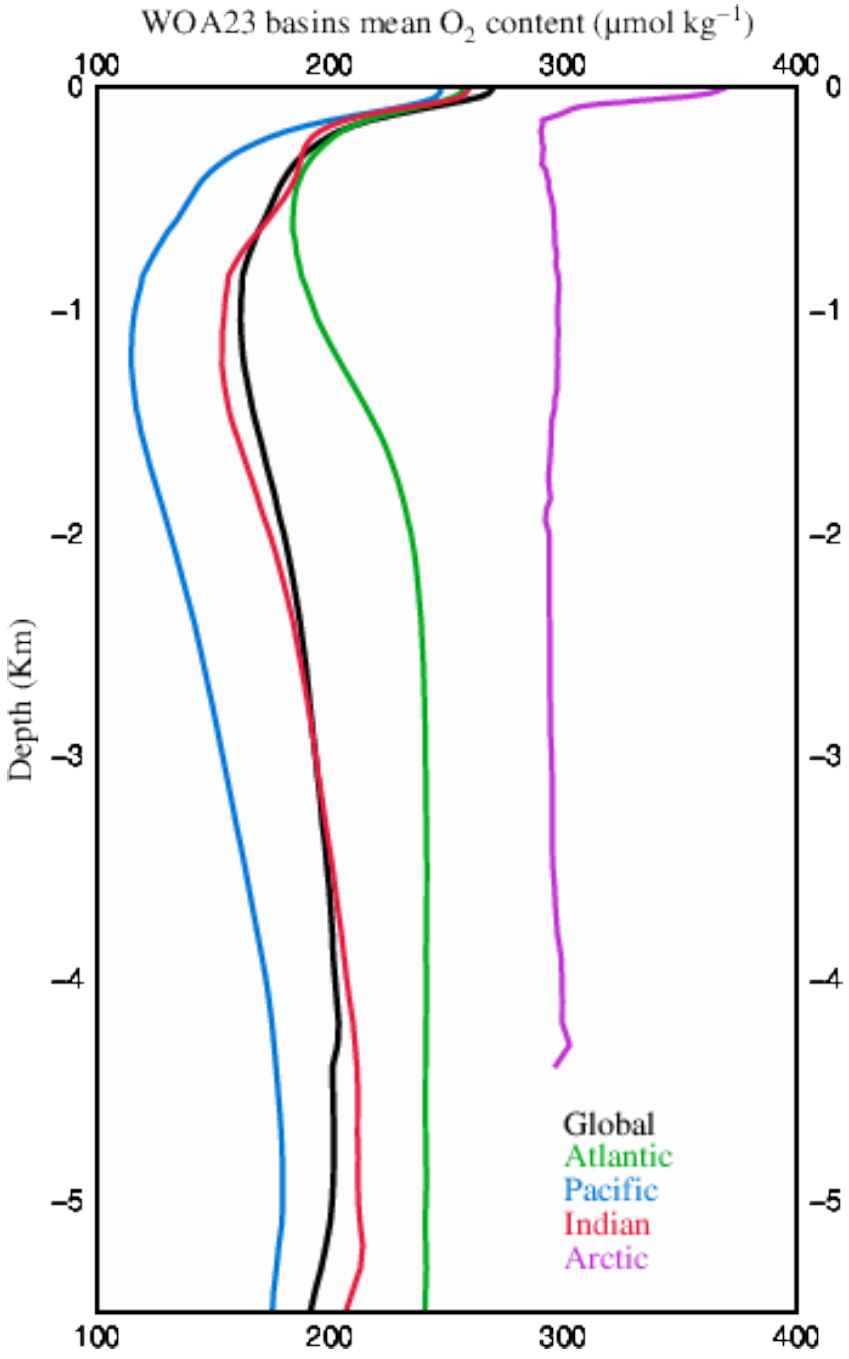

Figure 5a. WOA23F objectively analyzed annual mean O_2 content (µmol·kg^{-1}) in different basins as a function of depth (km).
Notes: Figure 8 a,b show ocean coverage for different basins.

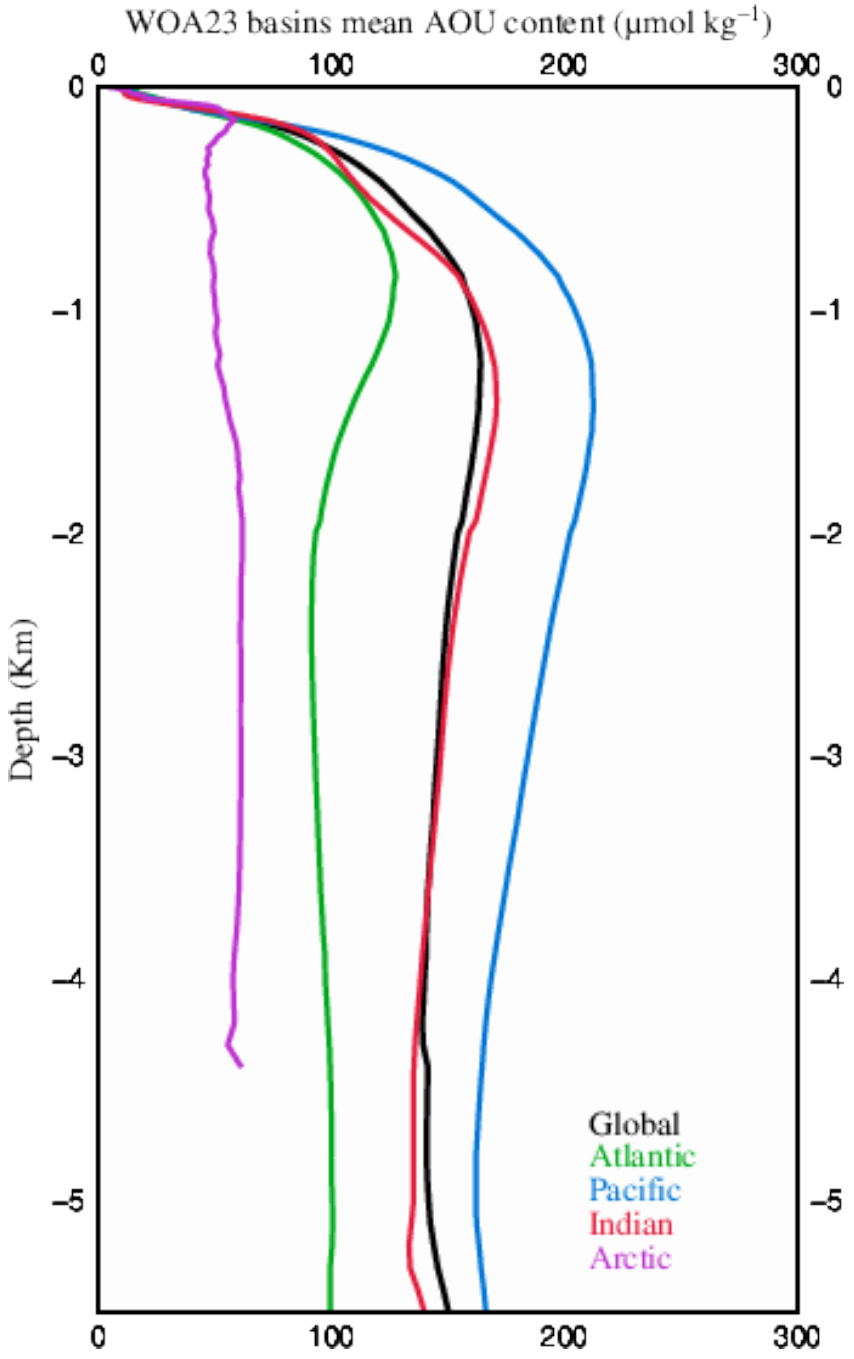

Figure 5b. WOA23F objectively analyzed annual mean AOU content (µmol·kg^{-1}) in different basins as a function of depth (km).
Notes: Figure 8 a,b show ocean coverage for different basins.

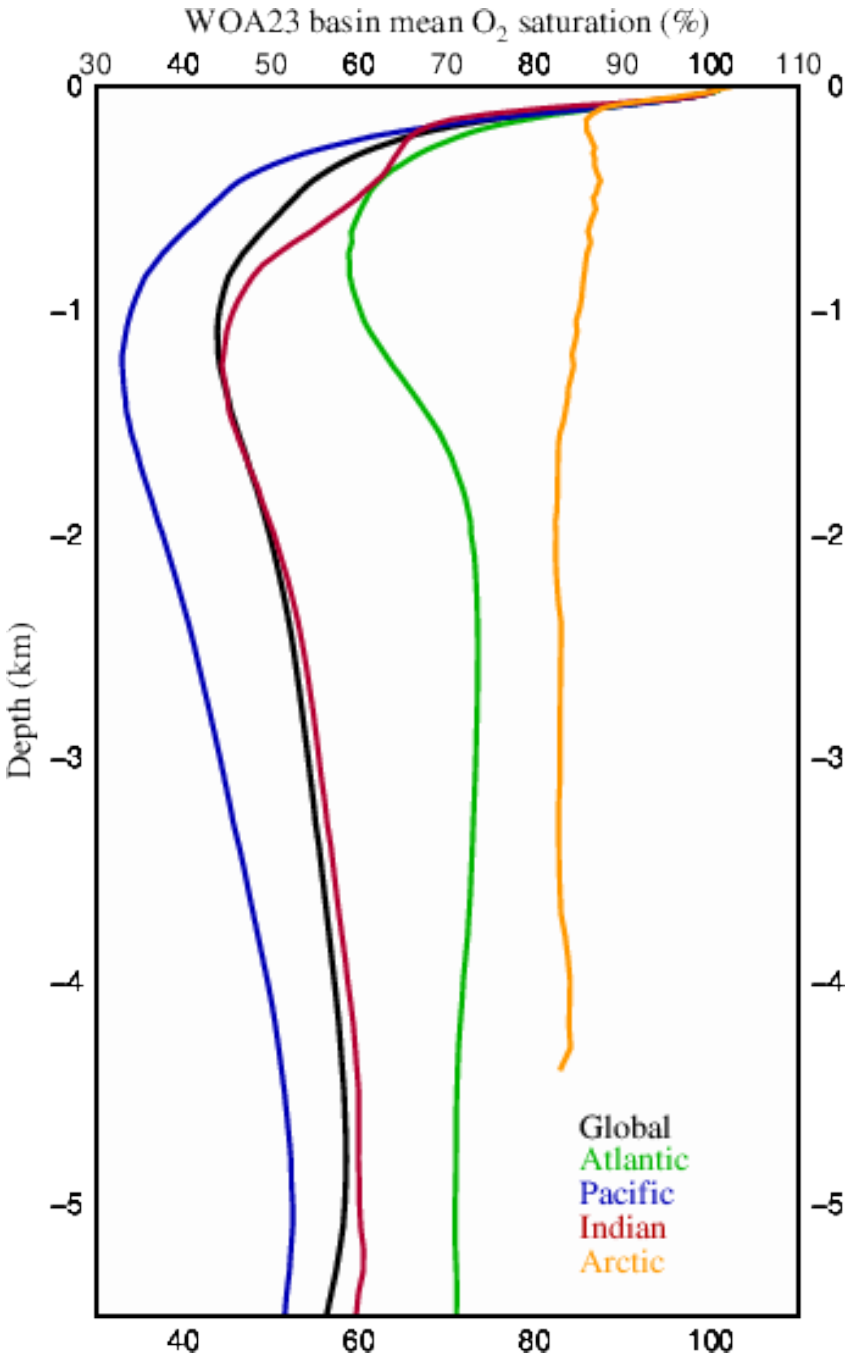

Figure 5c. WOA23F objectively analyzed annual mean O2S (%) in different basins as a function of depth (km).
Notes: Figure 8 a,b shows ocean coverage for different basins.

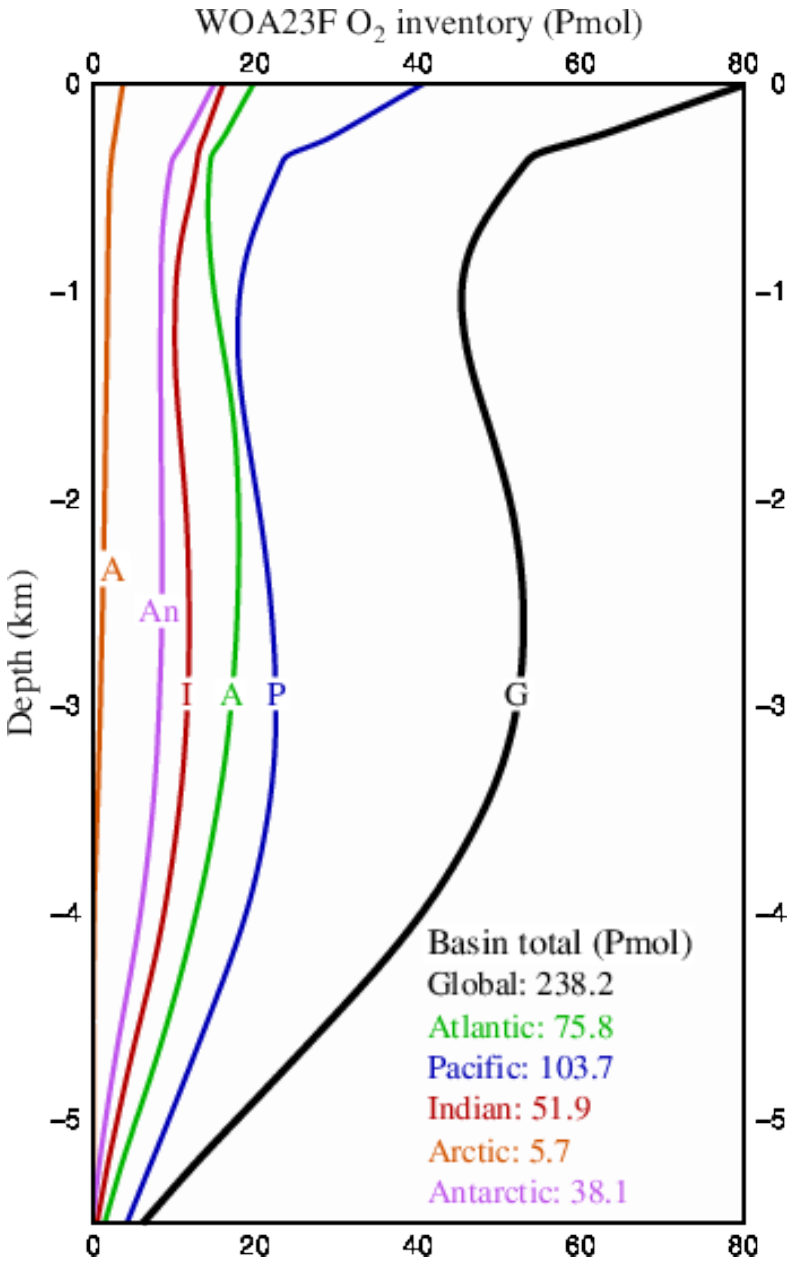

Figure 5d. WOA23F annual O_2 inventory (Pmol) in different ocean basins as a function of depth (km).
Notes: Figure 8 shows ocean coverage for different basins. The Antarctic inventory corresponds to O_2 content values ≤ 50°S.

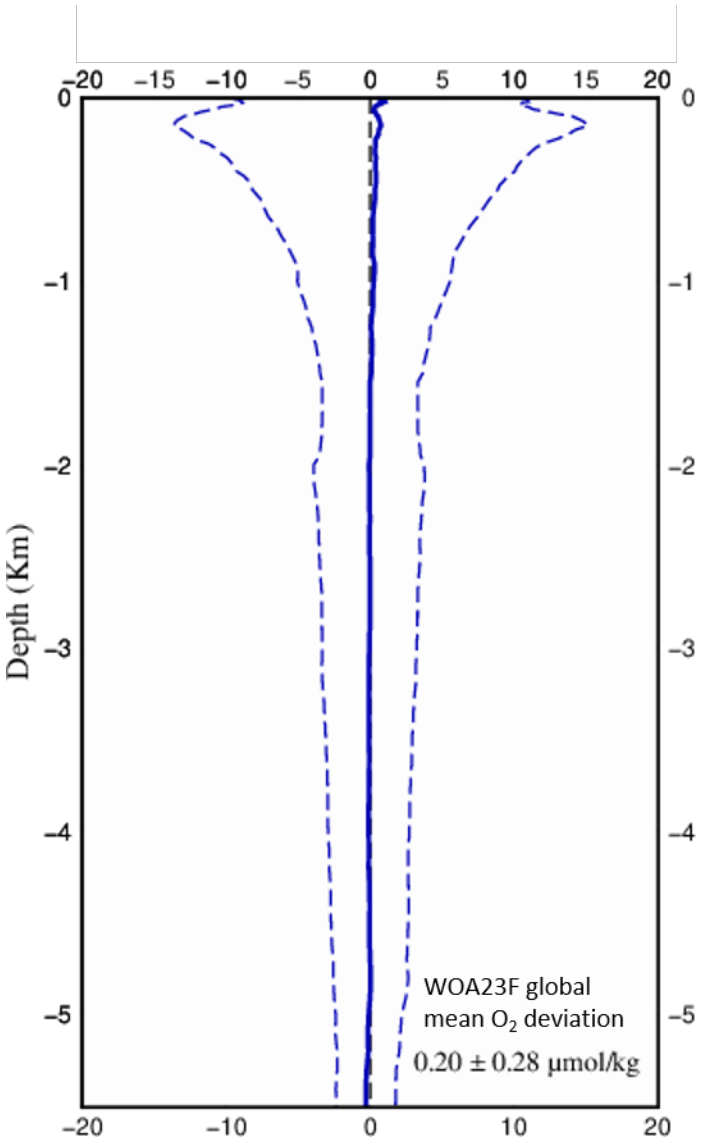

Figure 6a. WOA23F global annual O_2 content (µmol·kg^{-1}) mean difference of the statistical mean minus the objectively analyzed climatology as a function of depth (km).

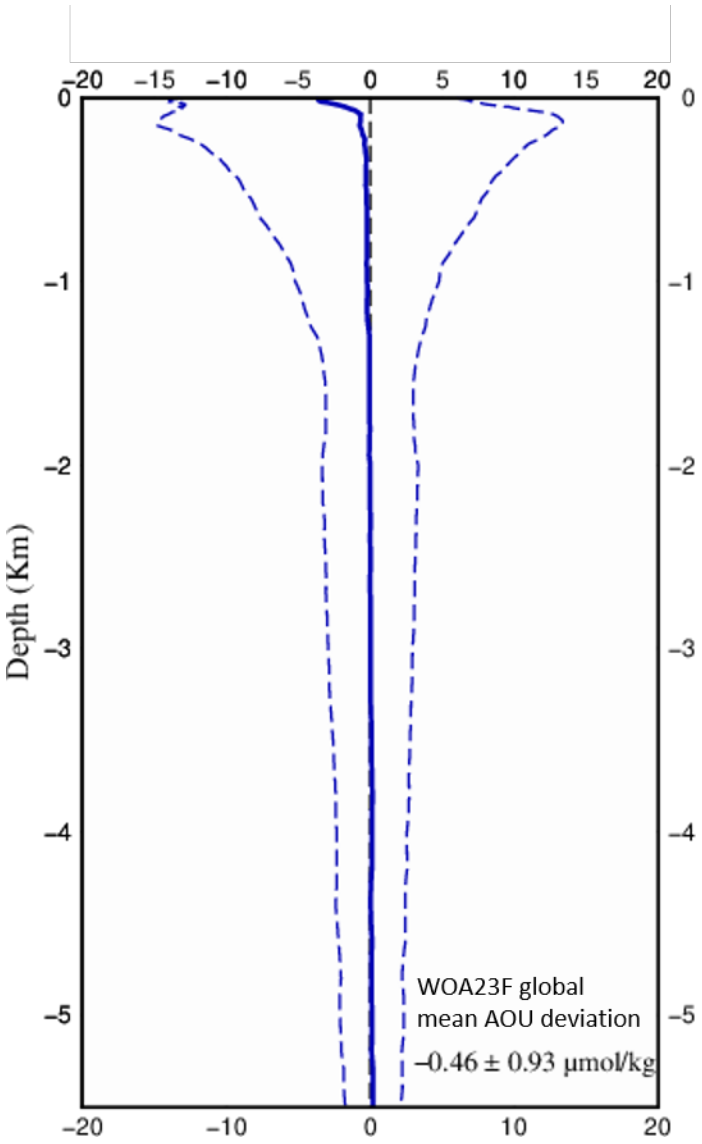

Figure 6b. WOA23F global annual AOU content (µmol·kg^{-1}) mean difference of the statistical mean minus the objectively analyzed climatology as a function of depth (km).

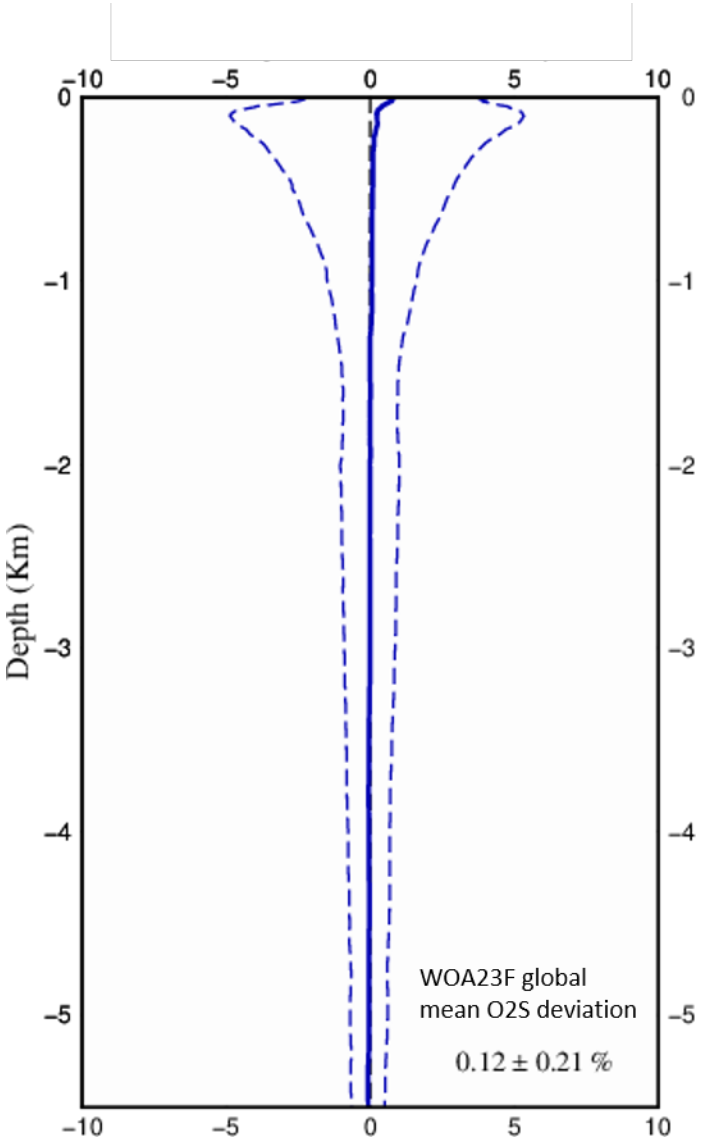

Figure 6c. WOA23F global annual mean O2S (%) difference of the observed statistical means minus the objectively analyzed climatology as a function of depth (km).

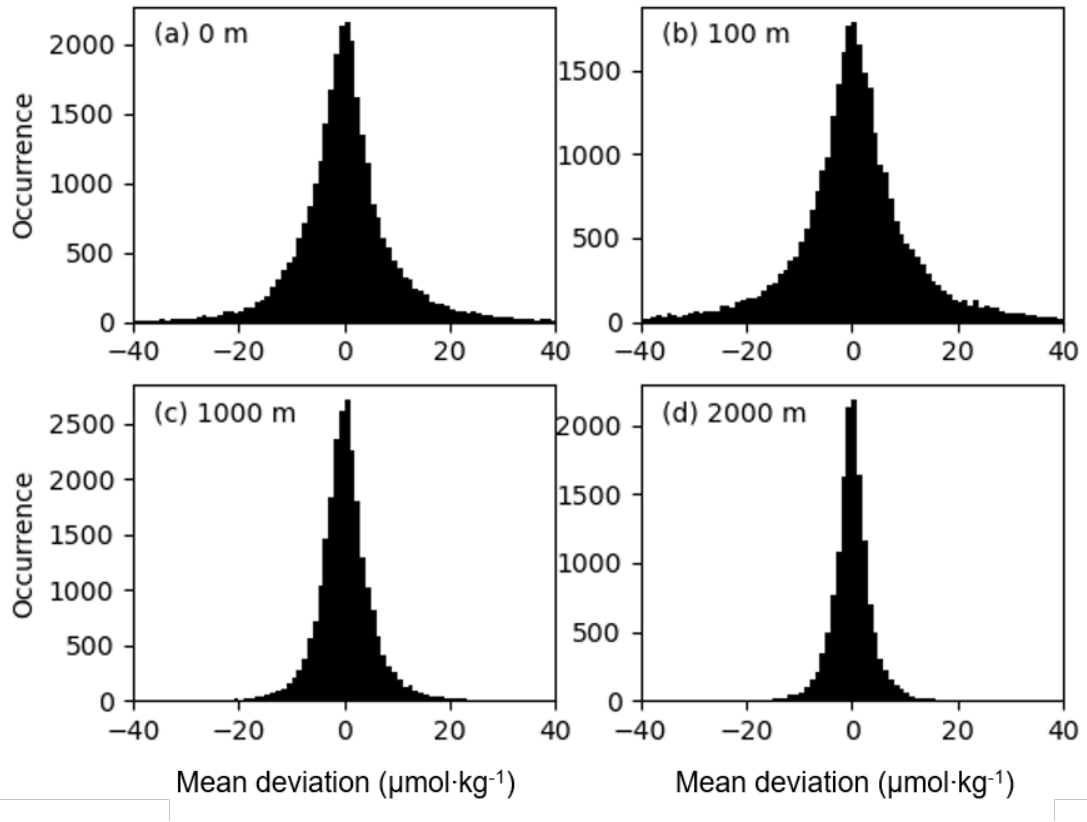

Figure 7. WOA23F globally averaged deviation between the annual mean O_2 content (μmol·kg^{-1}) statistical mean of the observations and the objectively analyzed values at different depths.

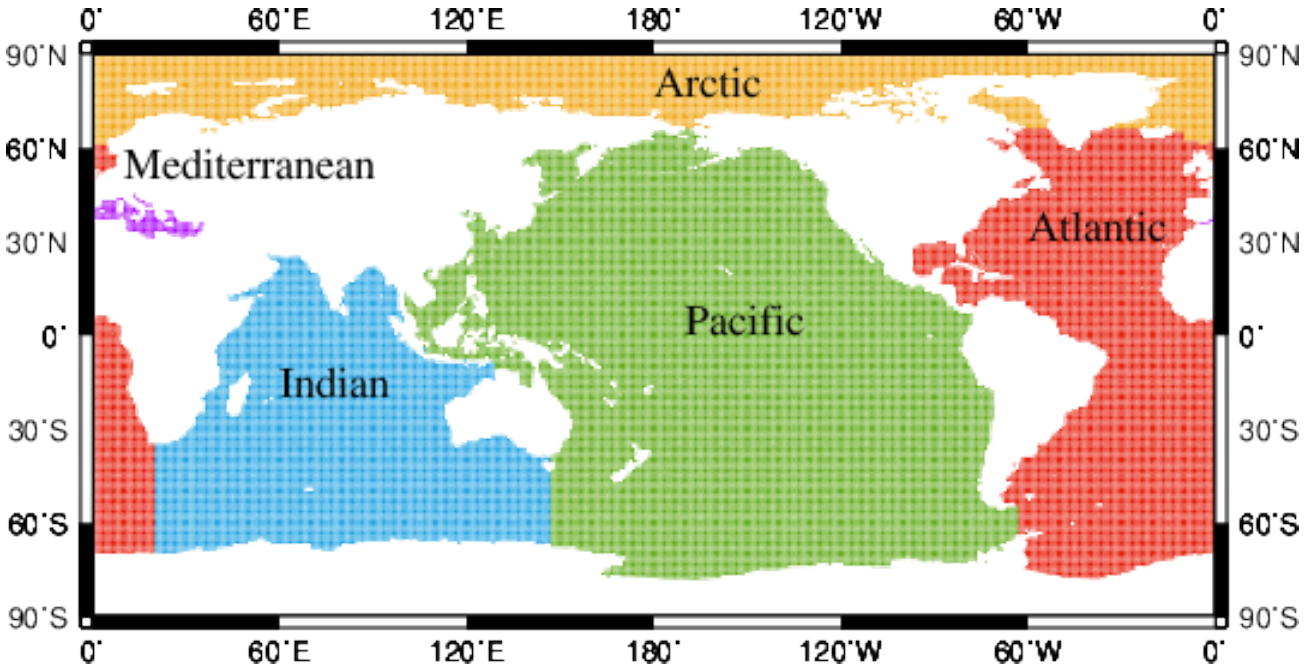

Figure 8a. WOA23 ocean coverage for different basins.

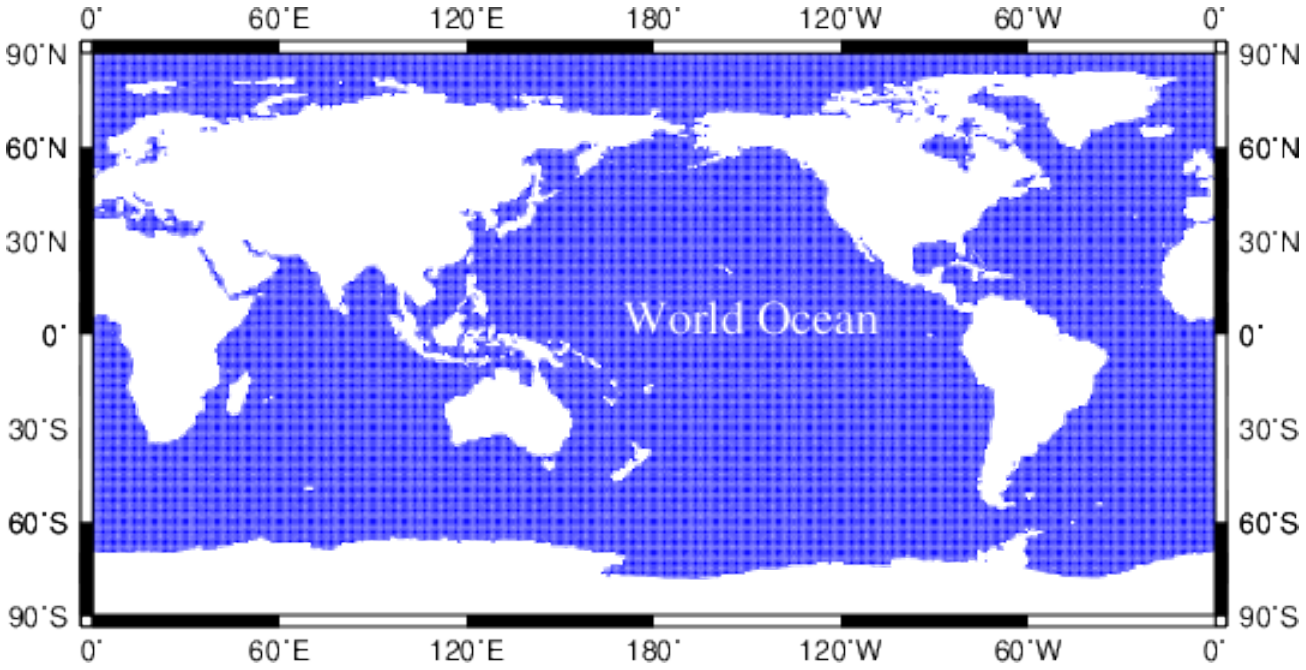

Figure 8b. WOA23 global ocean boundary.

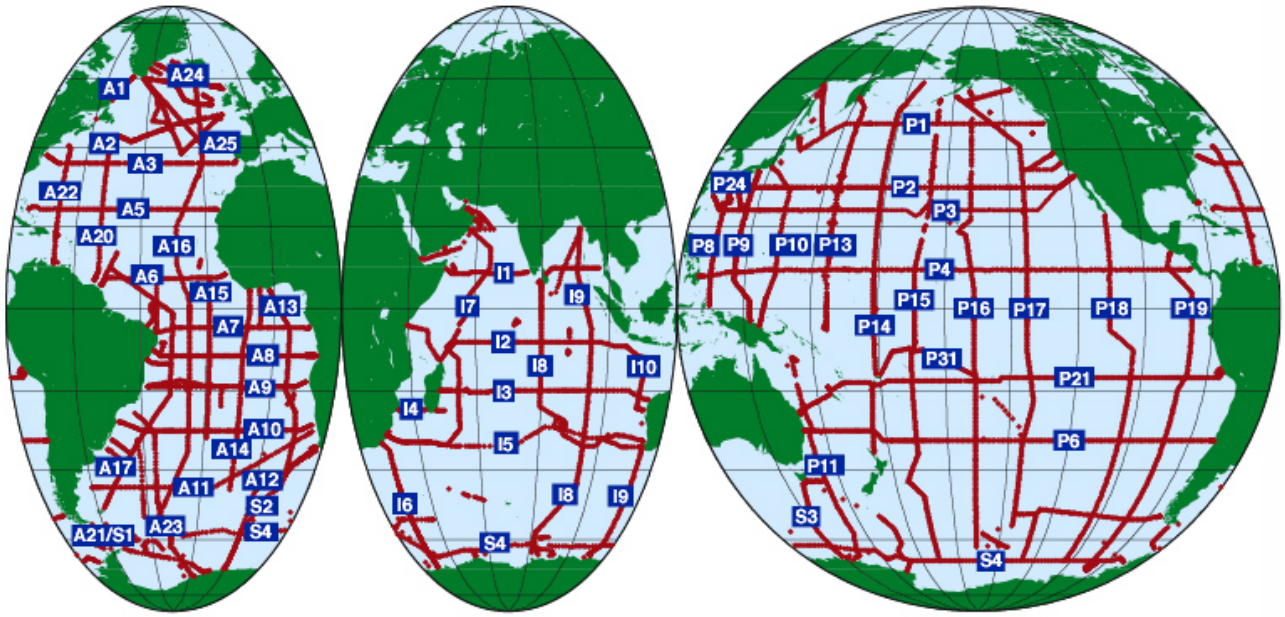

Figure 8c. Stations occupied during the WOCE One-Time Survey

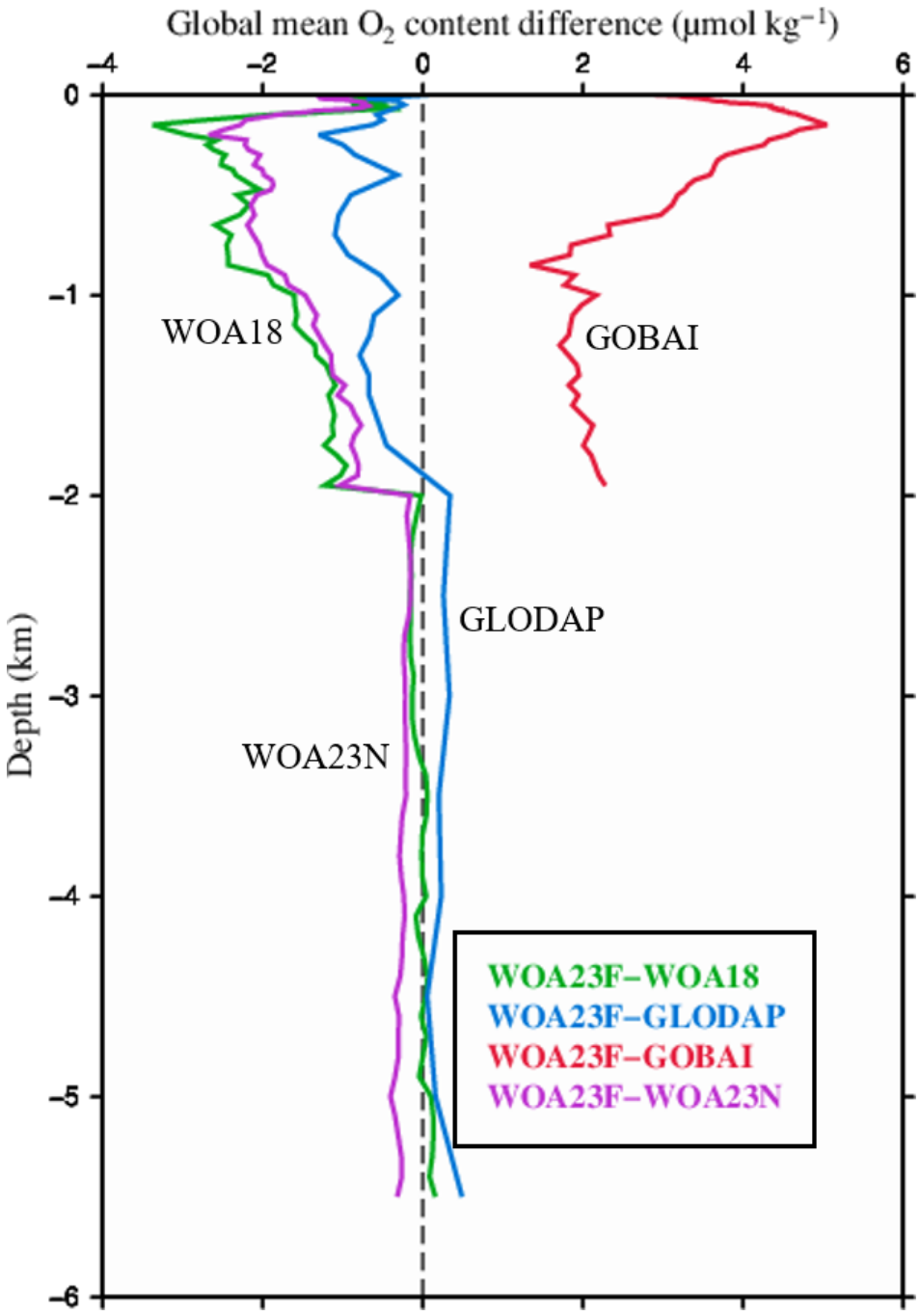

Figure 9. Global annual mean O_2 content (µmol·kg^{-1}) differences as a function of depth (km) between WOA23F and WOA23N, WOA18, GLODAP, and GOBAI.
Notes: Table 9 provides O_2, AOU, and O2S statistical mean differences between WOA23F and WOA18 (Garcia *et al.* 2018), GLODAP (GLODAPv2.2016b, Olsen *et al.* 2016, Lauvset *et al.* 2022), and GOBAI (Sharp *et al.* 2023).